

The John A. Blume Earthquake Engineering Center

Department of Civil Engineering
Stanford University

SEISMIC ZONING AND GROUND MOTION PARAMETERS FOR EL SALVADOR

by

**Celso S. Alfaro
Anne S. Kiremidjian
and
Randall A. White**

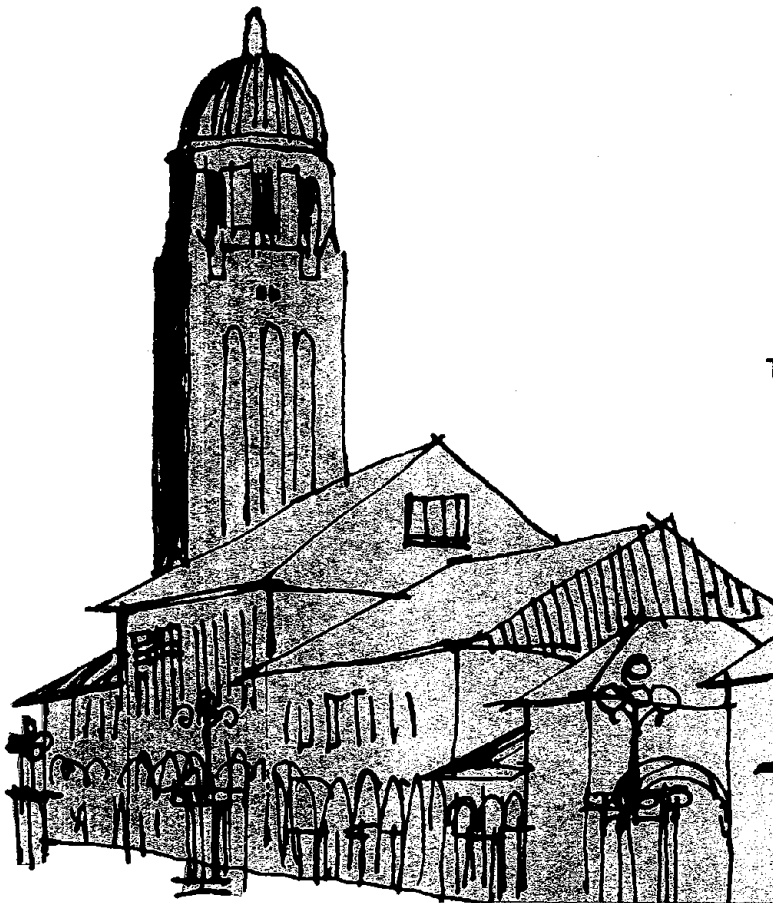
This research was partially
supported by

The Agency for International Development
(American Embassy in El Salvador)

The Organization of American States

The National Science Foundation
NSF Grant CES-8721370
and

The John A. Blume Earthquake
Engineering Center



Report No. 93

REPRODUCED BY
U.S. DEPARTMENT OF COMMERCE
NATIONAL TECHNICAL
INFORMATION SERVICE
SPRINGFIELD, VA 22161

December 1990

The John A. Blume Earthquake Engineering Center was established to promote research and education in earthquake engineering. Through its activities our understanding of earthquakes and their effects on mankind's facilities and structures is improving. The Center conducts research, provides instruction, publishes reports and articles, conducts seminars and conferences, and provides financial support for students. The Center is named for Dr. John A. Blume, a well-known consulting engineer and Stanford alumnus.

Address

The John A. Blume Earthquake Engineering Center
Department of Civil Engineering
Stanford University
Stanford, California 94305

**SEISMIC ZONING AND GROUND MOTION
PARAMETERS FOR EL SALVADOR**

DECEMBER 1990

BY

CELSO S. ALFARO
ANNE S. KIREMIDJIAN
RANDALL A. WHITE

THE JOHN A. BLUME EARTHQUAKE ENGINEERING CENTER
DEPARTMENT OF CIVIL ENGINEERING
STANFORD UNIVERSITY
STANFORD, CA 94305

THIS RESEARCH WAS PARTIALLY
SUPPORTED BY

THE AGENCY FOR INTERNATIONAL DEVELOPMENT
(AMERICAN EMBASSY IN EL SALVADOR)

THE ORGANIZATION OF AMERICAN STATES

THE NATIONAL SCIENCE FOUNDATION
NSF GRANT CES-8721370

AND

THE JOHN A. BLUME EARTHQUAKE
ENGINEERING CENTER

ACKNOWLEDGMENTS

The authors of this report would like to thank Ing. Fabio W. Alfaro, director of the computer center of the Direccion de Planificacion of the Ministerio de Obras Publicas in El Salvador for his cooperation on the gathering of data. The cooperation of the Senator William V. Roth, senator for Delaware and Scott G. Stevens, director of the English Language Institute at the University of Delaware is very much appreciated. We also like to thank the research team of the seismology department of the U.S. Geological Survey specially to David Harlow and Gerald Brady for many useful and stimulating discussions.

The partial support provided by the Agency for International Development (American Embassy in El Salvador), the Organization of American States (OAS), the National Science Foundation (NSF Grant CES-8721370), and the John A. Blume Earthquake Engineering Center are gratefully acknowledged.

TABLE OF CONTENTS

	Page
ACKNOWLEDGMENTS	i
Chapter 1. INTRODUCTION	1
Chapter 2. TECTONIC SETTING AND SEISMIC PROVINCES	
2.1 Introduction	4
2.2 Tectonic Setting	4
2.3 Seismic Provinces	9
Chapter 3. SEISMIC DATA BASE	
3.1 Introduction	12
3.2 Historical Seismicity	12
3.3 Post - 1900 Seismicity	17
3.4 Sorting of Data	18
3.5 Quality of Data	20
Chapter 4. GEOMETRICAL MODELING	
4.1 Introduction	21
4.2 Geometrical Modeling	21
4.3 Frequency of Earthquake Occurrences	23
Chapter 5. PROBABILISTIC HAZARD ANALYSIS MODELING	
5.1 Introduction	26
5.2 Bayesian Hazard Model	26
5.3 Markow Renewal Hazard Model	30
5.4 Parameter Estimation	35
5.5 Contribution of a Single or Several Seismic Sources	39

Chapter 6.	STRONG GROUND MOTION PARAMETER ESTIMATION	
6.1	Introduction	41
6.2	Data Base	41
6.3	Variables	41
6.4	Ground Motion Model	45
6.5	Regression Analysis	46
Chapter 7.	APPLICATION OF THE MODELS	
7.1	Introduction	53
7.2	Iso-acceleration Maps	53
7.3	Site-specific Seismic Loading	54
Chapter 8.	SUMMARY AND CONCLUSIONS	
		76

REFERENCES

Appendix A	EARTHQUAKE DATA FROM 1525 TO 1710
Appendix B	EARTHQUAKE DATA FOR EL SALVADOR SORTED BY SOURCES
Appendix C	SEISMIC PROVINCES
Appendix D	EARTHQUAKE RECURRENCE RELATIONSHIPS
Appendix E	BAYESIAN PARAMETERS

CHAPTER 1

INTRODUCTION

On October 10, 1986, the capital of El Salvador, San Salvador, experienced a moderate magnitude earthquake. The surface wave magnitude of this event was 5.8. The hypocentral location was 13.67°N and 89.19°W with average depth of 10.00 kilometers. Despite the moderate magnitude of this earthquake, the city was severely damaged. Ground motion records with epicentral distances ranging from 1 to 8 kilometers showed peak ground accelerations from 0.31g to 0.72g.

The high values of ground motion and the resulting building damage caught the attention of engineers and seismologists from all over the world. A previous study done by White and Harlow (1988) shows that San Salvador is hit by earthquakes like the one described above, approximately every 30 years. Considering the high seismic activity rate of this zone and the potential danger for life and property loss, the study "Seismic Zoning and Strong Ground Motion Parameters for El Salvador" was initiated at Stanford University. The area covered by this study is bounded by the latitudes 11.00°N and 16.00°N and the longitudes 82.00°W and 91.00°W. It includes all of El Salvador and part of Guatemala, Honduras, and Nicaragua (see Figure 2.1).

For this region, similar studies have been conducted by Kiremidjian et al. (1979), Kiremidjian et al. (1977), and Shah et al. (1975). In another study, an Italian group of engineers has brought to completion a detailed study of the dynamic properties of the soils within the city of San Salvador, in an attempt to perform a seismic microzonation of the city (Conorzio Salvador e., 1988). However, the study is specialized only in the eastern part of San Salvador and the attenuation models used in this study are the ones developed for the western United States.

The evaluation of the seismic hazard in a region requires a seismicity model, an attenuation model, and an exposure evaluation model. This study will include a comprehensive evaluation of the seismic environment of El Salvador and surrounding regions, a study of the available hazard analysis models applicable to this seismic environment, and the development of peak ground acceleration attenuation functions needed for the application of the hazard models.

Briefly, the major topics to be studied are outlined as follows:

- Tectonic Setting and Seismic Provinces.
- Seismic Data Base.
- Geometrical Modeling.
- Probabilistic Hazard Analysis Modeling.
- Strong Ground Motion Parameter Estimation.
- Application of the Models.

In order to evaluate the seismic hazard of a region, it is first necessary to study and model its seismicity. In Chapter 2, the seismo-tectonic environment of El Salvador is studied as a part of a more extensive system. In this region, three different tectonic regimes are found: the Caribbean Plate Boundary which is composed of the Chixoy-Polochic, Motagua, and Jocotan-Chamelecon faults; the Volcanic Chain which is composed of a line of volcanoes that goes from Guatemala to Costa Rica; and the Central American Trench which is formed by the subduction of the Cocos Plate beneath the Caribbean Plate (see Figure 2.1).

In chapter 3, the existing data for the study region is analyzed. Two kinds of data are found: non-instrumental and instrumental. For both types of data, a methodology of how to calculate earthquake parameters is described and their relation to the seismic provinces is evaluated.

Faults and areas of earthquake activity are represented by lines and polygonal dipping planes defining the geometrical source modeling for the region. The seismicity of the region is gathered and sorted according to this geometrical source model. Seismic parameters such as earthquake recurrence relationships, maximum credible earthquake, slip rates, and energy release are calculated for each seismic province. The results from this evaluation are presented in Chapter 4.

In order to obtain hazard estimates, the Bayesian model (Mortgat and Shah, 1979) and the slip-predictable model (Kiremidjian and Suzuki, 1987) are used in this study. The Markov renewal model is applied to a segment of the Benioff Zone. The remaining sources are modeled using the Bayesian model; the results from the two models are combined to obtain hazard estimates throughout El Salvador. For comparison purposes, hazard

estimates are computed for all sources using the Bayesian model as well. A review of both hazard models and calculation of parameters are presented in Chapter 5.

In Chapter 6, strong ground motion attenuation functions are discussed extensively. Since several tectonic regimes are found in the region of study and travel paths and stress conditions from near source and far sources are likely to vary (Campbell, 1981), the attenuation functions depend on the seismic source and source-to-site conditions.

The seismicity model, the stochastic hazard models, and the attenuation functions indicated above are used to develop iso-acceleration maps for El Salvador. In addition, site specific seismic loading (peak ground acceleration) are computed at eleven important cities and places in El Salvador. The results from this analysis are presented in Chapter 7.

In summary, the final results of this study represent a set of seismic hazard maps and a set of site specific loading estimates for El Salvador. Further implementation of the result of this study in seismic code regulations for a seismic code for lateral loads, will narrow the gap of the actual engineering practices in El Salvador with the ones performed in countries with modern seismic codes.

CHAPTER 2

TECTONIC SETTING AND SEISMIC PROVINCES

2.1 Introduction.

In this chapter, a study of the tectonic and seismological setting of El Salvador and surrounding regions is undertaken. The area covered by the study is bounded by the latitudes 11.00°N and 16.00°N and the longitudes 82.00°W and 91.00°W. It includes all of El Salvador and part of Nicaragua, Honduras, and Guatemala. This area is divided in several regions and their tectonic and seismological characteristics are described.

2.2 Tectonic Setting

El Salvador is located in the western part of the Caribbean Plate which contains several tectonic regions (see Figure 2.1). Along the Pacific coast of Central America lies a very narrow chain of active volcanoes (Carr et al., 1982). Southwest of El Salvador, the Cocos Plate subducts under the Caribbean Plate forming the Middle America Trench (White and Cifuentes, 1988). To the northwest is the North American-Caribbean Plate boundary which crosses Guatemala and is principally expressed by the Chixoy-Polochic and Motagua faults. To the northeast, El Salvador is bounded by a series of en-echelon grabens which form the Honduras Depression (Kiremidjian et al., 1979).

2.2.1 Volcanic Chain

A chain of active volcanoes with evidence of holocene activity (White and Harlow, 1988) lies parallel to the Middle America Trench from Guatemala to Costa Rica. The chain lies 160 to 180 km from the trench (Carr et al., 1982), and it is formed by about 75 volcanoes which are higher at the ends of the chain. In Guatemala and Costa Rica, the volcanoes have elevations from 2700 to over 4200 meters and are spaced from 18 to 30 km. At the middle of the chain, the volcanoes are lower with elevations from 512 to 2182 meters and are spaced from 12 to 18 km apart (White and Harlow, 1988).

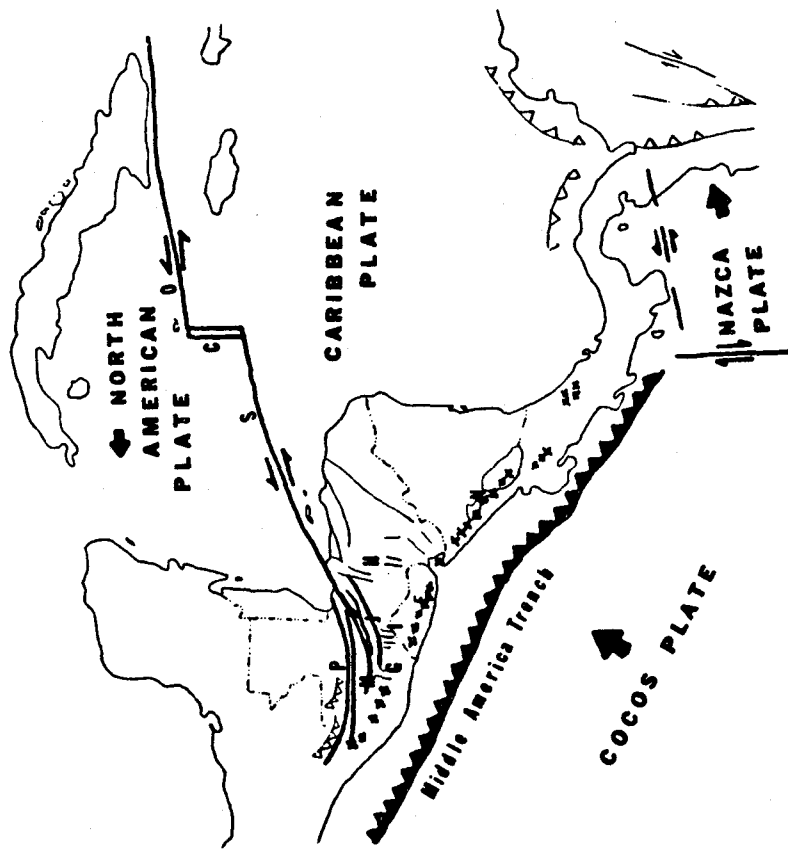


Figure 2.1. Major structures and boundaries of the western Caribbean Plate. P - Chixoy-Polochic Fault Zone, M - Motagua Fault Zone, J - Jocotan-Chamelecon Fault Zone, G - Guatemala City Graben, I - Ipala Graben, H - Honduras Depression, E - Fosa Central de El Salvador, N - Nicaraguan Depression, S - Swan Fracture Zone, C - Mid-Cayman Rise, O - Oriente Fracture Zone, x - Active Quaternary Volcanoes. (Modified from Jordan, 1975.)

Faults between the volcanoes that trend normal and parallel to the axis of the chain are associated with left-lateral and right-lateral displacements respectively. Fault displacements for both the 1986 San Salvador and 1972 Managua earthquakes were left-lateral on faults perpendicular to the trend of the chain. The intensity contours and the foreshock distribution of the 1965 San Salvador earthquake indicate a right-lateral fault motion along a fault parallel to the chain (Harlow et al., 1988).

2.2.2 Middle America Trench

At the Middle America trench, the Cocos Plate, which is composed of a gently sloping seafloor (20 to 40 m.y.) of smooth topography (White and Cifuentes, 1988), subducts under the Caribbean Plate at moderate angles and defines the Benioff Zone. The Benioff Zone appears to be formed by two parts. The shallower part is inclined at about 15° to 25° and the deeper part is inclined at approximately 40° to 55°. This interpretation of the subduction zone is suggested from the hypocentral cross sections (see Figure 2.2) of the Middle America Trench given in Burbach et al.(1984).

The convergence rate and average coseismic slip rate for the Cocos and Caribbean Plate boundary have been estimated to be about 6.5 cm/yr and 5.0 ± 1.6 cm/yr respectively in a region off western El Salvador (White and Cifuentes, 1988).

2.2.3 The Chixoy-Polochic and Motagua Faults

The North American and Caribbean Plate boundary through Guatemala is comprised principally by two parallel, left-lateral, strike-slip faults; the Chixoy-Polochic and Motagua faults (see Figure 2.3). However, for the purposes of this study, another subparallel fault will be considered as part of this boundary, the Jocotan-Chamelecon fault. The Chixoy-Polochic fault can be mapped for about 340 km across Guatemala and southern Mexico (Schwartz et al.,1979). The Motagua fault is traceable for over 300 km from the Atlantic coast to central Guatemala, where it is concealed by quaternary volcanic deposits (Anderson et al., 1973; Dengo and Bohnenberger, 1969; Schwartz et al., 1979).

The nature and amount of displacement along this boundary has been a subject of controversy (Kiremidjian et al., 1979). However, focal plane solutions for events occurring at this boundary and an average offset of 1.1 meters observed in the 1976 Motagua earthquake, show undoubtedly a left-lateral sense of movement (Molnar and Sykes,1969; Bucknam et al., 1978).

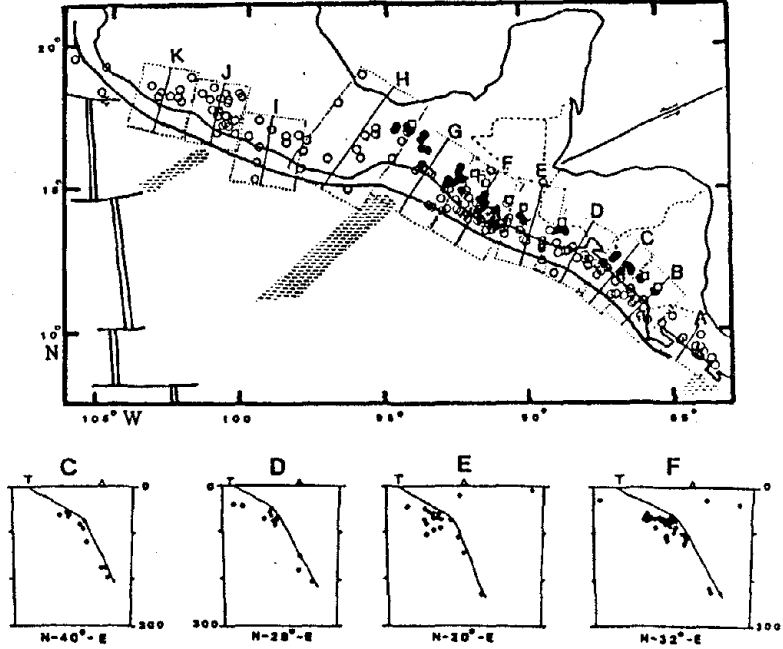


Figure 2.2. Cross sections of the Subduction Zone at some points in the Middle America Trench (After Burbach et al., 1984.)

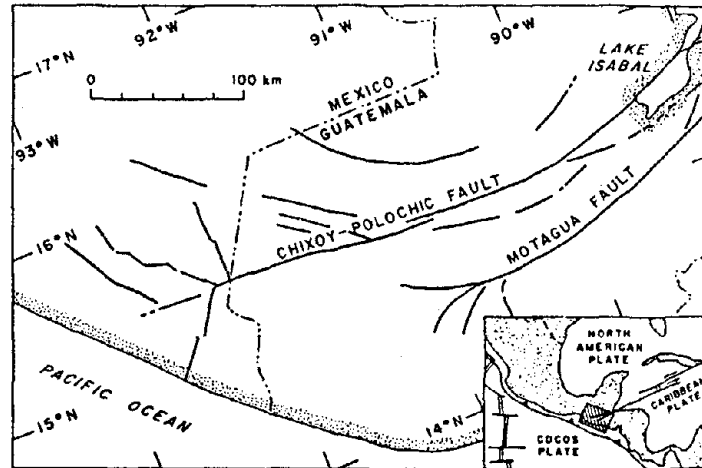


Figure 2.3. Location map of majors faults in central Guatemala and southern Chiapas (modified from Muehlberger and Ritchie, 1975). Inset shows the location of this map and the plate tectonic setting of the region (After R. White, 1984.)

2.2.4 Honduras Depression

Some faults in Central America are oriented north-south and they either compose transverse boundaries between longitudinal faults or compose graben structures in the Caribbean plate. The largest graben is the Honduras Depression which is a group of disconnected grabens or basins that extend from the Caribbean to the Pacific (see Figure 2.4).

The focal plane solution of an earthquake in this region indicates oblique slip with a component of thrust faulting (Dean and Drake, 1978). However, uncertainty about the nature of the displacements of this faults is still present.

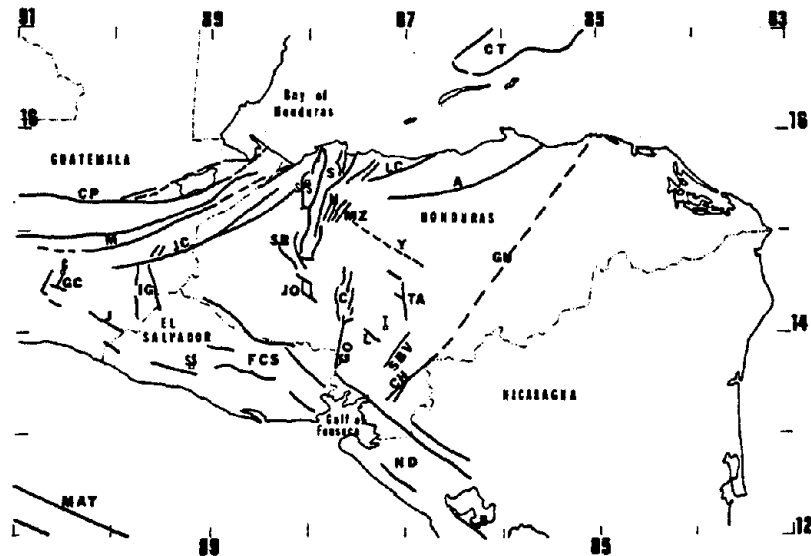


Figure 2.4. Major faults of the Honduras Region. (Honduras Depression faults from Muehlberger, 1976; figure modified from Motor Columbus, 1978.)
CT - Cayman Trough, CP - Chixoy-Polochic fault zone, M - Motagua fault zone, JC - Jocotan-Chamelecon fault zone, GC - Guatemala City graben, IG - Ipala Graben, J - Jalpataga fault, FCS - Fosa central de El Salvador, ND - Nicaraguan Depression, S - Sula graben, N - El Negrito graben, MZ - Morazan graben, SB - Santa Barbara graben, Y - Yoro graben, JO - Jesus de Otoro graben, C - Comayagua graben, GO - Goascoran fault, TA - Talanga fault, SBV - San Buenaventura fault, CH - Choluteca fault, GU - Guayape fault, LC - La Ceiba Fault, A - Aguan fault, L - Laparetique fault, G - Guatemala City, SS - San Salvador, T - Tegucigalpa, M - Managua, SPS - San Pedro Sula.
(After Kiremidjian et al., 1979.)

2.3 Seismic Provinces

In order to model the seismicity of El Salvador and surrounding areas, the region is divided into seismic provinces. The division is done based on the geologic and seismic features of the provinces themselves. Consequently, a seismic province in this study is defined as a very well identified fault or zone which spatially comprise earthquakes with similar seismic parameters such as focal plane solution, magnitude, epicenter, and focal depth.

Therefore, following the definition presented above and similar to the classification given by others (Carr and Stoiber, 1976; Kiremidjian et al., 1979) the following seismic provinces were identified (see Figure 2.5):

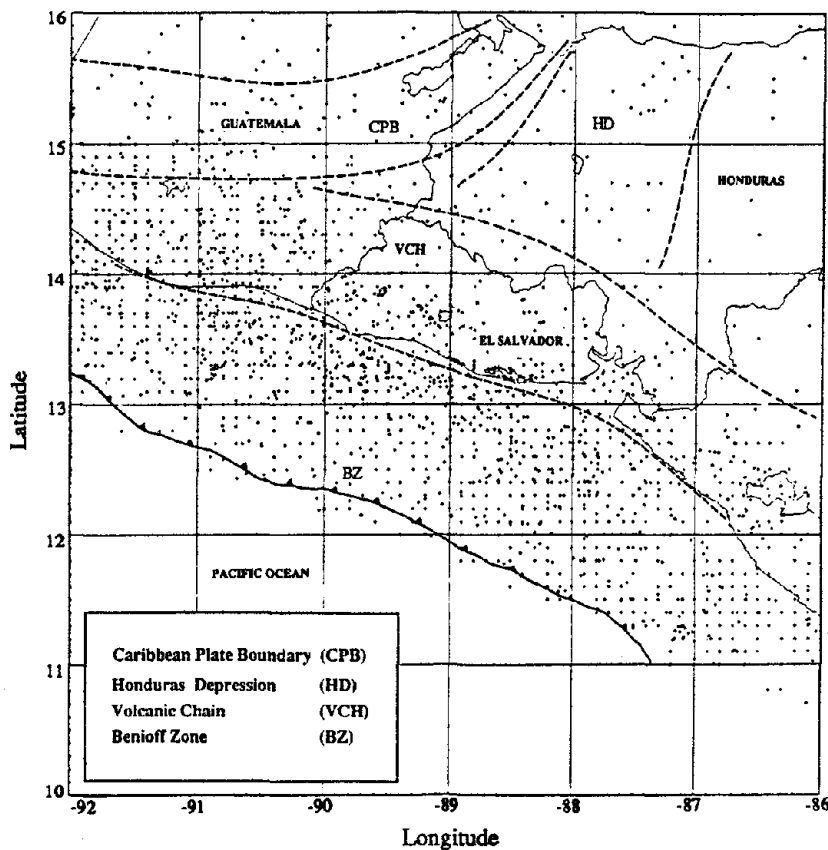


Figure 2.5. Tectonic provinces and epicenter locations of the Central American region.

- | | |
|-----------------------------|--------|
| 1) Volcanic Chain Zone | (VCH) |
| 2) Benioff Zone | (BZ) |
| • Shallow Benioff Zone | (SHBZ) |
| • Intermediate Benioff Zone | (IBZ) |
| • Deep Benioff Zone | (DBZ) |
| 3) Caribbean Plate Boundary | (CPB) |
| 4) Honduras Depression | (HD) |

2.3.1 Volcanic Chain Zone

The Volcanic Chain Zone is identified as a narrow band along the pacific coast of Central America which groups regions of similar tectonic and seismic patterns. Focal mechanisms of events within this band show strike slip displacements with one plane parallel to the volcano axis (White and Harlow, 1988). Fault motions of left-lateral sense have occurred in faults perpendicular to the trend of the chain and right-lateral slip has probably occurred along faults parallel to the chain.

In addition, events in this band exhibit very similar seismic parameters. For instance, epicentral locations fall within a very narrow band, focal depths of very well constrained events are within 5 and 15 km (White and Harlow, 1988), and maximum magnitudes of earthquakes range from M_S of 5.4 to 6.8. Consequently, the Volcanic Chain Zone is defined in this study as a narrow band along the pacific coast of Central America. The depth of the crust of the earth is believed to be 20 km; however, in the estimation of the earthquake magnitude and epicentral location the value of 35 km is often used. Thus it was decided to define the maximum depth of this source at 35 km for consistency with the data.

2.3.2 Benioff Zone

The Benioff Zone, described before as the subducting part of the Cocos plate under the Guatemalan, El Salvadoran, and Nicaraguan coasts is characterized by several geologic and seismic features. As suggested in Burbach et al. (1984), the underthrusting plate is formed by two parts separated at an average depth of 60 km. The magnitude of earthquakes in the shallower plate increases as we go deeper on the plate; from a catalog by White and Cifuentes (1988), the maximum magnitude, M_S , is found to be 7.1 at a range of hypocentral depths from 0 to 35 km. The magnitudes range up to M_S of 8.1 for a range of hypocentral depths from 40 to 60 km.

Taking into account these features of the zone, three segments are identified: a Shallow Benioff Zone (0-35 km), an Intermediate Benioff Zone (36-60 km), and a Deep Benioff Zone (61-260 km).

2.3.3 Caribbean Plate Boundary

The Caribbean Plate Boundary is formed by the Chixoy-Polochic, Motagua, and Jocotan-Chamelecon faults. The zone is characterized by left-lateral, strike-slip faults which are clearly mapped. The seismic activity is shallow (<35 km for this study) and the two main faults have already ruptured at least once. In 1785 an earthquake M_w of 7.3 to 7.5 ruptured the eastern portion of the Chixoy-Polochic fault and in 1816 another earthquake M_w of 7.5 to 7.7 ruptured its western portion. In 1976 an earthquake of M_w 7.5 ruptured the Motagua fault (White, 1988). The depth of this source zone will be considered to be between 5 to 15 km.

2.3.4 Honduras Depression Zone

The Honduras Depression zone is located at the central part of Honduras and has the following characteristics. The zone groups all the faults of central Honduras which form part of a sequence of en-echelon grabens. Its seismicity is very low with magnitudes ranging from M_s of 3.0 to 6.3, and is shallow in origin.

In conclusion, El Salvador is surrounded by the following tectonic regions: the Volcanic Chain, Benioff Zone, Caribbean Plate Boundary, and Honduras Depression. The Volcanic Chain is defined according to the kind of faulting around the axis of the chain and some features of earthquake parameters such as magnitude, focal depth and epicentral location. The Benioff Zone is defined according to the magnitude of events and hypocentral depth in the 3 sub-zones described before. The Caribbean Plate Boundary is defined on the delineation and seismic activity of each fault between the zone. And finally, the Honduras Depression Zone is defined by the location of the group of faults in the grabens.

CHAPTER 3

SEISMIC DATA BASE

3.1 Introduction.

Instrumental records for earthquakes in Central America became available in 1900 (Harlow et al., 1988). Catalogs with instrumental records, however, almost never include more than one cycle of large earthquakes for specific seismic sources. Since the instrumental data are insufficient to estimate the recurrence of large earthquakes, it is important to consider non-instrumental data as well.

Before 1900, intensity scales which describe physical damage at sites were the only records available to measure the severity of an earthquake (e.g. Rossi-Forel and Milne scales). Thus, this study distinguishes between historical seismicity which defines descriptive seismicity before 1900; and post-1900 seismicity, which includes both instrumental and descriptive data obtained after 1900.

3.2 Historical Seismicity.

General studies have been conducted on historical seismicity for the Central American region. White (1984), White and Cifuentes (1988), White (1988), White and Harlow (1988), and Harlow et al. (1988) have searched for primary sources on historical seismicity. They found information on Subduction, Shallow Focus and Plate Boundary earthquakes from more than 1000 historical documents. This information made it possible to construct intensity maps for at least the two highest intensity contours. Thus, approximated magnitudes and moment centroid locations became available.

For this period a total of 111 earthquakes were found. Only a brief description of the damage was available for the oldest forty events (see Appendix A). Since the remaining events were better documented, approximated magnitudes, moment centroid locations, and rupture lengths were determined (see Appendix B.) The methodology followed in these calculations is explained below.

For earthquakes for which at least two of the highest contours of the Modified Mercalli Intensity could be constructed, all of the seismic parameters mentioned before were determined. Following Aki (1966) and Kelleher et al. (1973), it is assumed that the rupture area corresponds to the aftershock area of an earthquake. Based on White and

Harlow (1988), the aftershock area and the area of damage covered by the intensity contour of MMI VII gives for the subduction zone the following relationship:

$$L_{VII} = 200 (M - 6.77) \quad (3.1)$$

where L_{VII} is the diameter of the MMI VII isoseismal line which is assumed to be the diameter of the rupture area, and M is the magnitude. Similarly, for upper crustal earthquakes the following equation was developed,

$$L_{VII} = 200 (M - 6.37) \quad (3.2)$$

which gives the minimum diameter of the damage area of MM intensity VII for a given earthquake.

Discrimination of damaging events that have occurred on the Benioff zone from those that have occurred in a upper-crustal seismic province is difficult since the MMI contour lines of an earthquake from either seismic province can lie along the Volcanic Chain. White and Cifuentes (1988) characterize a damaging Benioff Zone earthquake by A_{VII} (Area of MMI VII) $> 10,000 \text{ km}^2$, and slow attenuation of intensity with distance. On the other hand, a damaging upper-crustal earthquake has $A_{VII} < 600 \text{ km}^2$ and fast attenuation of intensity with distance.

Following this criteria, White and Harlow (1988) determined epicentral and hypocentral locations. For upper-crustal events (see Figure 3.1), the epicenters were set at the location of the center of the highest intensity contour and the hypocenter was constrained to the crust (see Chapter 2). For Benioff Zone earthquakes, this scheme was not applicable. The hypocenters were set according to the location of the sliding interface between the Cocos and Caribbean Plates then the hypocenters were constrained between 40 to 60 km of depth. The epicenters were located moving normally to the trench the location of the moment centroid showed along the Volcanic Chain (see Figure 3.2) to the point where the hypocenters were between 40 to 60 km. Deeper or shallower regions were not considered since earthquakes occurring at these locations will not produce MMI VII areas as shown in Figure 3.2.

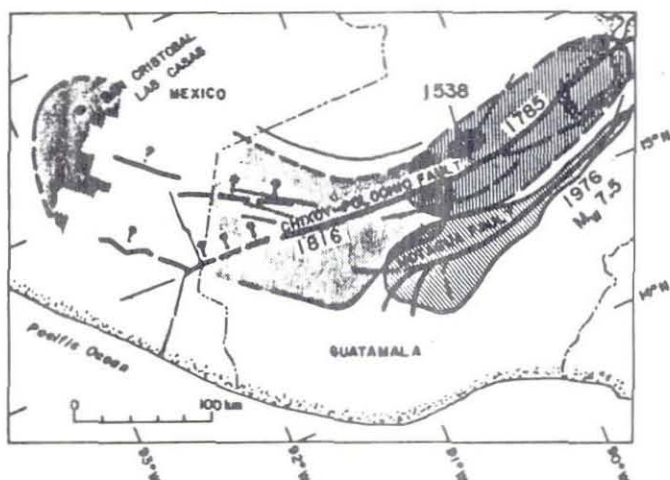


Figure 3.1. MMI contour lines for main earthquakes that occurred in the Caribbean Plate Boundary Zone (After White, 1988.)

Following this procedure, a segment belonging to the Intermediate Benioff Zone was defined (see Figure 3.3). Further analysis of energy release, rupture length, and recurrence time for this segment is presented in Chapter 4.



Figure 3.2. MMI contour lines for earthquakes that occurred in the Subduction Zone since 1690 (After White and Cifuentes, 1988.)

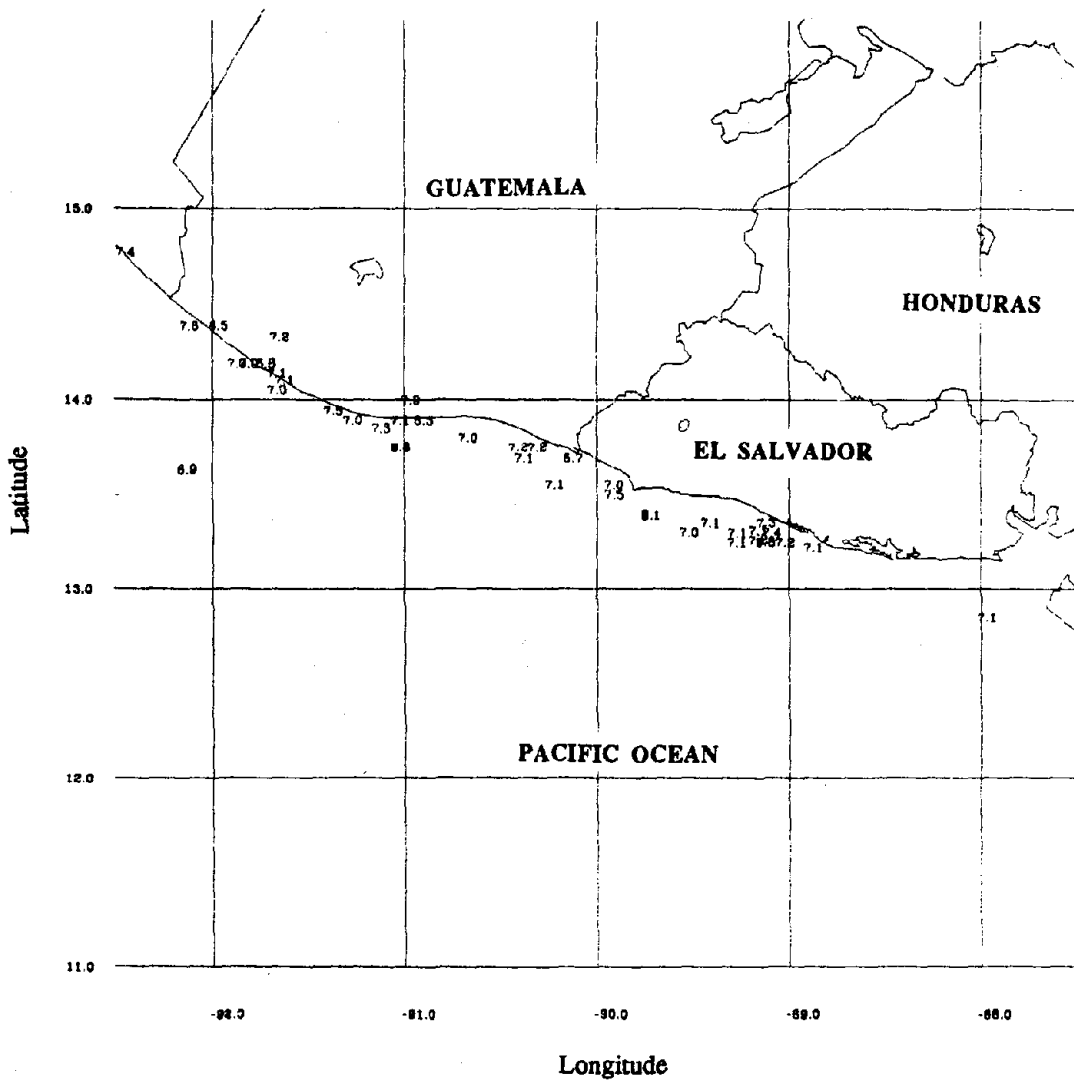


Figure 3.3. Seismic events that occurred in the Intermediate Benioff Zone (between 40 and 60 km depth) for $M_s \geq 7.0$.

3.3 Post - 1900 Seismicity

For the post - 1900 period, a search in several catalogs was conducted to collect both descriptive and instrumentally recorded seismicity. The descriptive seismicity catalogs provided a total of 42 events (see Figures 3.2 and 3.4) from a total of 3501 events for this period. The remaining recorded events were obtained from the International Seismological Center (ISC), the Coast and Geodetic Survey (CGS), Preliminary Determination of Earthquakes (PDE), the catalog of R. Geller (GELL), the catalog of L. Sykes (SYKES), and the Bulletin of the Seismological Society of America (BSSA).

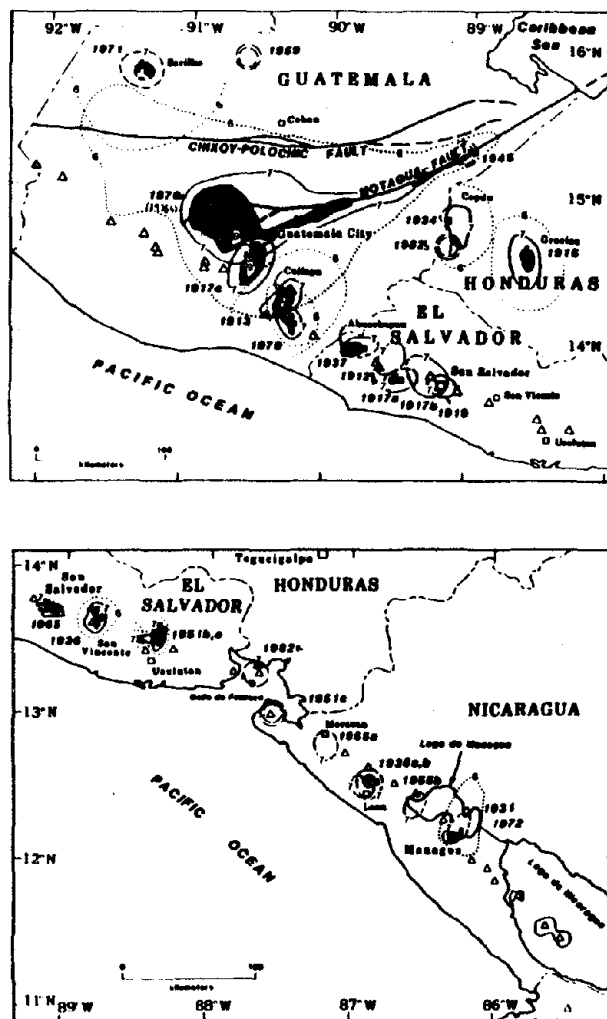


Figure 3.4. MMI contour lines for upper-crustal earthquakes of $M_s \geq 5.5$ since 1900 (After White and Harlow, 1988.)

The catalog for this period of time contains in most cases the following information: reference, date, time (Greenwich Meridian Time), epicenter location (in degrees, longitude and latitude), hypocentral depth (in km), body wave magnitude, and local magnitude.

The estimation of seismic parameters was done depending on the seismicity analyzed. Descriptive seismicity was treated according to the procedures described in Section 3.1. For instrumental seismicity, depths were assigned based on schemes for each seismic province presented in Chapter 2.

For many events, only the body wave magnitude was given. To convert this magnitude to local magnitude the following linear relationships was used:

$$M = a + mb \quad (3.3)$$

where a and b are regressive constants with the value of -3.47 and 1.61 respectively (Shah et al., 1975).

Appendix B contains a listing of all the data described in this section.

3.4 Sorting of data.

For hazard analyses purposes, the gathered seismicity needs to be sorted in seismic provinces. In this study, earthquakes were assigned following the definitions of the seismic provinces as described in chapter 2. The sorted seismicity for each seismic province is shown in table 3.1 and their epicenters and corresponding magnitudes are plotted in Figures C.1 to C.9 (see Appendix C.)

Epicenters in the Volcanic Chain province comprise a band of variable width (see Figure C.2). Some of the earthquakes farthest inland may not qualify as volcanic origin events because of their inland location. However, they are of low magnitude, thus their inclusion will not affect subsequent analyses. It is important to note that the largest magnitudes in this source have occurred in places where the distance between volcanoes is the longest. White and Harlow (1988) developed an equation to estimate maximum possible magnitude M_S using the distance between adjacent volcanoes,

$$M_S < 0.82 \log (D) + 5.1 \quad (3.4)$$

where D is the distance between adjacent volcanoes in kilometers.

Earthquake epicenters for the Shallow, Intermediate and Deep Benioff Zones are shown in Figures C.3 to C.5. Shallow and Intermediate events are spread mostly offshore

Central America. At deeper focal depths (>60 km) the earthquake epicenter band moves to the northeast as is expected. The major events of this seismic province ($M_S \geq 7.0$) are located in the Intermediate Zone in a section of about 280 km long which extends from Central Guatemala to Central El Salvador.

The Caribbean Plate Boundary is formed by the Chixoy-Polochic, Motagua and Jocatan-Chamelcon faults. Earthquake epicenters corresponding to these faults are plotted in Figures C.6 to C.8. One of the largest events of this seismic province is the $M_W=7.5$ on the Motagua fault. A similar magnitude event, $M_W=7.6$, occurred on the Chixoy-Polochic fault in 1816.

The Honduras Depression Zone has the lowest rate of seismicity of all seismic sources in the study area. Its catalog is formed by 32 earthquakes with magnitudes between 3.0 to 6.3.

Seismic Province		Number of events of $M \geq 3.0$
Volcanic Chain		416
	Shallow	1163
Benioff Zone	Intermediate	448
	Deep	1418
Caribbean Plate Boundary		95
Honduras Depression		32

Table 3.1. Number of earthquakes assigned to each seismic province.

Earthquake epicenters of this province are plotted in Figure C.9. As it can be seen, most of the earthquakes have occurred in the eastern boundary of the province. The most active fault seems to be located to the northeast of the Aguan Fault. To the southeast, the

Santa Barbara, Jesus de Otoro, and Comayagua appear to be the most active grabens of the zone. It is interesting to note that the biggest magnitude earthquake ($M_S=6.3$) occurred in a place where no faults have been mapped.

3.5 Quality of Data

The data in the catalog of appendix B are extremely variable in quality. Inhomogeneities, as well as uncertainties associated with epicentral locations and magnitudes, are inherent to the data. Missing lower magnitude data is one of the most frequent problems with data catalogs. With increased instrumentation, considerably more events with $M < 5.0$ have been recorded. The coverage of small magnitude earthquakes increased dramatically since 1962 when the World Standardized Seismographic Network (WWSN) was installed (Molnar and Sykes, 1969). This increase in earthquake recording in recent years has resulted in an apparent increase of earthquake occurrence with time. This problem is not seen for the highest magnitudes since large events are felt over greater areas and are thus more likely of being recorded. The catalog shown in appendix B is probably complete for $M \geq 7.0$ since 1711, $M \geq 7.0$ since 1920, $M \geq 6.0$ since 1940, and $M \geq 4.8$ since 1962.

Uncertainties in the data are also associated with the assignment of magnitudes and epicentral locations. The data from catalogs of descriptive seismicity may have errors of $\pm 1/4$ of a magnitude; the moment centroids can have errors of location of 10 to 25 km. For the data for which instrumental records exist, the values of magnitudes also can have errors as much as $\pm 1/4$ units of magnitude. Errors in epicentral location depend on the seismic source where the earthquake originated. For subduction earthquakes, epicenters can have error in location of ± 50 km for the period from 1900 to 1963 and error of ± 25 to ± 30 km for post-1963 records. For an upper-crustal seismic source, the error in epicentral location can be as much as ± 25 km for any period.

In summary, the existing data was treated according to the seismicity in consideration. The data were sorted according to the seismicity patterns of each seismic source. These data are used in the following chapter to develop earthquake recurrence relationships for each source.

CHAPTER 4

SEISMIC SOURCE MODELING

4.1 Introduction.

For hazard analysis purposes, a geometrical source model for the study region is defined. Faults and areas of earthquake activity are represented by lines and polygonal dipping planes. In addition, seismic parameters such as earthquake recurrence relationships and maximum credible earthquake are calculated for each seismic source.

4.2 Geometrical Modeling.

The model proposed for seismic hazard analysis purposes consists of a combination of fault zones and line sources. For seismic sources where a well defined fault trace was identified, the line source model was adopted. Seismic provinces where earthquakes cannot be assigned to a specific fault but fall within an active region are modeled as generalized fault zones.

4.2.1 Volcanic Chain Zone.

The limits of this zone are those for the seismic province defined in Chapter 3. A band of about 30 km wide that follows the axis of the chain of volcanoes is defined for this zone. A sectioned model for this band is considered to represent best the seismicity of the region. Three segments are defined (see Figure 4.1): the Guatemalan Segment (GS), which extends from the Mexico-Guatemala border to the Guatemala-El Salvador boundary; the Central El Salvador Segment (CESS) that extends from the eastern boundary of the previous segment to central El Salvador; and the Eastern El Salvador-Nicaragua Segment (EESS), which is situated from central El Salvador to central Nicaragua.

For hazard analysis purposes independent computations were performed for each segment. The focal depths for each of these subzones were considered to be 10 km.

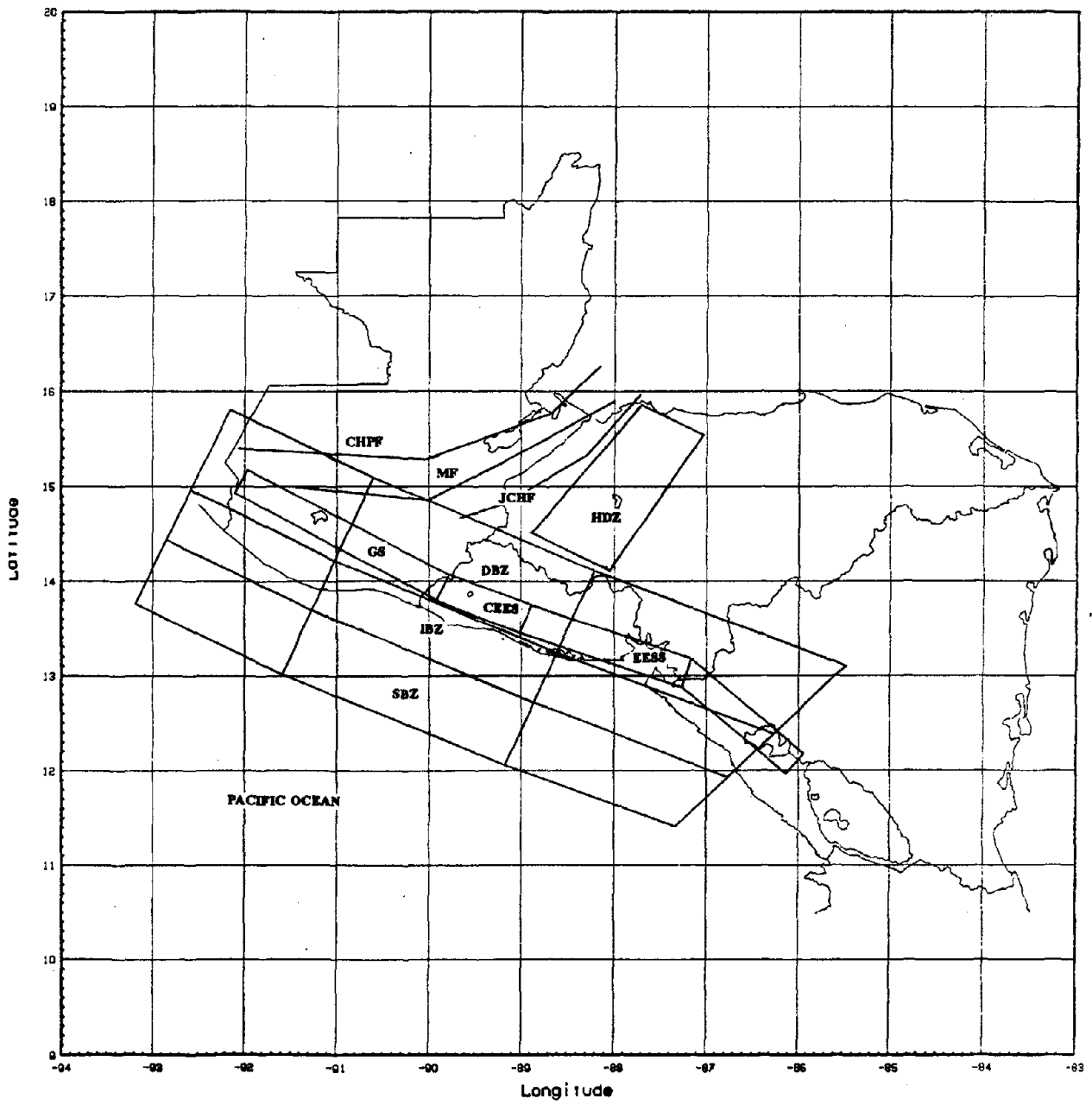


Figure 4.1. Seismic zone and fault line model.

4.2.2 Benioff Zone.

The boundaries of the Benioff Zone are the same defined for the seismic source in Chapter 3. Within this zone three subzones that vary with depth are identified: the Shallow (SBZ), Intermediate (IBZ), and Deep Benioff (DBZ) Zones. In addition each of these subzones is divided into three sections based on the segmentation of the Benioff Zone as discussed in Chapter 3. For the nine segments of this zone (see Figure 4.1), independent hazard calculations were computed. The focal depths are considered as follows: for Shallow Benioff Zone depths go from 0 to 35 km, for the Intermediate Benioff Zone depths go from 36 to 60 km, and for the Deep Benioff Zone depths go from 60 to 260 km.

4.2.3 Caribbean Plate Boundary.

Line source models were adopted for this seismic source and were located approximately along the geologic fault traces. The faults are the Chixoy-Polochic (CHPF), Motagua (MF), and Jocotan-Chamelecon (JCHF) faults and were sectioned in three segments, roughly according to historical ruptures of the faults themselves (see Figure 4.1). Independent computations were performed for each line model. Their focal depths were set at 7 km.

4.2.4 Honduras Depression Zone.

The boundaries of this zone (HDZ) correspond to the seismic province discussed in Chapter 3. The focal depth considered for this zone model is 8 km.

4.3 Frequency of Earthquake Occurrences.

For the purposes of hazard analysis, a statistical relationship between the frequency of earthquake occurrences and range of magnitudes is developed for each seismic province.

Some problems arise when searching for the statistical relationship that best represents earthquake occurrences in a region. The problem arises when more than one source of information is available. As discussed in Chapter 3, the information available for the study region is originated from two sources, historical and instrumental catalogs which also have different quality and completeness levels.

Several methods were considered in the development of earthquake recurrence relationships. These include the least squares method, the maximum likelihood method, and the maximum entropy method. After a detailed investigation it was determined that the

least squares method gives the best results and it was adopted for the recurrence calculations of all sources (for further discussion see Appendix D). Recurrence relationships are obtained by fitting a regression line through all earthquake data with $M \geq 3.0$ (M is defined as M_L for $M \leq 6.0$ and M_S otherwise). In general, the number of earthquakes, $N(M)$, that occur above a given magnitude M is given by the following relationship:

$$\ln N(M) = \alpha + \beta M \quad (4.1)$$

where

$N(M)$	=	Number of events above magnitude M
M	=	Magnitude
α and β	=	Regression constants

α is a measure of the number of events above magnitude zero for a given source and β is the measure of the seismic severity for a given source.

For some of the sources, a single regression line fitted through the data resulted in a recurrence relation which overestimates the number of occurrences at large magnitudes. Due to the lack of completeness of earthquake occurrences in the low magnitude range over time, the regression line shifts down at the low magnitudes decreasing the slope of the line. Following Kiremidjian et al. (1979) and Shah et al. (1975), a bilinear recurrence relationship was used to fit the data where differences in slope were observed between small and large magnitude frequency of occurrence (see Figures D.1-D.16 in Appendix D). Earthquake recurrence parameters based on the maximum likelihood method were also obtained to take in account the missing data in various time and magnitude intervals (Weichert, 1980); however, the results were found inadequate primarily due to the large differences of observation time for the different magnitude intervals (see Appendix D). Consequently, this approach was abandoned.

Table 4.1 shows values of α and β , the break point magnitude (BPM), and the upper cutoff magnitude (CM). The parameters α and β are values obtained from the regression analysis. The break point magnitude is the magnitude where the slope of the recurrence lines change. The maximum cutoff magnitude is a value determined based on fault length, rupture area (equations 3.1 or 3.2), distance between adjacent volcanoes (equation 3.4) or maximum magnitude known for the seismic source.

Seismic Sources	Regression constants, break point magnitude (BPM), and upper cutoff magnitude (CM)					
	α_1	β_1	α_2	β_2	BPM	CM
• Volcanic Chain						
Guatemala Segment	7.765	-1.081	-	-	-	6.8
Central El Salvador Segment	4.544	-0.310	17.745	-2.633	5.68	6.5
Eastern El Salvador Segment	5.526	-0.296	14.435	-1.958	5.35	6.6
• Benioff Zone						
Shallow Benioff Zone						
Segment 1	9.343	-1.410	-	-	-	7.7
Segment 2	8.479	-1.079	-	-	-	8.1
Segment 3	9.406	-1.192	-	-	-	7.9
Intermediate Benioff Zone						
Segment 1	5.760	-0.525	16.134	-2.028	6.90	7.8
Segment 2	5.639	-0.363	23.369	-2.901	6.99	8.2
Segment 3	8.856	-1.306	-	-	-	7.8
Deep Benioff Zone						
Segment 1	10.226	-1.364	-	-	-	7.9
Segment 2	10.604	-1.312	-	-	-	8.2
Segment 3	7.108	-0.505	11.555	-1.499	4.47	8.2
• Caribbean Plate Boundary						
Chixoy-Polochic Fault	4.428	-0.384	11.193	-1.403	6.64	7.8
Motagua Fault	4.513	-0.342	6.929	-0.898	4.35	7.7
Jocotan-Chamelecon Fault	4.371	-0.575	-	-	-	7.4
• Honduras Depression Zone	3.367	-0.143	7.529	-1.225	3.85	6.2

Table 4.1. Regression constants for the seismic sources as defined by equation 4.1.

CHAPTER 5

PROBABILISTIC HAZARD ANALYSIS MODELING

5.1 Introduction.

This chapter reviews the two stochastic seismic hazard models used in the development of the seismic hazard maps for El Salvador. These include the Bayesian model (Mortgat and Shah, 1979) and the slip-predictable model (Kiremidjian and Anagnos, 1984) which are discussed briefly.

The purpose of seismic hazard analysis is to predict earthquake occurrences in a form of an expected number of events or probability of exceedence of a given earthquake magnitude for a period of time t (Anagnos and Kiremidjian, 1988). For engineering purposes, the hazard estimates are often expressed in terms of probabilities of exceeding various ground motion levels in future time t . In order to obtain these hazard estimates, the Bayesian model, which is based on homogeneous Poisson assumption with fault rupture model and Bayesian parameters, and the Markov renewal model are used in this study. The main difference between these models is the assumed underlying earthquake generating mechanism.

5.2 Bayesian Hazard Model.

A variety of stochastic occurrence models for earthquakes based on the Poisson process have been developed (see Anagnos and Kiremidjian, 1988). The Poisson process assumes independence of earthquake sequences in time and space. However, the model to be used for hazard mapping purposes, the Bayesian model, has the advantage over the simple homogeneous Poisson models in that it includes subjective information for earthquake occurrences.

It is well known that the use of incomplete historical data to determine the future seismic activity of a region can result in erroneous conclusions. In such cases, as is the case of the seismic data for El Salvador, consideration of geological and seismological information can improve considerably the reliability of the predictions of the seismicity of the region.

5.2.1 Model Formulation.

The Bayesian model considers the parameters of the distributions as random variables. This defines a compound distribution (Benjamin and Cornell, 1970) which is a distribution of a random variable with parameters that are also random variables. The marginal distribution of the random variable independent of the parameters can be written as,

$$f_X(x) = \int f_X(x|\tilde{\theta})f_{\Theta}''(\tilde{\theta})d\tilde{\theta} \quad (5.1)$$

where

$$\begin{aligned} \tilde{\theta} &= \text{a vector of parameters defined on } \Theta. \\ f_X(x) &= \text{the Bayesian distribution on } X. \\ f_X(x|\tilde{\theta}) &= \text{the model distribution on } X \text{ given the parameters } \tilde{\theta}. \\ f_{\Theta}''(\tilde{\theta}) &= \text{the posterior distribution of } \tilde{\theta}. \end{aligned}$$

the posterior distribution on the parameters $\tilde{\theta}$ is given as follows:

$$f_{\Theta}''(\tilde{\theta}) = N_1 L(\tilde{\theta})f_{\Theta}'(\tilde{\theta}) \quad (5.2)$$

where

$$\begin{aligned} f_{\Theta}'(\tilde{\theta}) &= \text{the prior distribution on } \tilde{\theta}. \\ L(\tilde{\theta}) &= \text{the likelihood function on } \tilde{\theta}. \\ N_1 &= \text{a normalizing constant.} \end{aligned}$$

Following this scheme and using the concept of conjugate distributions, Mortgat and Shah (1979) developed expressions for the marginal distribution on the number of occurrences (n) and a distribution on the number of earthquakes of fixed magnitude (M_i) given that n earthquakes have occurred. In their model, earthquake occurrences are assumed to form a Poisson process with mean rate of occurrence λ . The parameter λ is treated as a random variable and Bayesian statistics are applied to include subjective knowledge on historical data. The subjective probability distribution on λ (prior distribution) is chosen to be gamma with parameters λ' and ν' . Using recorded data on earthquake occurrences,

the sample likelihood function on λ can be obtained. The posterior distribution on λ is determined by combining the prior distribution and the sample likelihood function on λ and applying Bayes' theorem given by Equation 5.2. Convolving the conditional Poisson process for the number of earthquake occurrences with the posterior distribution on λ , the marginal Bayesian distribution of the number of occurrences n is derived (for detailed information see Mortgat and Shah, 1979).

The generating process for the number r_{M_i} of events of any specific M_i given that a total of n events have occurred is assumed to be binomial, with probability of success P_{M_i} . The parameter P_{M_i} is treated as a random variable. The conjugate prior distribution on P_{M_i} is assumed to be beta with parameters η_{M_i} and ϵ_{M_i} which can be obtained from subjective information. For this study, the fitted lines for earthquake recurrences determined in Chapter 4 constitute this subjective input. For each source, the relationship that describes the recurrence of the various M_i magnitudes is given as follows:

$$\ln N(M) = \alpha + \beta M \quad (4.1)$$

(repeated)

where

- $N(M)$ = number of events above magnitude M
- M = magnitude
- α and β = regression constants.

The parameter η_{M_i} represents the subjective information about the number of events that occurred in a seismic source above a given lower bound, and ϵ_{M_i} represents an equivalent number of events of magnitude M_i .

Using occurrence data, the sample likelihood function on P_{M_i} can be obtained from the generating binomial process. Thus, having determined the parameters of the prior distribution and the sample likelihood function, the posterior parameters η_{M_i}'' and ϵ_{M_i}'' , which completely defines the posterior probability distribution on P_{M_i} of magnitude M_i , can be determined using the concept of conjugate distribution. Finally, the conditional generating process of r_{M_i} and the posterior distribution on P_{M_i} , are convolved to obtain the marginal distribution on the number of success M_i 's.

Marginal Distribution on the Number of Magnitudes. Combining the Bayesian distributions discussed above, a distribution that describes the seismicity of the source considered is obtained in terms of two parameters, the magnitude (M_i) and the number of occurrences (n). This distribution is written as follows, (Mortgat and Shah, 1979):

$$P_R(r_{M_i}) = \sum_{n=0}^{\infty} \left[C_n^{r_{M_i}} \frac{\Gamma(\eta''_{M_i})}{\Gamma(\varepsilon''_{M_i}) \Gamma(\eta''_{M_i} - \varepsilon''_{M_i})} \cdot \frac{\Gamma(r_{M_i} + \varepsilon''_{M_i}) \Gamma(n + \eta''_{M_i} - r_{M_i} - \varepsilon''_{M_i})}{\Gamma(n + \eta''_{M_i})} \right] \left[\frac{\Gamma(n + v'') t^n \lambda''^{v''}}{n! \Gamma(v'') (t + \lambda'')^{n + v''}} \right] \quad (5.3)$$

where

- $P_R(r_{M_i})$ = probability that there are r_{M_i} events of magnitude M_i .
- $\lambda'' = \lambda' + T$ = parameter of the posterior distribution on λ .
- $v'' = v' + N$ = parameter of the posterior distribution on λ .
- $\varepsilon''_{M_i} = \varepsilon_{M_i} + R_{M_i}$ = parameter of the posterior distribution on P_{M_i} .
- $\eta''_{M_i} = \eta_{M_i} + N$ = parameter of the posterior distribution on P_{M_i} .
- $C_n^{r_{M_i}} = \frac{n!}{r_{M_i}! (n - r_{M_i})!}$ = the binomial coefficient.
- r_{M_i} = integer describing the number of events with magnitude M_i ($0 \leq r_{M_i} \leq n$).

Using this equation, the computation of hazard estimates in terms of the ground motion parameter (peak ground acceleration, PGA) is provided. The distributions that describe the seismicity of all sources (equation 5.3) are combined with the distributions on the attenuation of peak ground acceleration (see Chapter 6). The contribution of all sources is superimposed to obtain the probability of exceeding of peak ground acceleration. This procedure is used to obtain risk consistent design parameters which when applied to the study region, seismic hazard maps can be obtained and further related to seismic zones for structural design code formulation (Kiremidjian et al., 1979).

5.3 Markov Renewal Hazard Model.

As it has been indicated in other studies (Kiremidjian and Anagnos, 1984; Kiremidjian and Suzuki, 1987; and Anagnos and Kiremidjian, 1988), the assumptions of temporal and spatial independence of the earthquake generating process is violated when characterizing large infrequent events or when modeling seismic hazard for regions with a regular earthquake occurrence patterns. In this study, the Markov renewal model (Kiremidjian and Suzuki, 1987) is applied to a segment of the Benioff Zone which is characterized by large infrequent earthquakes (see Figure 5.1). The remaining sources are modeled using the Bayesian model. The results from the two models are combined to obtain hazard estimates throughout El Salvador.

5.3.1 Model Formulation.

Kiremidjian and Anagnos (1984), postulated the hypothesis that the size of future events depends on the elapsed time since the last event. Interarrival times of events are assumed to be Weibull distributed random variables and the sequence of earthquakes then can be represented as a Markov renewal process.

Figure 5.2 shows schematically the assumptions of the slip-predictable model.

Let $E = [1,2,\dots,N]$ be the state space for N discrete stress levels (see Figure 5.2c) and

Y_n = the size of the n th event

T_n = the time of the n th event

The set $\{Y_n : n \geq 0\}$ are random variables assuming values in E and the set $\{T_n : n \geq 0\}$ is such that $0 < T_0 < T_1 < \dots$. The stochastic process $\{Y_n, T_n : n \geq 0\}$ is a Markov renewal process provided that

$$\begin{aligned} P[Y_{n+1} = j, T_{n+1} - T_n \leq t | Y_0 \dots Y_n : T_0 \dots T_n] \\ = P[Y_{n+1} = j, T_{n+1} - T_n \leq t | Y_n = i] = Q(i,j,t) \end{aligned}$$

$$\text{for all } i,j \in E; \text{ and } t \geq 0. \tag{5.4}$$

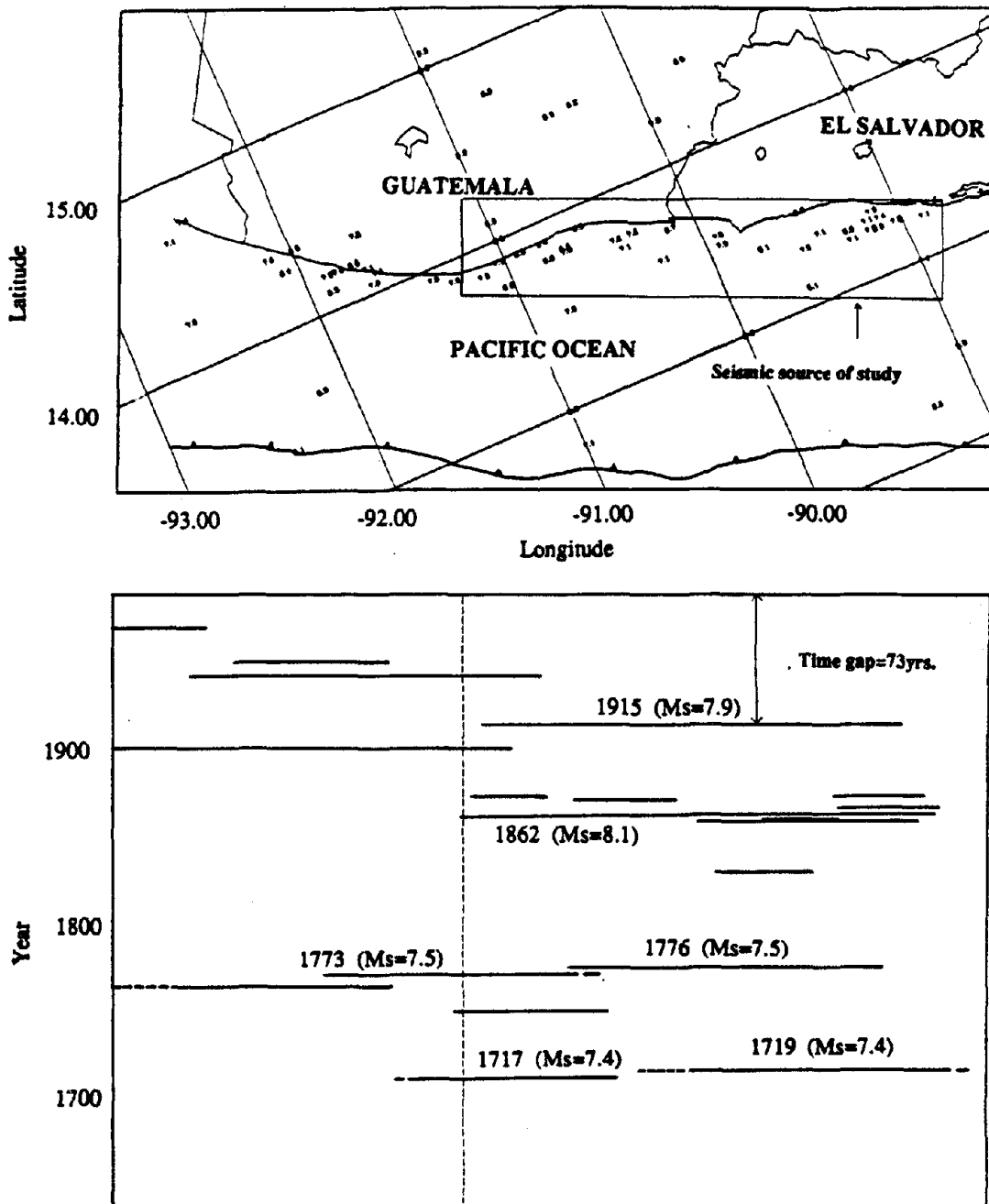


Figure 5.1. Benioff Zone earthquakes ($M_S \geq 7.0$) since 1711 along a section of the Middle America Trench near El Salvador.

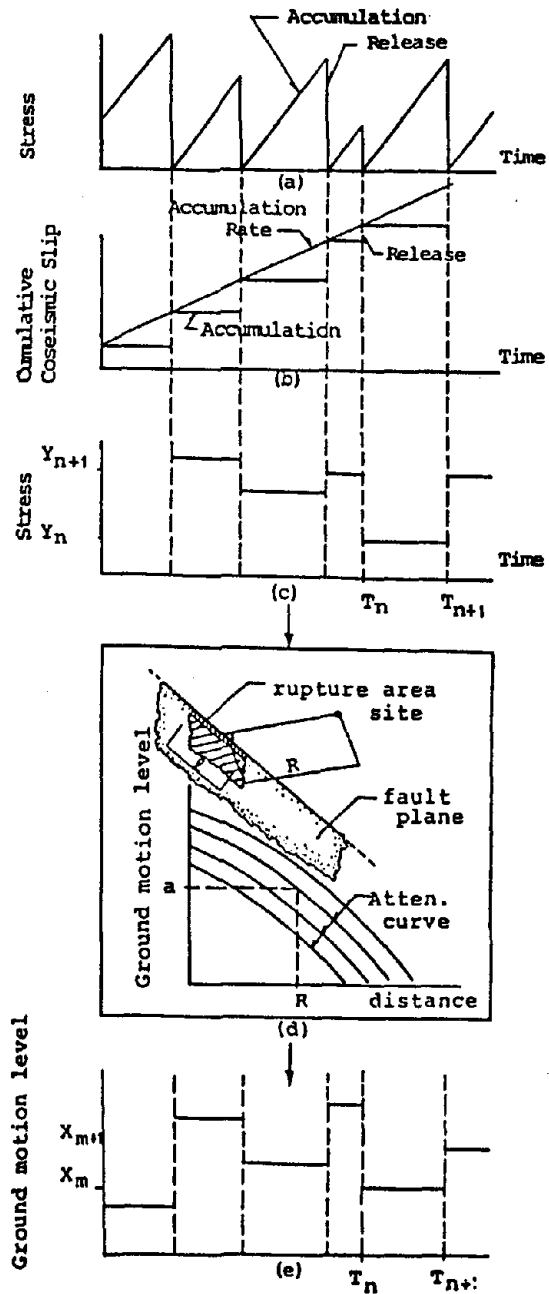


Figure 5.2. Schematic representation of: (a) slip-predictable model; (b) cumulative coseismic slip in time; (c) corresponding sample path for the Markov renewal process; (d) the source-to-site characterization; and (e) the resulting site-hazard sample path. (From Kiremidjian and Suzuki, 1987)

Thus, the joint probability of Y_{n+1} and $T_{n+1} - T_n$ depends only on the state visited at time T_n . In other words, the size of the next event depends only on the time of occurrence of the last event.

Furthermore, Kiremidjian and Suzuki (1987) redefine this state space E to information on site ground motion. This transformation is schematically shown in Figure 5.2d and the final state space is represented in Figure 5.2e.

Thus, in order to determine the probability of exceedence from all possible events of a specific level of ground motion, the following state space is defined:

$$U = [U_1, U_2, \dots, U_N, U_{N+1}, \dots, U_{2N}] \quad (5.5)$$

where

$$\begin{aligned} U_i &= \{a < a_0 \text{ and } Y_n = i\} && \text{for } i = 1, 2, \dots, N, \\ U_i &= \{a > a_0 \text{ and } Y_n = i - N\} && \text{for } i = N+1, \dots, 2N. \end{aligned}$$

The states U_i describe the joint event that a ground motion level, a_0 , is not exceeded when the size of the n th event is i , for $i = 1, 2, \dots, N$, or that the ground motion level a_0 is exceeded when the size of the n th event is $i - N$, for $i = N + 1, \dots, 2N$. The set $\{X_n : n \geq 0\}$ are random variables assuming values in U and the set $\{T_n : n \geq 0\}$ is such that $0 < T_0 < T_1 < \dots$. Thus, X_n 's visit states U_i at times T_n . In order to define the process, the holding time distribution, $h_{ij}(t)$ and the transition probabilities need to be described.

The holding time distributions are defined on the basis of the Weibull interarrival times with cumulative probability distribution given as follows:

$$F_T(t) = 1 - \exp(-\phi_1 t^{\phi_2}) \quad \text{for } \phi_1, \phi_2 > 0, t \geq 0 \quad (5.6)$$

where ϕ_1 and ϕ_2 are the parameters of the distribution. This distribution has an increasing hazard rate for values of ϕ_2 greater than 1.

For the transition probabilities, let

$$\begin{aligned} q_{ij} &= P \{ \text{process enters state } j \text{ next / it was last in state } i \} \\ &= \int_{R_e} \int_{R_e} f_{E|Y,R}(\xi) f_{R|Y}(r) p_{ij} dr d\xi \end{aligned} \quad (5.7)$$

where $f_{a|Y,R}(\xi)$ is the distribution of the scatter on the ground motion acceleration, a , assumed to be lognormal with unit median and variance $\sigma_{\ln \xi}^2$; $f_{R|Y}(r)$ is the probability density of the nearest distance from the rupture to the site, and the p_{ij} 's are the transition probabilities of the process $\{Y_n : n \geq 0\}$.

Thus, the probability of exceeding a level of acceleration a_0 at least once in time $(0,t]$ given that state i is entered at time 0 is denoted by $G_i(X \geq j, k \geq 1|t)$. This probability is calculated by considering the complementary probability of zero events of size $X \geq j$ in $(0,t]$; in other words,

$$G_i(X \geq j, k \geq 1|t) = 1.0 - G_i(X \geq j, k=0|t) \quad (5.8)$$

and

$$G_i(X \geq j, k=0|t) = \sum_{r=1}^N \int_0^t q_{ir} h_{ir}(\tau) G_r(X \geq j, k=0|t-\tau) d\tau + H_i(t) \quad (5.9)$$

where $H_i(t)$ is the complementary cumulative holding time distribution. Computations of probabilities of exceeding a ground motion level are provided by this equation.

The probability of at least one event of size $X \geq j$ in time $(t_1, t]$, given that there were no occurrences in time $(0, t_1]$, that is in a duration gap t_1 , is computed for hazard analysis purposes. The probability of no events of any size in time $(0, t_1]$ is given by $G_i(0|t_1) = H_i(t_1)$. Thus, the joint probability of no events of size $X \geq j$ in time $(t_1, t]$ and no events of any size in time $(0, t_1]$ is given by

$$G_i(X \geq j, k=0, t_1|t) = \sum_{r=1}^N \int_{t_1}^t q_{ir} h_{ir}(\tau) G_r(X \geq j, k=0|t-\tau) d\tau + H_i(t) \quad (5.10)$$

Considering the complementary probability of equation (5.10), the probability of at least one event of size $X \geq j$ in time $(t_1, t]$ given that there were no events in time $(0, t_1]$ is given by

$$G_i(X \geq j, k \geq 1|t_1, t) = 1.0 - G_i(X \geq j, k=0, t_1|t) / H_i(t_1) \quad (5.11)$$

Using these equations the computation of the site hazard in terms of the ground motion parameter a (peak ground acceleration, PGA, for this study), is provided. These

computations are functions of the forecast time t (the economic life of the structure) and the duration of the gap, t_1 .

5.4 Parameter Estimation.

In this section, an evaluation of the parameters needed for the application of the hazard models is conducted. For the Bayesian model, a search for a fault rupture model, and the evaluation of the parameters of the posterior distribution on the mean rate of occurrence λ and the posterior distribution on the probability of success, P_{M_i} , of the number of events of any specific magnitude given that a total number of events have occurred are conducted for all sources. For the Markow hazard model, a calculation of the fault rupture-site geometry model, and the evaluation of the parameters for the holding time distribution and the coseismic slip rate are conducted for the Intermediate Benioff Zone segment .

5.4.1 Bayesian Model Parameter Estimation.

In this model it is assumed that the maximum ground motion is caused by waves arriving from the nearest point on the rupture length on the fault zone. For the case of line sources, fault rupture is considered along the length of the fault. For area sources, the length of the rupture is given by a magnitude-rupture relationship and the width is calculated as half of the length of the rupture area. In addition, the rupture process near the ends of the fault are required to satisfy geometric as well as seismic constraints (Mortgat and Shah, 1979).

Among the magnitude-rupture relationships available are these developed by White and Cifuentes (1988), Schwartz et al.(1984), and Bonilla et al. (1984) (see Figure 5.3). For Subduction Zone seismic sources, the relation from White and Cifuentes is chosen because it fits the model segmentation proposed in Chapter 4. For instance, for $M_S = 8.2$ the rupture length is about 280 km which corresponds roughly to the length of the middle segment of the Subduction Zone. For local faults the relationship from Schwartz et al. is selected. For these faults, the equation of White and Cifuentes was disregarded since it saturates for earthquakes in a range of $M_L < 6.37$. For the 1976 earthquake on the Motagua Fault, $M_W = 7.5$ (M_W is approximately equal to M_S at values of 7.5), the fault ruptured about 200 km. The relationship by Bonilla et. al. (1984), was considered inappropriate since for a magnitude $M_S = 7.5$ the rupture length is found to be 85 km. The relationship by Schwartz et al. (1984) gives a better approximation, for a magnitude of 7.5 the rupture length is 170 km.

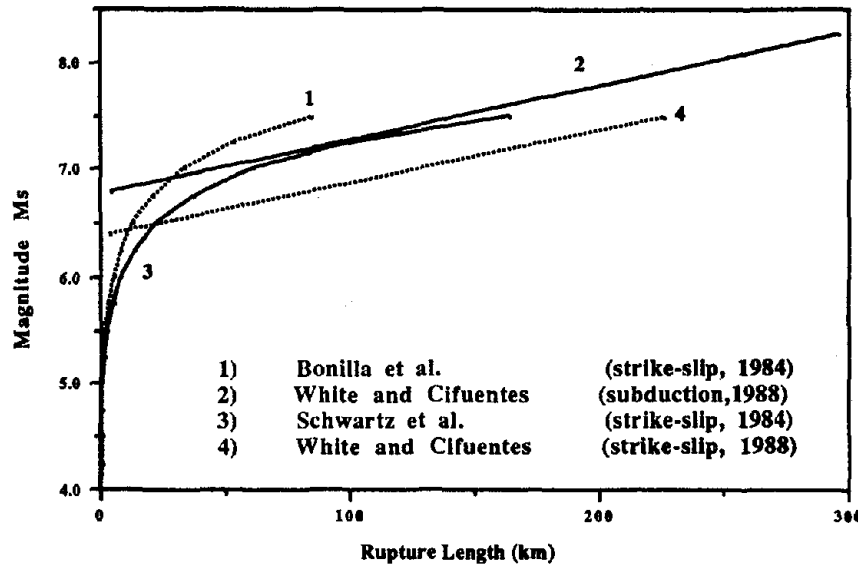


Figure 5.3. Fault rupture relationships.

Parameter estimation. The parameters needed to implement the model are of two kinds: the available data, presented in Chapter 3, and the subjective input introduced through Bayesian analysis.

The parameters T and N of the sample likelihood for the mean rate of occurrence, λ , are determined from the data. T represents the time base for which data is available. For instance, T is 256 years for the Guatemalan Segment of the Volcanic Chain (see Table E.1 in Appendix E). N represents the total number of occurrences observed on the source considered during this period of time.

The parameters λ' and ν' of the prior Gamma distribution on λ are determined from the subjective input of the analyst. In this study, it is assumed that the numerical values of λ' and ν' are respectively equal to T and N for each corresponding source. In other words, the analyst has the same confidence in the data available and in his subjective input.

The values for λ'' and ν'' , the parameters for the posterior distribution on λ , are based on the values of λ' , ν' , T and N . Then, probability function for λ for the source considered during a future time t is defined, in a posterior sense.

The parameters N and R_{M_i} of the sample likelihood function for P_{M_i} can be determined from the data available. N as before, represents the total number of events observed on the source under consideration and R_{M_i} represents the number of earthquakes of magnitude M_i recorded on the same source. R_{M_i} must be determined for each source and each M_i .

The parameters η'_{M_i} and ϵ'_{M_i} of the conjugate beta prior distribution on P_{M_i} are determined from the subjective input of the analyst. For this study, the subjective input is constituted by the analytical recurrence relationships fitted in Chapter 4 for each seismic source.

Finally, the values for η''_{M_i} and ϵ''_{M_i} , the parameter for the posterior distribution on P_{M_i} , can be determined based on the values for η'_{M_i} , ϵ'_{M_i} , N , and R_{M_i} . Thus, in a posterior sense, the probability distribution of P_{M_i} of magnitude M_i for a source is determined. The values for all the parameters defined before are summarized in Tables E.1 to E.16 in Appendix E.

5.4.2 Markov Hazard Model Parameter Estimation.

In Equation (5.7), $f_{R|Y}(r)$ is the probability density function of the nearest distance from the rupture zone to the site and depends on the fault-to-site geometry. For hazard analysis purposes, the region of study was discretized in partitions of 0.20° in both directions (N-S and E-W directions). Fault-to-site geometries were calculated for each nodal point (see Figure 5.4). All the possible geometries calculated are covered by the four geometric models developed by Kiremidjian and Suzuki (1987), for which the cumulative probability distribution for the nearest distance from the source to the site are also developed.

Parameter Estimation. In order to implement the hazard model, the slip rate, the interarrival times, and the holding times were determined for the Intermediate Benioff Zone segment. Thatcher and Hank's (1973), Davies and Brune's (1971), and Utsu and Seki's (1954) relationships were used for moment-magnitude, moment-average seismic slip, and magnitude-fault rupture area, respectively (see Table 5.1).

The seismic source to be applied to the model is shown in Figure 5.1. From this figure, it can be appreciated a periodic release of energy (foreshock, mainshock, and aftershocks); therefore, the applicability of a temporal dependent earthquake generating process was investigated. Figure 5.5 shows a plot of the cumulative moment release vs. time for this segment; clearly, a dependence of the amount of energy release with the time elapsed since the last major release of energy is obvious. In addition from Figure 5.5, the slip-predictable model with constant slip rate seems to fit adequately. The interarrival time of release of energy was estimated to be 65 years with a standard deviation of 18 years. The estimated slip rate was of 3.13 cm/yr.

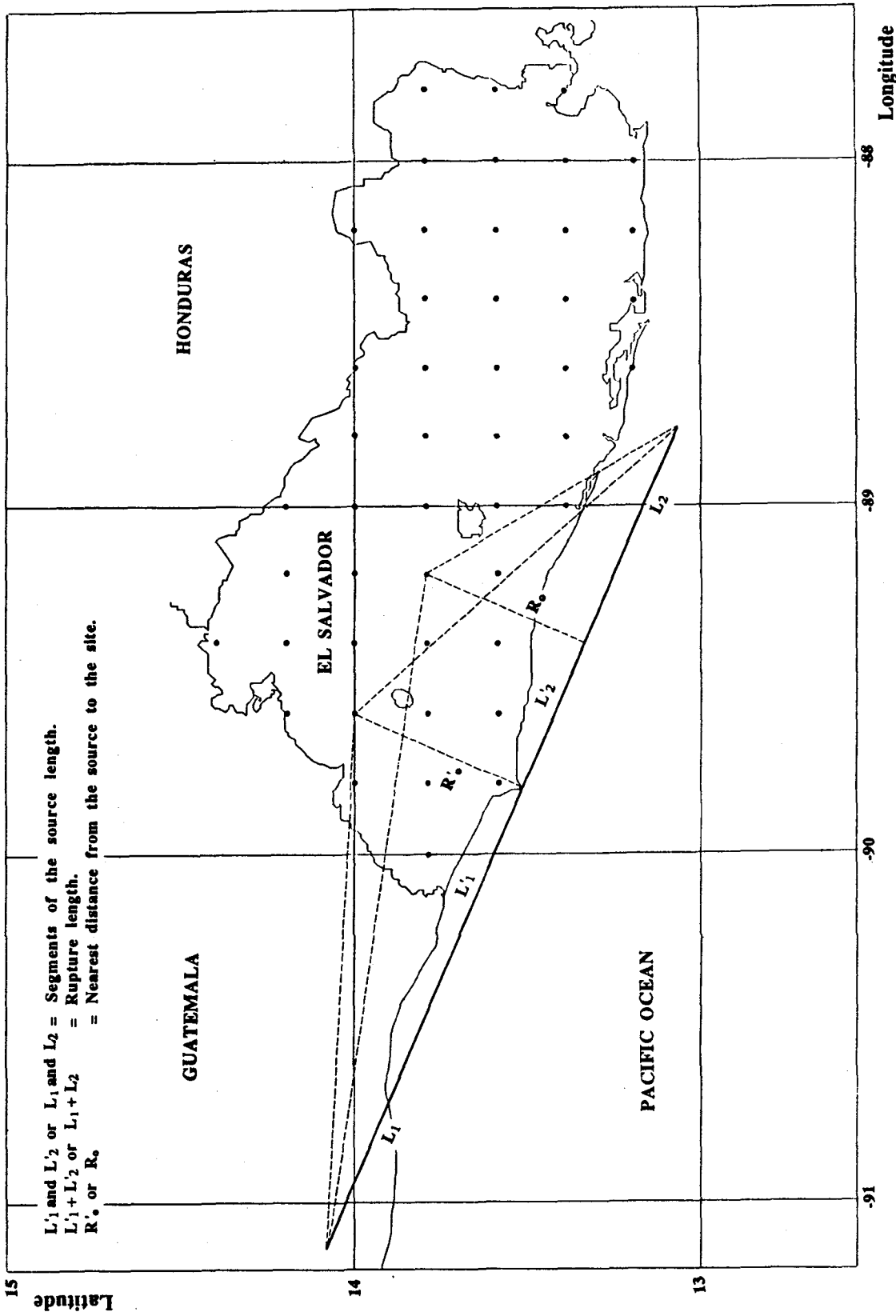


Figure 5.4 Source to site geometries for two sites in El Salvador for the Markov hazard model. The source-to-site geometry was developed for each nodal point shown on the map (dots). The source is at 50 km depth and the sites at the surface.

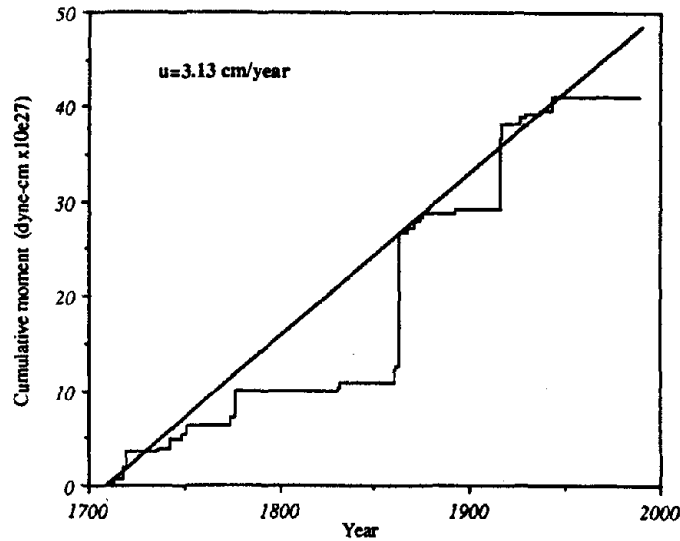


Figure 5.5 Cumulative moment release vs. time in the segment of study (see Figure 5.1), the slip rate is estimated from the best fit through the data.

Using this constant slip rate, the holding time threshold values were estimated (see Table 5.1). The interarrival times of major releases of energy are assumed to be Weibull distributed. Using the method of moments, the parameters ϕ_1 and ϕ_2 of equation (5.6) are determined from the average interarrival time. The values obtained are 0.28×10^{-7} and 4.06 respectively. It is important to note, that for all the site hazard computations of this seismic source a gap time of 75 years was included since the last large earthquake in the region was in 1915.

5.5 Contribution of a Single and Several Seismic Sources.

In order to determine the ground motion hazard at a site the contribution of all sources must be integrated. For this purpose Equations 5.3, 5.11 with parameters specific to each seismic source are combined with a seismic ground motion model (see Chapter 6) to determine the probability of exceeding various ground motion levels at the specified site.

State	Magnitude (Ms)	Moment M_0 ($\times 10^{27}$ dyne-cm)	Rupture Area $S(\text{km}^2)$	Displacement u (cm)	Holding Time ($\dot{u}=3.13$ cm/yr)
1	$7.50 < M \leq 7.75$	4.22	7852	162.9	52
2	$7.75 < M \leq 8.00$	10.00	14125	214.5	68
3	$8.00 < M \leq 8.25$	23.70	25410	282.6	90
4	$8.25 < M \leq 8.50$	56.20	45709	372.6	119

Table 5.1. Parameters for the slip-predictable Model-Middle America Trench, El Salvador.

The contribution from all seismic sources to a single site is computed assuming spatial independence. The composite probability of exceedence of a given acceleration level is obtained as follows:

$$P_T = 1.0 - \prod_{i=1}^N (1.0 - P_i) \quad (5.12)$$

where P_T is the probability of exceedence of a given acceleration, a , in a future time t when events occur in all seismic sources. P_i is the probability of exceedence for a given level of acceleration, a , in time t for the i th source.

In summary, this chapter reviews the two seismic hazard models used in this study. Their application to the seismicity of El Salvador and discussion of results will be presented in Chapter 7.

CHAPTER 6

STRONG GROUND MOTION PARAMETER ESTIMATION

6.1 Introduction.

In this chapter, strong ground motion attenuation functions are developed specifically for El Salvador. As it was indicated in a previous chapter, several tectonic regimes are found in the study region. Since subduction earthquakes are different in travel paths and stress conditions from near-source events (Campbell, 1981), the analysis will dependent upon the origin of the events.

6.2 Data Base.

The data base consists mainly of accelerograms produced by earthquakes that occurred in Central America. Recordings were obtained from basements, first floors, and free field sites by SMA-1 and AR-240 strong ground motion instruments (Knudson et al., 1973; Shakal et al., 1987).

As indicated above, for analysis purposes the data base was classified according to the origin of the events. Tables 6.1 and 6.2 show the data base used for the near-source and far-source regression analysis. For the near-source data base, seven records come from the San Salvador earthquake in 1986, eight records are from the mainshock, foreshocks, and aftershocks of the Nicaragua earthquake in 1972, and the remaining five records come from the mainshock and aftershocks of the motagua earthquake in 1976. For the far-source data base, all records are from different events recorded at the Observatorio in San Salvador.

6.3 Variables.

As in many other studies (Hasegawa et.al., 1981; Sabetta and Pugliese, 1987; and Joyner and Boore, 1988), the peak ground acceleration (PGA) was chosen as the ground motion parameter. They were taken from digitized strong ground motions when available; otherwise they were scaled from the original accelerograms. From the three components of motion, the larger of the two horizontal acceleration components was selected for purposes of analysis.

Date	Time	Latitude (°N)	Longitude (°W)	M *	Depth (km)	R(Epi) (km)	amax (g)	Station	Site Geol.
01/04/68	10 03	12.11	86.25	4.6	5	2	0.13	3500Mana	1B
01/03/72	04 31	12.20	86.24	4.1	5	9	0.04	3500Mana	1B
01/03/72	04 31	12.20	86.24	4.1	5	11	0.15	3501Mana	1B
01/05/72	11 52	12.24	86.24	4.2	5	16	0.12	3502Mana	1B
01/05/72	11 52	12.24	86.24	4.2	5	14	0.22	3501Mana	1B
12/23/72	06 29	12.25	86.27	6.2	5	13	0.39	3501Mana	1B
12/23/72	07 17	12.14	86.33	5.0	5	1	0.19	3501Mana	1B
12/23/72	07 19	12.20	86.30	5.2	5	7	0.33	3501Mana	1B
02/04/76	09 01	14.87	90.51	7.5	10	23	0.60	3200Guate	2
03/07/76	02 54	14.67	90.99	5.1	7	33	0.20	254Chi	2
03/07/76	03 15	14.75	91.05	5.1	7	22	0.19	315Chi	2
03/09/76	07 42	14.70	91.05	5.2	7	27	0.12	742Chi	2
04/26/76	15 24	15.06	89.60	4.1	7	11	0.08	1524Zac	2
10/10/86	17 49	13.67	89.19	5.8	10	5	0.54	IGNSSalv	2
10/10/86	17 49	13.67	89.19	5.8	10	4	0.71	CIGSSalv	2
10/10/86	17 49	13.67	89.19	5.8	10	1	0.66	OBSSSalv	1A
10/10/86	17 49	13.67	89.19	5.8	10	6	0.72	IVUSSalv	--
10/10/86	17 49	13.67	89.19	5.8	10	5	0.47	HCRSSalv	1B
10/10/86	17 49	13.67	89.19	5.8	10	5	0.43	UCASSalv	1B
10/10/86	17 49	13.67	89.19	5.8	10	8	0.31	HSHSSalv	1B

*M as defined in section 6.3.

Table 6.1. Near-source strong ground motion data.

Date	Time	Latitude (°N)	Longitude (°W)	M *	Depth (km)	R(Epi) (km)	amax (g)	Station
05/26/65	04 58	13.40	90.70	5.2	39	168	0.005	3300SSalv
03/13/66	21 46	14.20	88.40	4.2	36	104	0.004	3300SSalv
11/18/67	12 17	13.40	89.20	5.1	70	33	0.014	3300SSalv
11/18/67	12 26	13.40	89.10	4.7	78	35	0.018	3300SSalv
09/10/78	23 24	12.27	91.50	5.6	94	298	0.017	3300SSalv
10/30/78	18 24	13.88	91.05	5.3	73	204	0.010	3300SSalv
12/06/78	11 53	13.14	89.64	5.9	50	78	0.016	3300SSalv
12/18/78	02 31	13.13	88.26	5.3	85	129	0.014	3300SSalv
10/27/79	14 36	14.20	90.88	7.0	58	193	0.048	3300SSalv
10/27/79	21 43	13.78	90.73	6.8	65	169	0.036	3300SSalv
11/04/80	16 21	13.86	90.93	5.4	83	191	0.007	3300SSalv
01/09/82	01 55	13.50	88.64	4.7	80	65	0.013	3300SSalv
03/06/82	21 24	12.90	88.45	4.9	65	121	0.013	3300SSalv
06/19/82	06 22	13.45	89.37	7.2	55	33	0.340	3300SSalv
06/20/82	14 23	13.45	89.33	5.4	55	31	0.026	3300SSalv
07/02/82	11 59	13.26	89.29	5.9	65	49	0.033	3300SSalv
10/27/82	07 41	13.46	89.42	5.1	70	33	0.060	3300SSalv
03/02/83	15 37	13.30	89.20	4.8	90	44	0.015	3300SSalv
04/29/83	01 02	13.42	89.18	4.9	82	31	0.034	3300SSalv
07/18/83	00 53	12.60	87.20	5.6	66	248	0.010	3300SSalv

*M as defined in section 6.3.

Site geology classification 1A.

Table 6.2. Far-source strong ground motion data.

A diversity of magnitude scales are used in characterizing the size of an earthquake (Heaton et al., 1982) and all except the moment magnitude tend to saturate as their size increase. In order to avoid this problem, the magnitude M is defined as the surface-wave magnitude M_S when both the local magnitude (M_L) and M_S are greater than 6.0 and is defined as M_L when the magnitudes are lower than this value.

Many distance measures used in attenuation equations have been proposed (Shakal and Bernreuter, 1981). Some have used a measure of the closest distance to the vertical projection of the fault rupture (Joyner and Boore, 1988) and argued that it is a more physically consistent source-to-station distance for large rupture zones. Because of the lack of information on the rupture zones, this study adopts the epicentral distance as the source-to-site measure. However, a careful analysis was made for the cases of large rupture zone (e.g. Motagua earthquake, 1976) since the epicentral distance in these cases can introduce misleading interpretations of ground acceleration attenuation.

Recording stations were classified being above stiff and soft soils by using the geological information available (Consorzio Salvador e., 1988; Michael Rymer, 1987; David Harlow, oral communications). The geology at stations in San Salvador have been classified as follows (Consorzio Salvador e., 1988):

Zone 1. This zone is characterized by a bedrock thickness of at least 65 m within the first 100 m of depth (e.g., minimum thickness of the lava layer that is assumed to behave as bedrock). This zone is subdivided into two subzones.

Zone 1A. This subzone is characterized by a lava layer that is exposed or is within 5 m from the surface (stiff soils).

Zone 1B. This subzone is characterized by a bedrock layer with a depth ranging from 5 m to 35 m (shallow soils).

Zone 2. This zone is characterized by a bedrock thickness of less than 35 m within the first 100 m of depth (deep soils).

The layer of soils that covers the bedrock at these sites is formed by two pyroclastic and epiclastics tuff units (Michael Rymer, 1987), the coffee-colored tuff (tobas color cafe) and the white earth (tierra blanca). The average shear-wave velocity (V_S) of these deposits range from 150 m/s to 450 m/s and their average compressional-wave velocity (V_P) range from 300 m/s to 1000 m/s (Consorzio Salvador e., 1988). The bedrock is formed by

compact andesitic lava flows with an average V_S ranging from 2000 m/s to 2600 m/s and an average V_P ranging from 2600 m/s to 3200 m/s.

The geologic classification at recording stations in Guatemala and Nicaragua were assumed as deep and shallow soils, respectively (David Harlow, oral communications). For site geology classification at these recording stations see Tables 6.1 and 6.2.

6.4 Ground Motion Model.

The functional form adopted for modelling the attenuation of near-field and far-field strong ground motion parameters is represented by the following equation:

$$\log Y = a + bM - c \log (r_0^2 + \Delta^2)^{1/2} \quad (6.1)$$

where Y is the strong ground motion parameter in consideration (PGA), and M is the generic magnitude defined above. In order to study the attenuation due to geometrical spreading the term $c \log (r_0^2 + \Delta^2)^{1/2}$ is present in the equation; r_0 , is the epicentral distance in kilometers and the parameter Δ is included to recognize that the strong ground motion comes from some depth below the surface and also to recognize the concept of saturation of the strong ground motion at short distances. Notice that terms representing anelastic attenuation and site geology are not included in the model. A preliminary test of the model including these terms showed the value of the anelastic attenuation term nearly zero and positive, it was therefore removed from the model. In addition, due to the lack of data a further categorization of the data base by soil condition was considered inadequate for regression analysis purposes, i. e. a poor constraint of the attenuation curves was evident when site geology was considered. Consequently, soft and stiff soil conditions are taken as the site geology for the near-source and far-source attenuation functions respectively (see Tables 6.1 and 6.2).

The value of Δ in the attenuation model is determined by a non-linear regression analysis (Neter et al., 1985), and the values of the coefficients a , b , and c are determined by a subsequent linear regression.

6.5 Regression Analysis.

Table 6.3 shows the results obtained in the regression analysis performed. The goodness of fit is represented by an r^2 value of 0.64 and 0.77, the correlation coefficient squared, for the near-source and far-source regression analyses, respectively. The 84 percentile values of PGA are obtained by multiplying the median value by a factor of 1.62 for both attenuation functions. Plots of both relationships for the 50 and 84 percentiles, as functions of distance and magnitude, are shown in Figures 6.1 and 6.2. For both plots, the curves representing the 50 percentile (heavy lines) are dashed whenever they are not constrained by data and caution is recommended when extrapolation is intended beyond these limits.

	a	b	c	Δ	$\sigma \log Y$
Near-field sources PGA	-1.116	0.312	-1.000	7.9	0.21
Far-field sources PGA	-1.638	0.438	-1.181	70	0.21

Table 6.3. Regression coefficients given by equation (6.1).

Residuals of the data with respect to the predicted values are analyzed to test for biases given by the attenuation functions developed in this study. Figure 6.3 shows plots of standardized residuals against epicentral distance for different magnitude classes, and magnitude for the near-source attenuation function. No obvious differences in trend are observed in these plots for the three different magnitude classes, probably due to the lack of data. Therefore, it was assumed that the shape of the attenuation curves obtained are independent with magnitude. A similar test was performed for the far-source attenuation function and similar results were obtained. Plots of standardized residuals against distance and magnitude for this attenuation function are shown in Figure 6.4.

In Figures 6.5 and 6.6, the predicted ground motions given by the attenuation functions developed in this study are compared with the data for observed peak ground acceleration. In these plots, the data have been grouped in magnitude intervals of 5.0 to

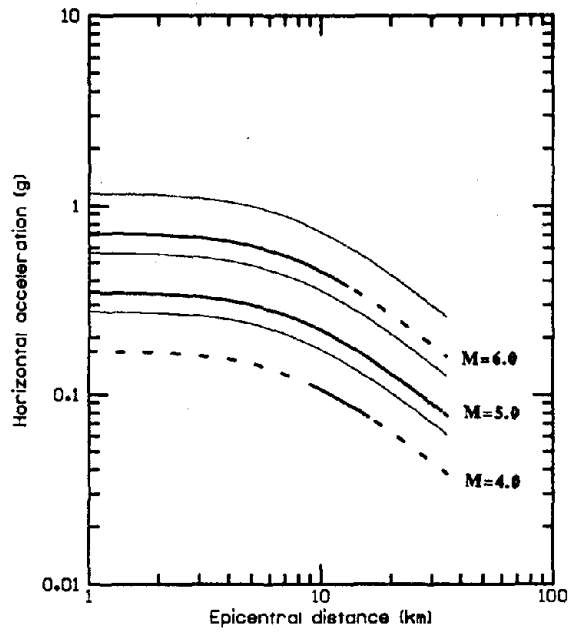


Figure 6.1. Peak ground acceleration attenuation function for near-sources in Central America. The plot shows the 50 percentile (heavy lines) and the 84 percentile (light lines) of the predictive attenuation function. The curves are dashed whenever they are not constrained by data.

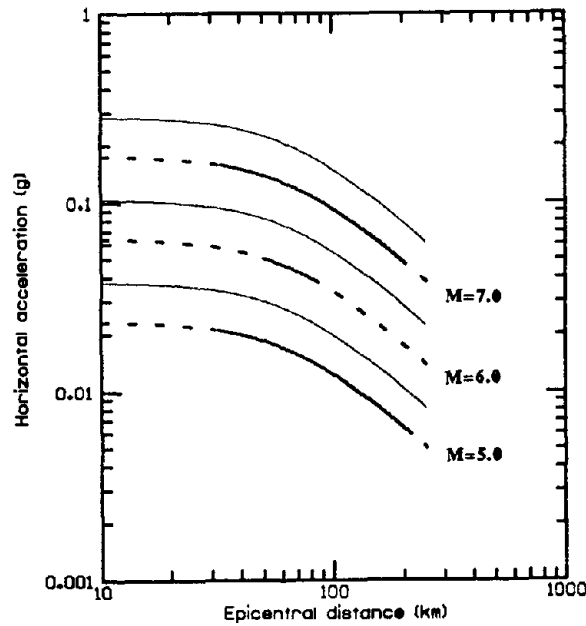


Figure 6.2. Peak ground acceleration attenuation function for far-sources in Central America. The plot shows the 50 percentile (heavy lines) and the 84 percentile (light lines) of the predictive attenuation function. The curves are dashed whenever they are not constrained by data.

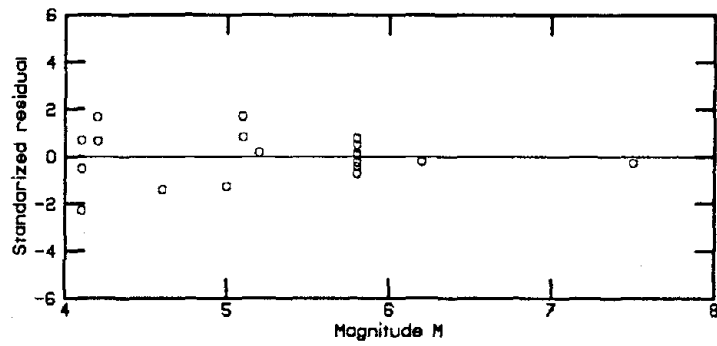
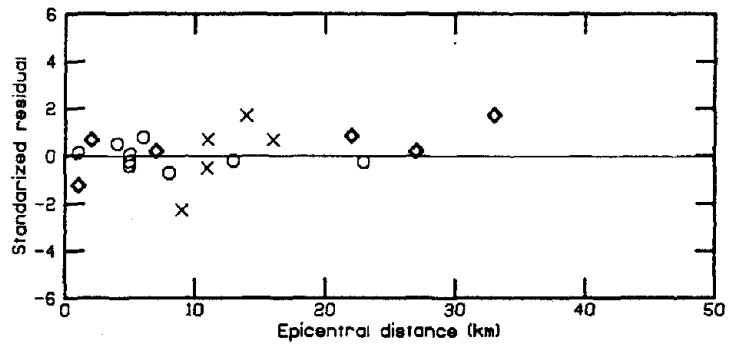


Figure 6.3. Standardized residuals of data respect to the near-source predictions from Equation (6.1). In the first plot, exes represent magnitudes from 4.0 to 4.5, diamonds represent magnitudes from 4.6 to 5.5, and circles represent magnitudes from 5.6 and above.

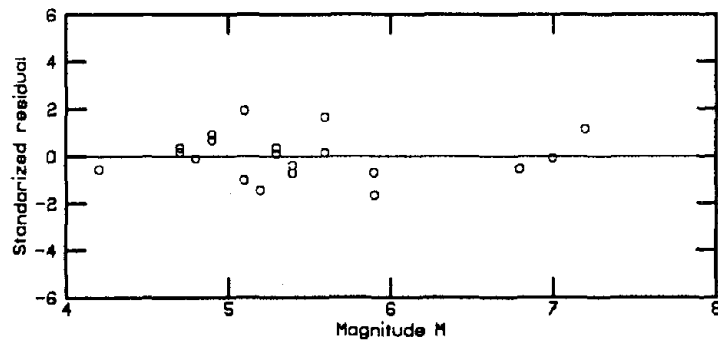
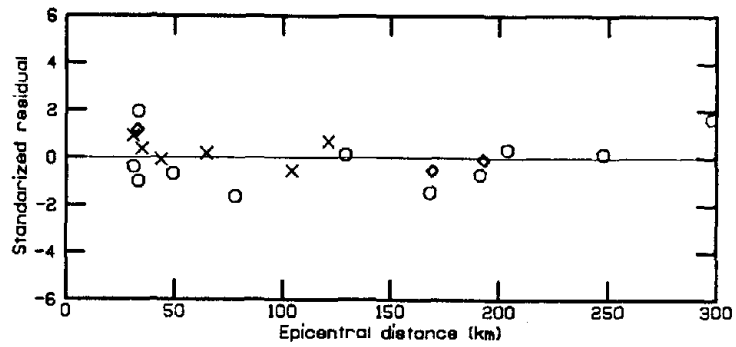


Figure 6.4. Standardized residuals of data respect to the far-source predictions from Equation (6.1). In the first plot, exes represent magnitudes from 4.0 to 5.0, circles represent magnitudes from 5.1 to 6.0, and diamonds represent magnitudes from 6.1 and above.

5.49 and 5.5 to 6.0. The heavy lines represent the 50 percentile curve for the magnitudes of 5.0 and 6.0. The light lines represent the 84 and 16 percentiles curves for the magnitudes of 6.0 and 5.0, respectively. It is observed in these figures that the predicted curves represent reasonably well the behavior of the data.

A comparison of the near-source attenuation function developed in this study with the ones developed by others (i.e., Joyner and Boore, 1988; Campbell, 1989) for western United States is very difficult. Since these authors used different definitions for the various variables (i. e., magnitude, distance, and site geology), a graphical comparison would require certain assumptions in order to reconcile these differences which in some cases it is almost impossible. For instance, Joyner and Boore (1988) used for the source-to-site distance, the closest distance of the vertical projection of the fault rupture to the recording station. In this study, instead, the epicentral distance is used for the source-to-site distance. Consequently, in this study, an overestimation on the prediction of the peak ground accelerations is expected, forehand.

Sabetta and Pugliese (1987) developed a relationship for the Italian strong ground motion data. They used similar definitions for the various variables adopted in this study. In addition the seismotectonic environment, and site geology are believed to be similar to the ones of the Central American volcanic chain. Figure 6.7 shows a comparison of the attenuation function developed in this study (heavy lines) with the relationship mentioned above (light lines). The comparison is made for the magnitudes 5.0 and 6.0, and for different site geologies. In this plot, one can note that the results from this study are comparable to their results for the shallow soils (bedrock depth within 5 m and 20 m). This site geology classification represents in sixty percent the near-source data set of this study (see Table 6.1).

In Figure 6.8, the relationship for the far-source obtained in this study is compared with the ones developed by Esteva and Villaverde (1974) and Kawashima et al. (1984) for the subduction zones of Mexico and Japan, respectively. A focal depth of 70 kilometers was assumed for the relationship of Esteva and Villaverde to make the comparison possible. The comparisons are made for magnitude 7.0. In this plot one can observe that the relationship of Esteva and Villaverde is comparable to the one developed in this study.

In summary, in this study a development of near-source and far-source attenuation functions for PGA was undertaken. These attenuation functions along with the probabilistic hazard models and geometrical model discussed in previous chapters are used in the next chapter to compute hazard values for the entire country and specific sites of El Salvador.

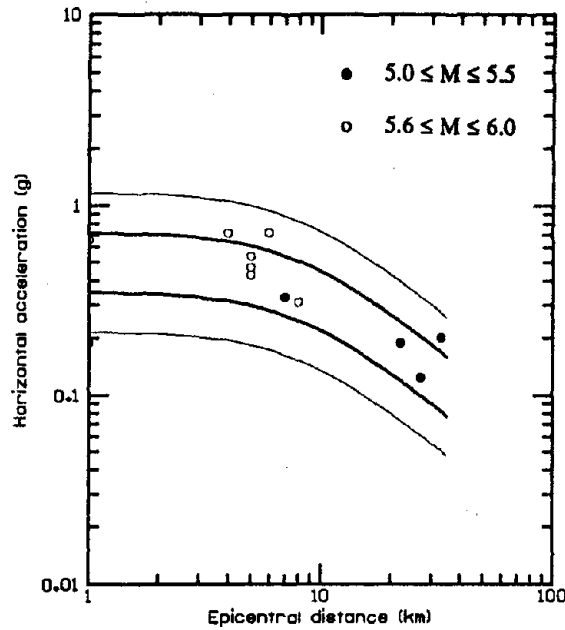


Figure 6.5. A comparison of the observed values of PGA with the near-source predicted values given by the coefficients of the Table 6.3. The heavy lines represent the 50 percentile for the magnitudes 5.0 and 6.0 and the light lines represent the 84 and 16 percentiles for the upper and lower bounds respectively.

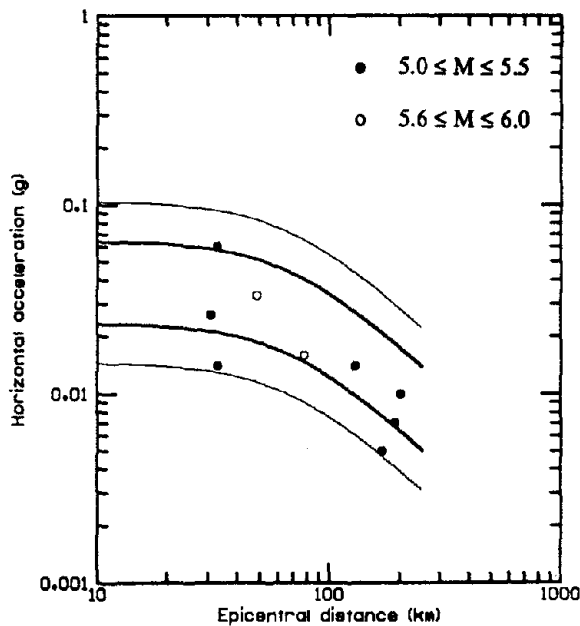


Figure 6.6. A comparison of the observed values of PGA with the far-source predicted values given by the coefficients of the Table 6.3. The heavy lines represent the 50 percentile for the magnitudes 5.0 and 6.0 and the light lines represent the 84 and 16 percentiles for the upper and lower bounds respectively.

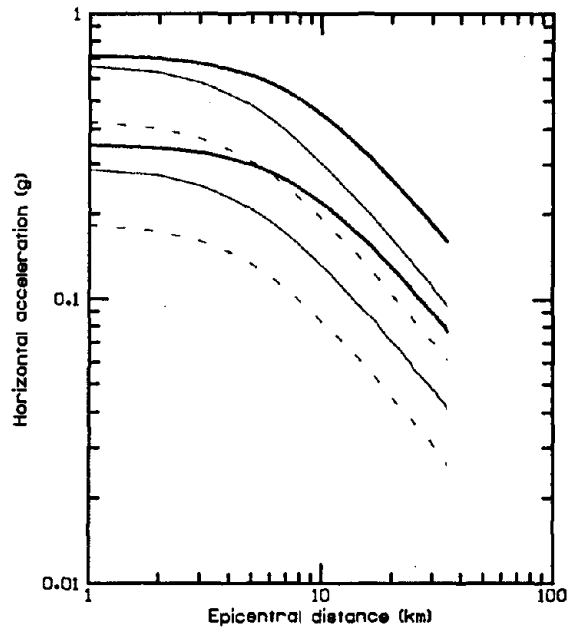


Figure 6.7. Comparison of the near- source attenuation function developed in this study (heavy lines) with the 50 percentile curves (light lines) from the relationship of Sabetta and pugliese (1987). The dashed-light lines represent the 50 percentile for deep soils (bedrock at depths greater than 20 mts) and rock, and the solid-light lines represent the 50 percentile for shallow soils (bedrock at depths within 5 and 20 mts).



Figure 6.8. Comparison of the far- source attenuation function developed in this study (heavy lines) with the 50 percentile curves (light lines) from the relationships of Esteva and Villaverde (1974), dashed-light lines; and Kawashima et al. (1984), solid-light lines.

CHAPTER 7

APPLICATION OF THE MODELS

7.1 Introduction.

Based on the seismotectonic setting of the region, a geometrical model was proposed for the study area in Chapter 4. In Chapter 5, two seismic hazard models are reviewed and their suitability for hazard forecast of the region is discussed. In Chapter 6, a study of strong ground motion attenuation functions for Central America was conducted. Two peak ground acceleration attenuation functions were developed. In this chapter, these models are combined to develop iso-acceleration maps for El Salvador. In addition, site-specific seismic loads are computed at eleven locations in El Salvador.

7.2 Iso-Acceleration Maps

In order to develop the hazard maps, the Markov renewal and Bayesian hazard models described in the previous chapter, are applied to the seismicity of El Salvador. As it was expected, for regions where a seismic gap exists the Markov model is more conservative than the Bayesian model giving higher peak ground acceleration values. For this reason, a combined Markov-Bayesian model is chosen for the final seismic hazard maps for El Salvador. The Markov model is applied to the seismic source of Figure 5.1 and the cumulative distribution function of peak ground acceleration (CDF) at each node is combined with the CDFs obtained by applying the Bayesian model to the remaining seismic sources. However, for comparison purposes hazard maps using only the Bayesian model for all sources are also developed.

All the seismic parameters described in Chapter 5 along with the seismic source and attenuation modeling are used to determine the CDF on peak ground acceleration (PGA). El Salvador and surrounding regions are divided into a grid of 115° longitude by 115° latitude spacings. The CDF of PGA at each node of the grid is computed by using the programs MARKOV. HAZARD (Kiremidjian and Suzuki, 1987) and SEISMIC. HAZARD (Chiang et al., 1984) to apply the Markov renewal and Bayesian models, respectively. Then for a specific hazard level the PGA values calculated from the CDFs at each node are evaluated using the computer program CONST. PROB.

Finally, the iso-acceleration lines are obtained by interpolation of the values of PGA between nodes. For a full explanation of these computer programs and parameters needed see Chiang et al. (1984).

Seismic hazard maps are developed for 10% chance of exceedence in 100 years, 10% chance of exceedence in 50 years, and 20% chance of exceedence in 20 years. These forecasts correspond to return periods of events of 100, 500, and 1000 years, respectively. Figures 7.1 to 7.3 show the iso-acceleration maps for these return periods by using the Markov-Bayesian combined model. Similarly, Figures 7.4 to 7.6 show the iso-acceleration maps by using only the Bayesian model. In all cases, high seismicity is observed along the axis of the Volcanic Chain, but also, its influence is only strongly observed to about 20 km away from its axis. This fact is a result of the attenuation relationship used for the Volcanic Chain, which has a sharp drop at epicentral distances of 10 km (see Chapter 6). This phenomenon is clearly seen when the Markov model is used for the Subduction Zone. In Figure 7.3 one can observe that the iso-acceleration line of 0.60g is governed by the Subduction Zone seismic sources until it gets closer to the axis of the Volcanic Chain axis where an uplift of this line is observed.

Comparing the hazard maps for the Bayesian and Markov-Bayesian models for 100 year return period, one can see that higher peak ground acceleration levels are forecasted by the Markov-Bayesian model. In Figure 7.1, one can observe that in the Markov-Bayesian model the subduction sources govern over the volcanic sources in the hazard mapping. On the other hand, in Figure 7.4 in the Bayesian model the volcanic sources govern over the subduction sources for the same hazard evaluation giving then lower peak ground accelerations. This observed differences are due to assumptions on which the Markov and Bayesian models are based and that we discussed in Chapter 5.

7.3 Site-Specific Seismic Loading

Eleven important sites, major population and industrial facilities locations, were selected for the site-specific hazard analysis:

1. San Salvador
2. Santa Ana
3. San Miguel
4. Ahuachapan
5. Sonsonate
6. San Vicente

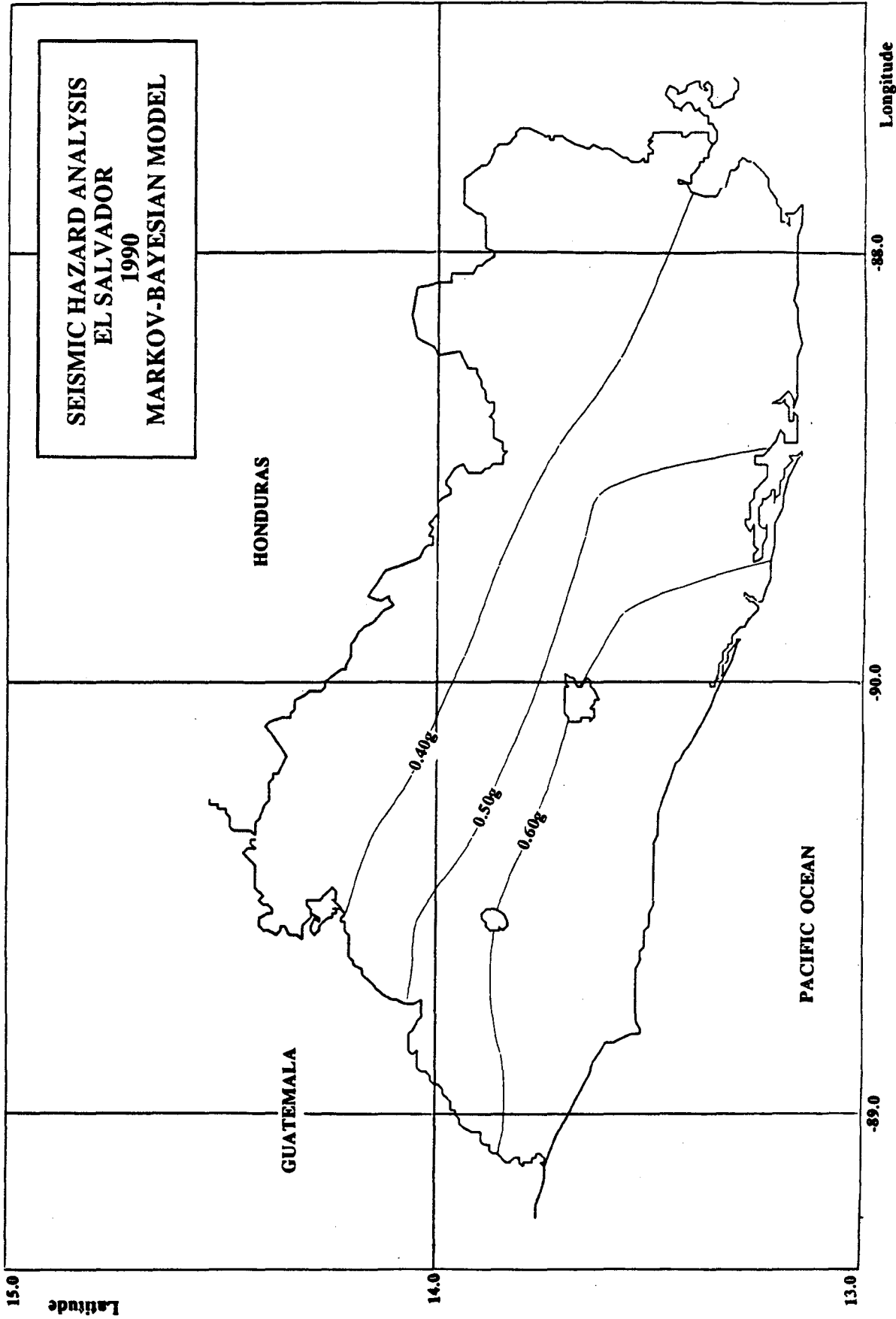


Figure 7.1. Preliminary iso-acceleration map for El Salvador for a future time of 20 yrs and 20% risk level.

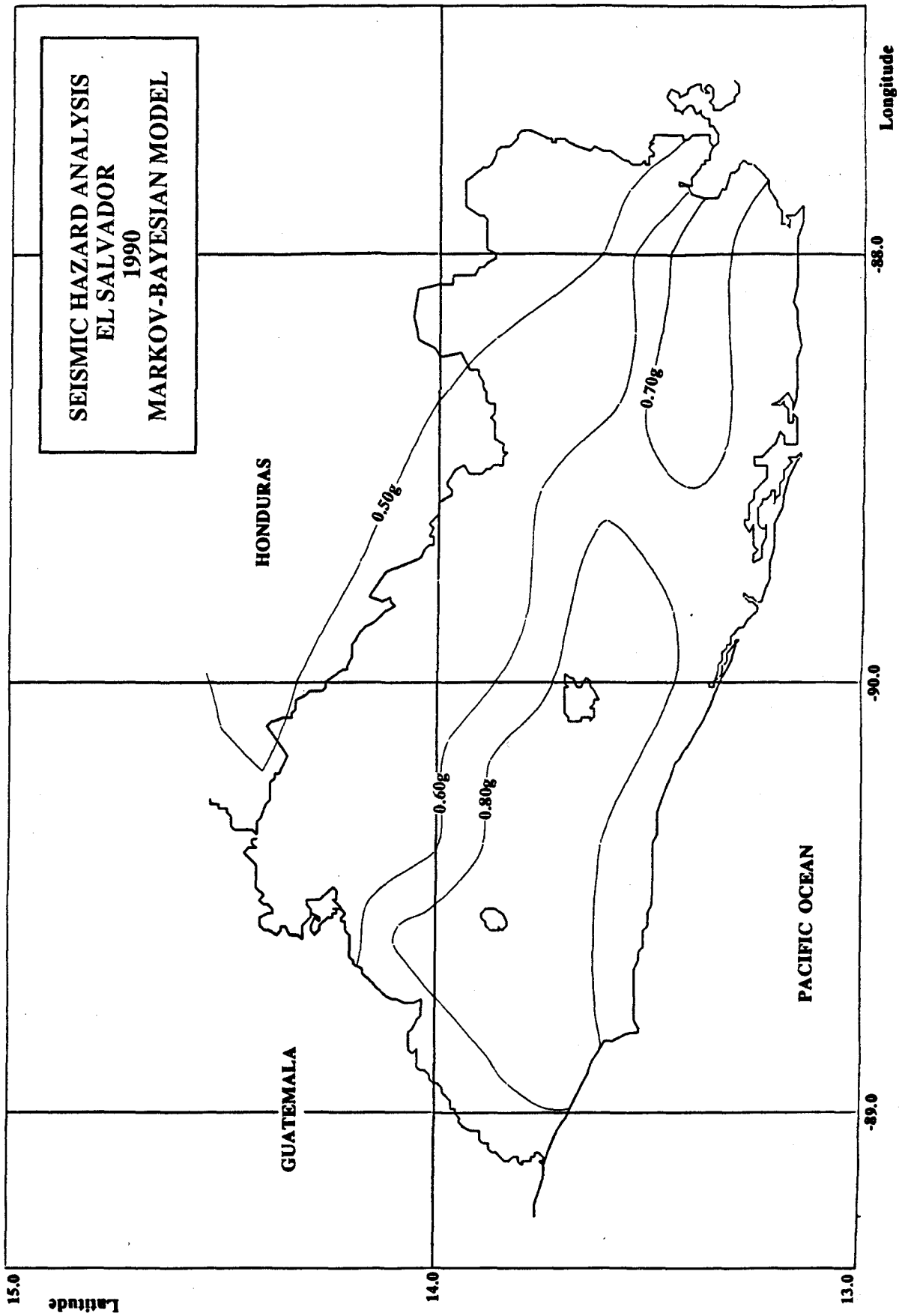


Figure 7.2. Preliminary iso-acceleration map for El Salvador for a future time of 50 yrs and 10% risk level.

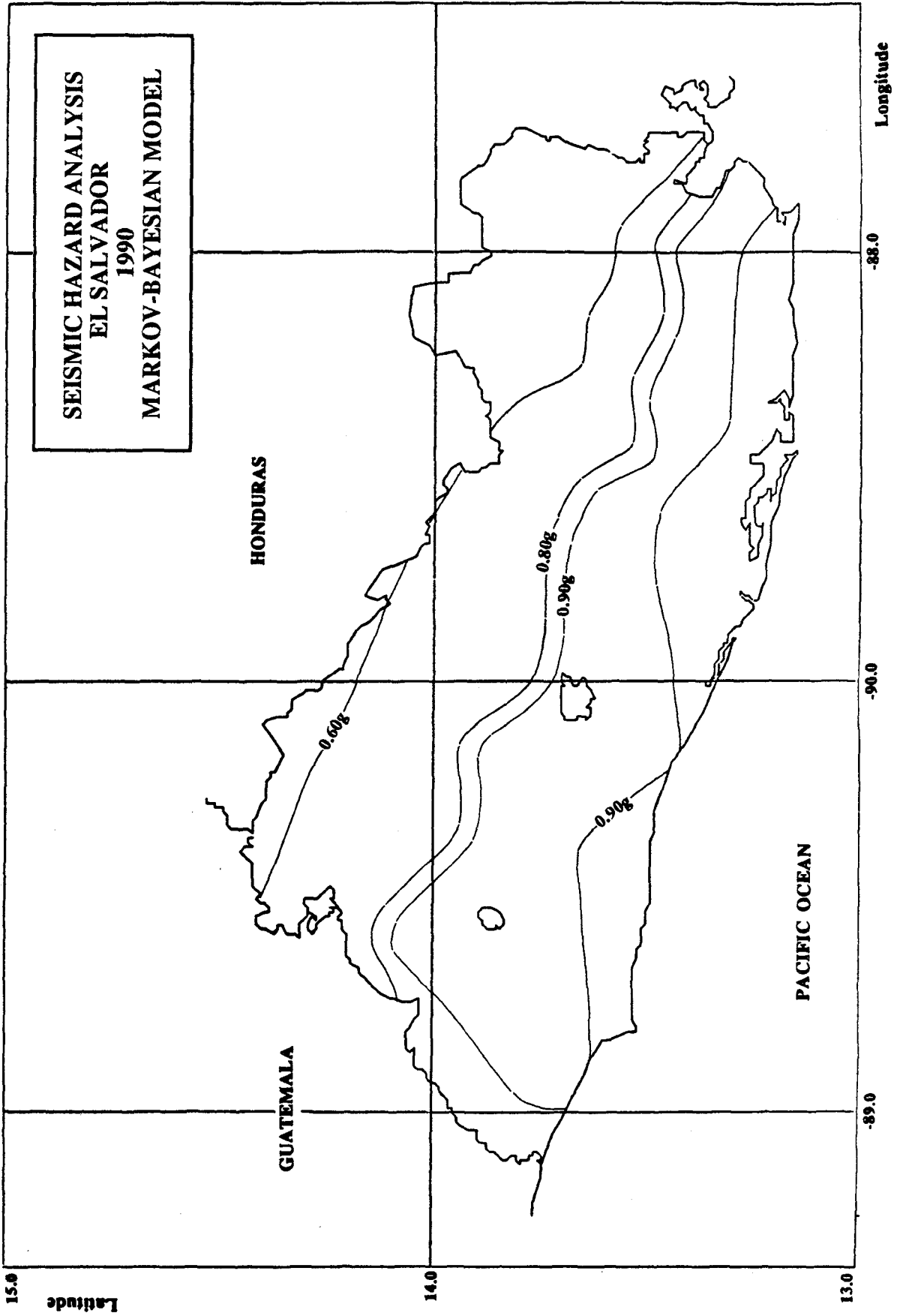


Figure 7.3. Preliminary iso-acceleration map for El Salvador for a future time of 100 yrs and 10% risk level.

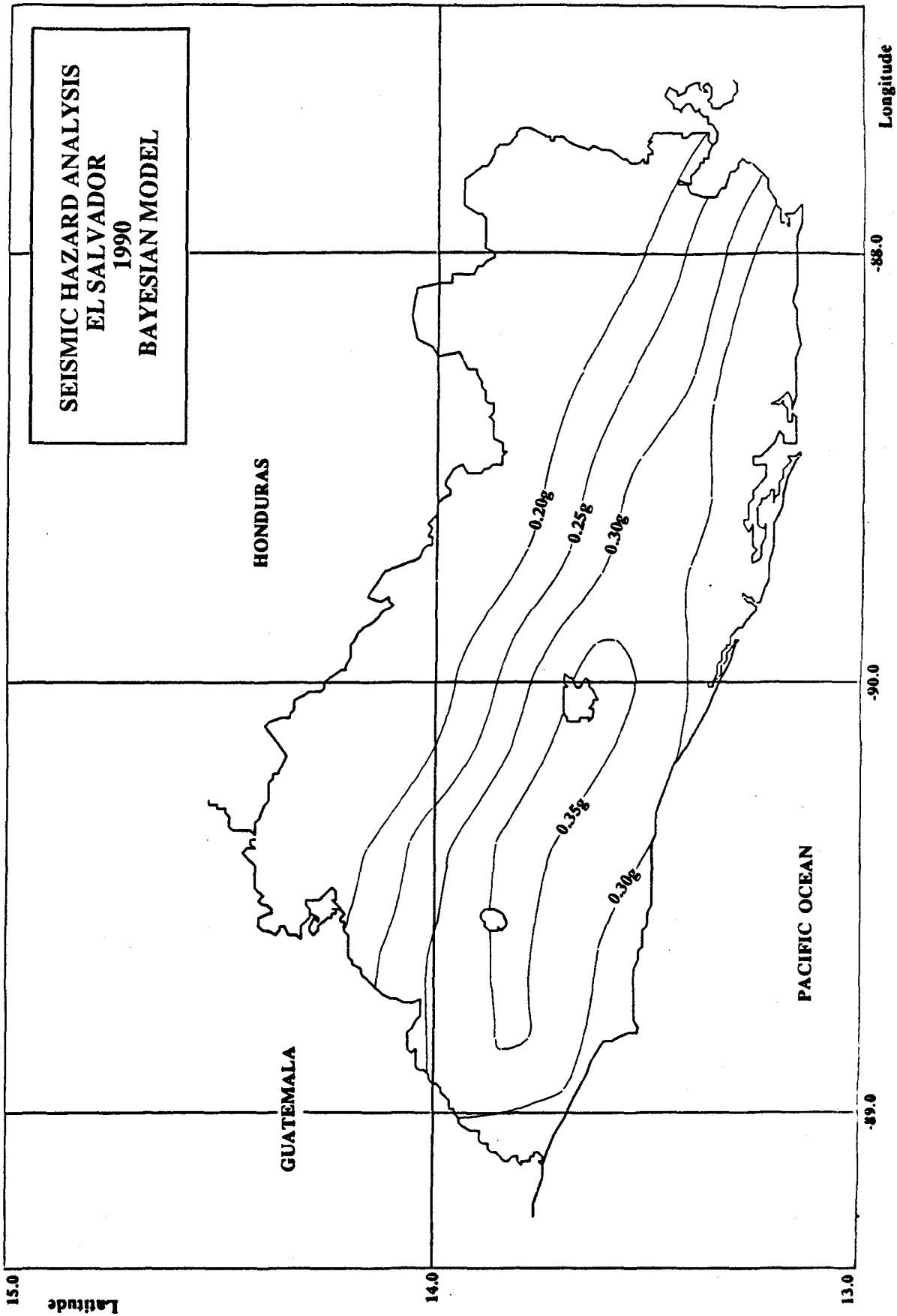


Figure 7.4. Preliminary iso-acceleration map for El Salvador for a future time of 20 yrs and 20% risk level.

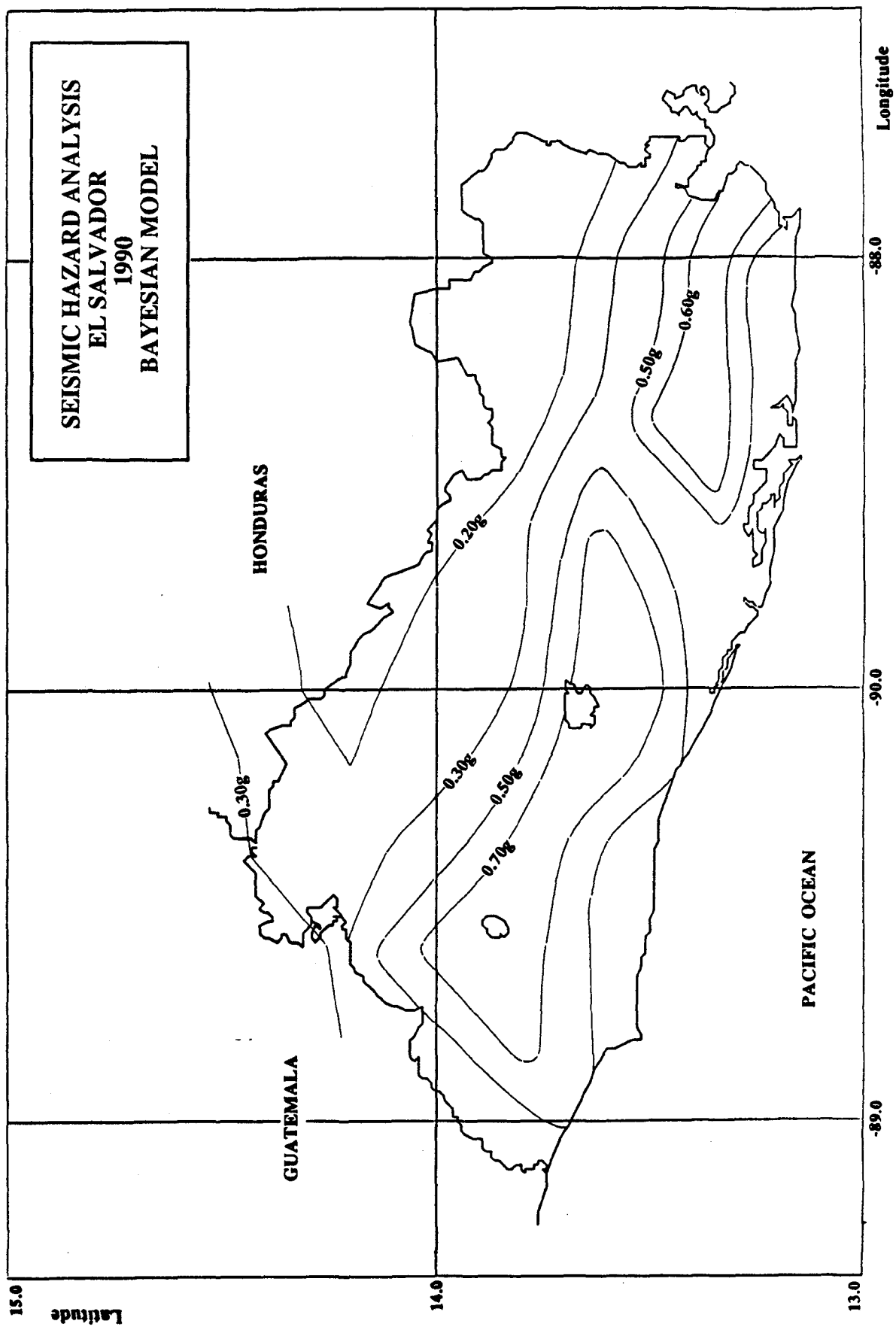


Figure 7.5. Preliminary iso-acceleration map for El Salvador for a future time of 50 yrs and 10% risk level.

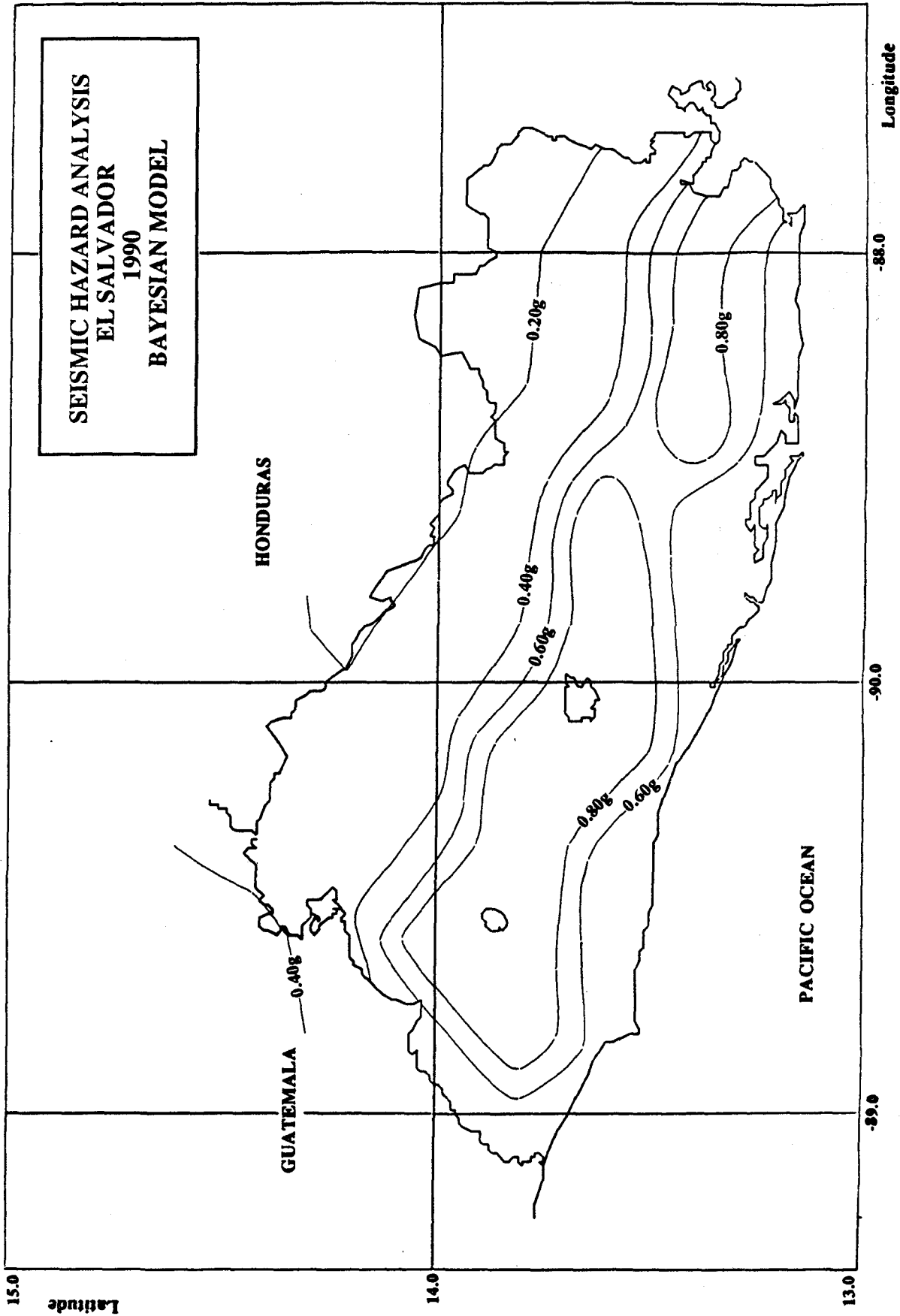


Figure 7.6. Preliminary iso-acceleration map for El Salvador for a future time of 100 yrs and 10% risk level.

7. Acajutla
8. La Union
9. Puente Cuscatlan
10. Puente de Oro
11. Presa 5 de Noviembre

The cumulative distribution function of PGA at these eleven locations were computed by using the Markov-Bayesian model. Also, the hazard at these locations can be represented in terms of acceleration zone graphs (AZG) (Kiremidjian et al., 1979). Figures 7.7 to 7.17 show the AZGs for the locations previously indicated.

In order to indicate the implications of the AZGs, the relationship between an acceptable level of risk, return period, and economic life are reviewed (see also, Kiremidjian et al., 1977 and Kiremidjian et al., 1979). The CDF of PGA based on the Markov-Bayesian model is obtained for a specified future time period. This time period is related to the economic life of the structure or facility, and the probability at selected PGA value indicates the hazard associated with this PGA level. The return period of a PGA value for a specified economic life and corresponding hazard level can be computed based on the Binomial distribution. Considering this distribution, the probability of r successes in n independent Bernoulli trials, with probability p of success at each trial is given by

$$P_n(r) = \binom{n}{r} p^r (1-p)^{n-r} \quad (7.1)$$

Thus, the probability of zero successes in ten trials (years) is

$$P_{10}(0) = \binom{10}{0} p^0 (1-p)^{10} = (1-p)^{10}$$

Let $P_{10}(0) = (1-p)^{10}$ be equal to 0.90. Then the probability of no occurrence (or success) of a certain level of loading in ten years is given by 0.90 or $(1-p)^{10} = 0.90$. Hence, $p = 0.01048$ or return period $RP = 95$ years.

In other words, for a structure whose economic life is ten years and for a acceptable risk level of exceeding the specified loading level by 10%, the structure should be designed for a return period of 95 years. Table 7.1 gives the relationship between acceptable risk level, economic life, and return period. For instance, if the acceptable risk level is 20% for a structure whose economic life is 20 years, then the loading level should correspond to a return period of 90 years. If the structure is to be built in San Salvador, the corresponding PGA is approximately 0.52g. If the same structure for the same risk level is to be built in

San Miguel, the corresponding PGA level is approximately 0.34g. Thus, for a given class and use of structure, having the same economic life (20 years) and the same acceptable risk (20%) the two consistent PGAs in San Salvador and San Miguel are 0.52g and 0.34g, respectively. This is the concept of consistent risk design in regions with different seismicity levels. Figure 7.18 shows the graph relating the risk level, economic life and return period independently of any region. Once an acceptable risk level for a given economic life is selected for a given class and use of structure, the corresponding return period is immediately obtained from Figure 7.18. Then, based on the graph of return period versus peak ground acceleration (Figures 7.7 to 7.17), the loading at a site can be determined.

Let consider another example. Consider two separate classes of structures to be built in San Salvador. Let an office building with an economic life of 40 years have an acceptable risk level of 20% and a warehouse with a 10 year economic life have a 40% acceptable risk level. Referring to Figure 7.18, the return period for which the office

Economic life (years) \ Probability of exceeding %	10	20	30	40	50	100
10	95	190	285	390	475	950
20	45	90	135	180	225	449
30	29	57	84	113	140	281
40	20	40	59	79	98	196
50	15	29	44	58	72	145
60	11	22	33	44	55	110
70	9	17	25	34	42	84
80	7	13	19	25	31	63
90	5	9	14	18	22	44
95	4	7	11	14	18	34
99	3	5	7	9	11	22
99.5	2	4	6	8	10	19

Table 7.1. Return Period as a function of economic life and probability of non-exceedence. (Kiremidjian et al., 1979)

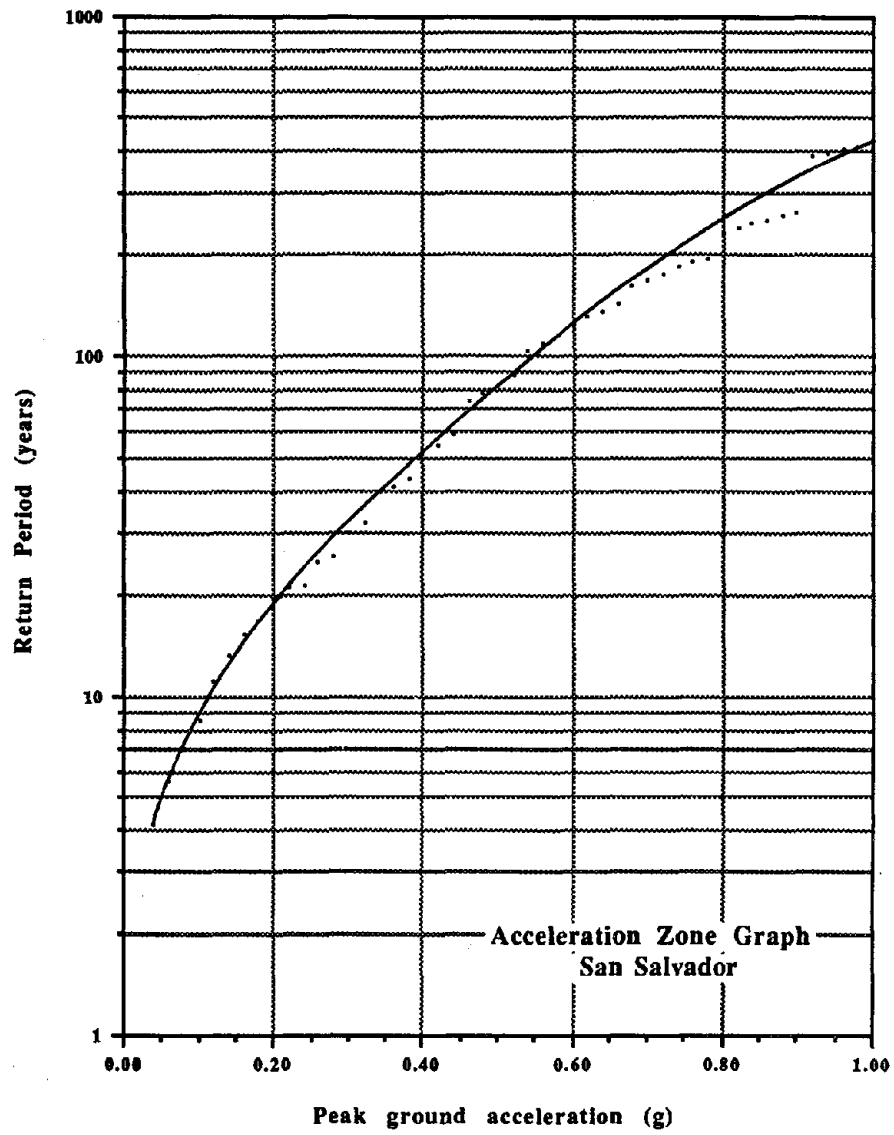


Figure 7.7.

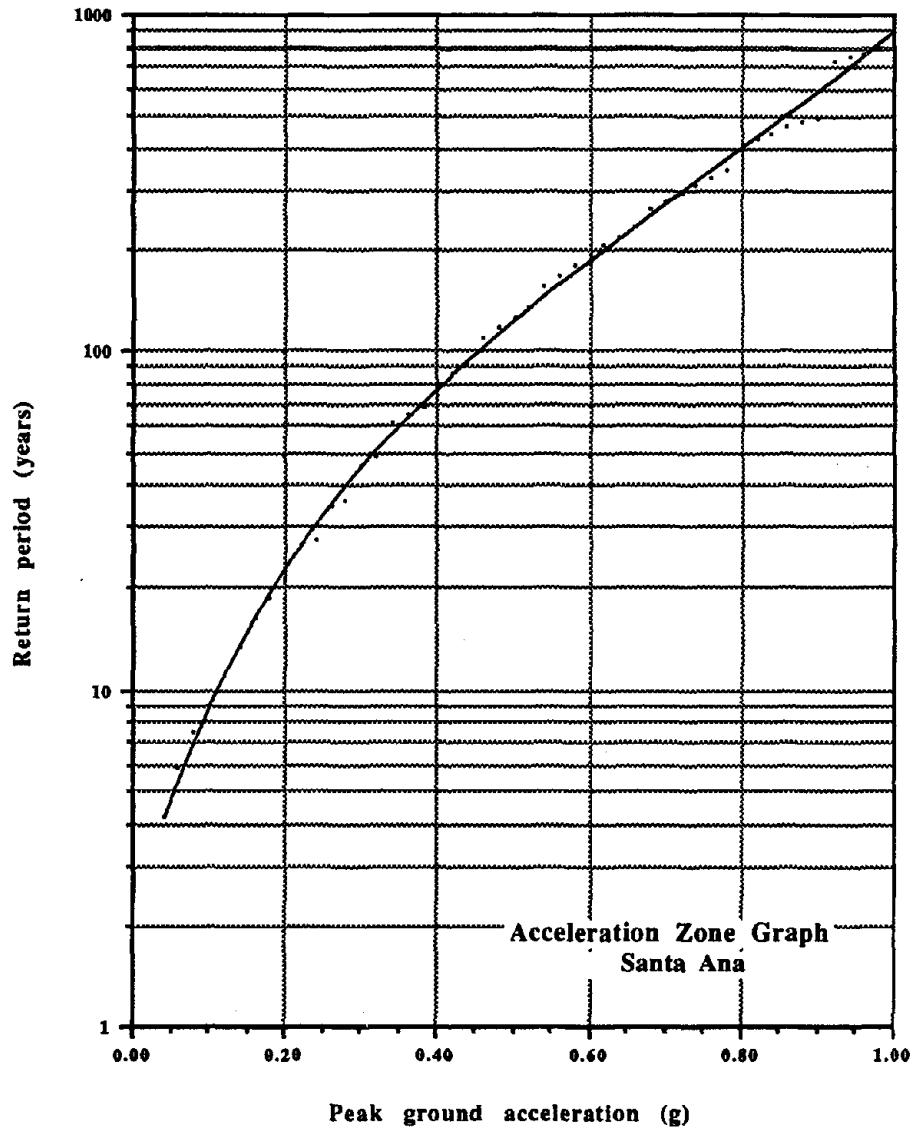


Figure 7.8.

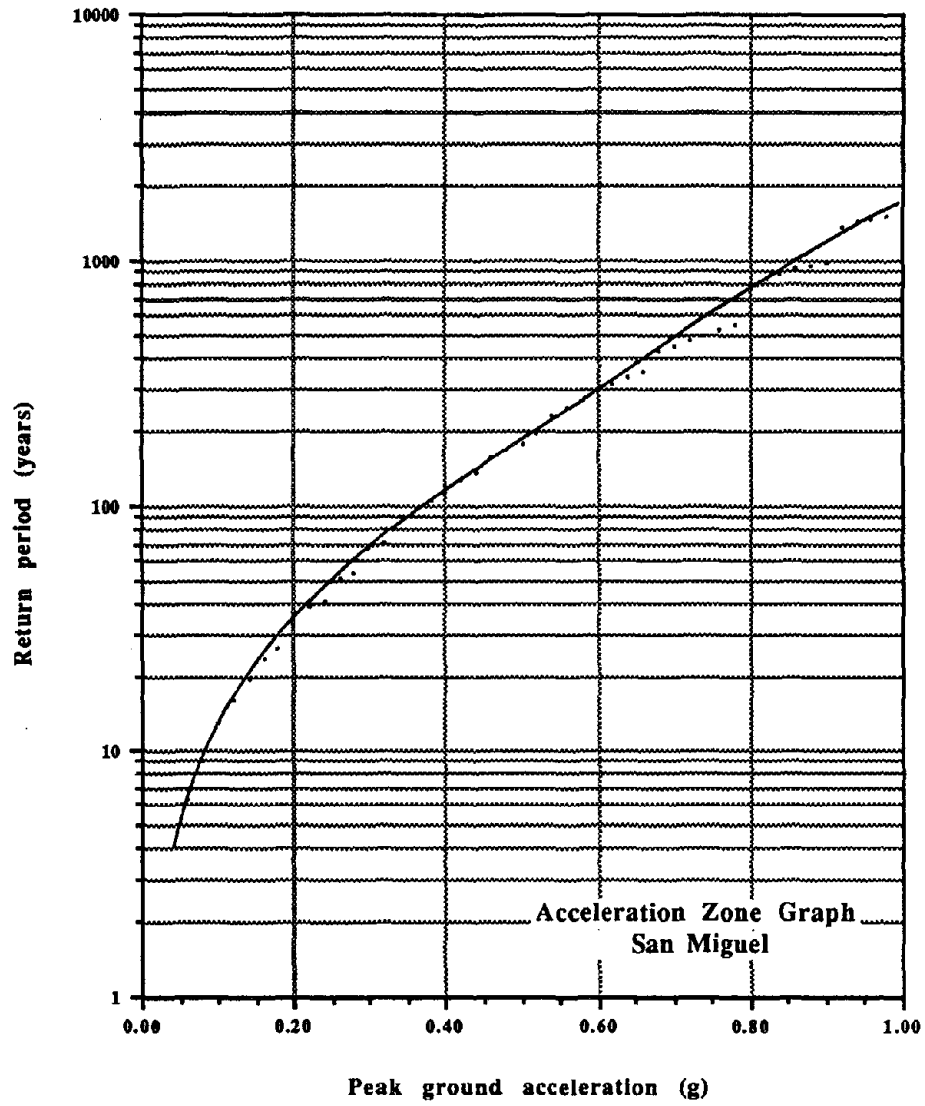


Figure 7.9.

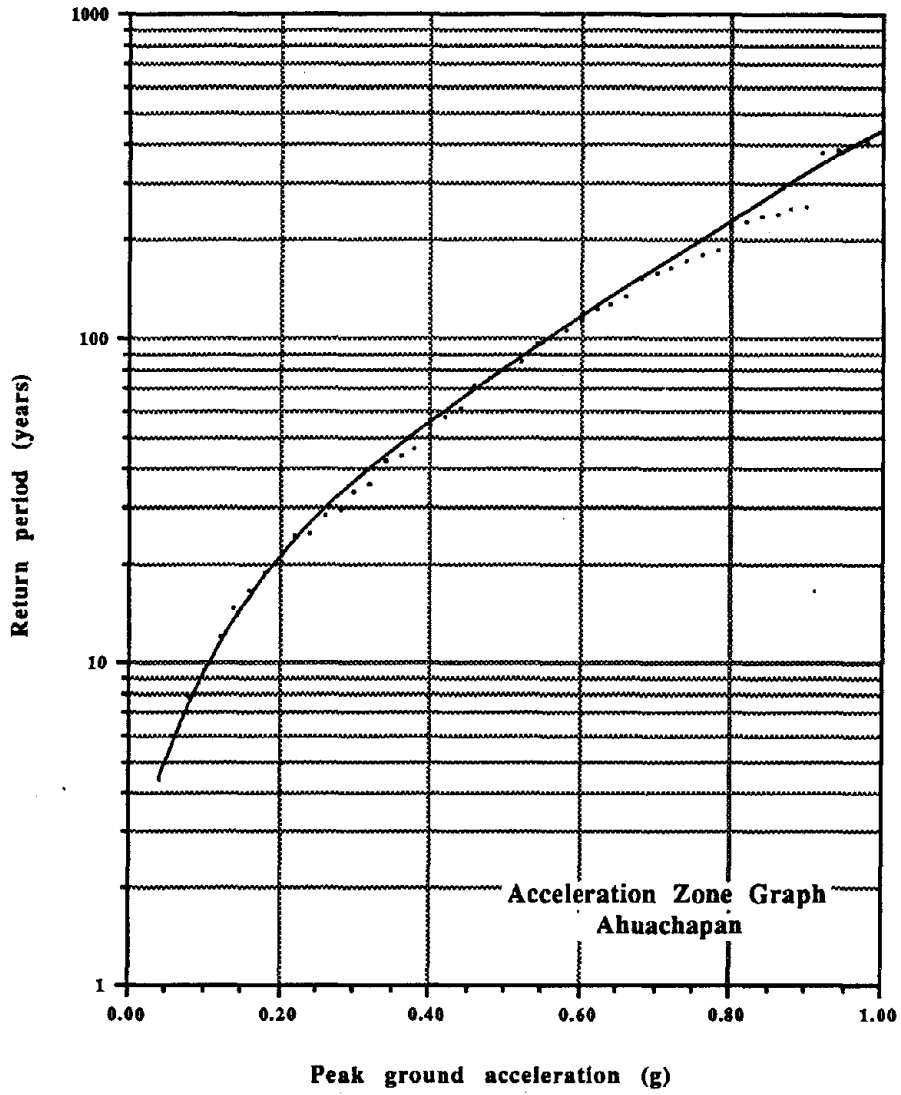


Figure 7.10.

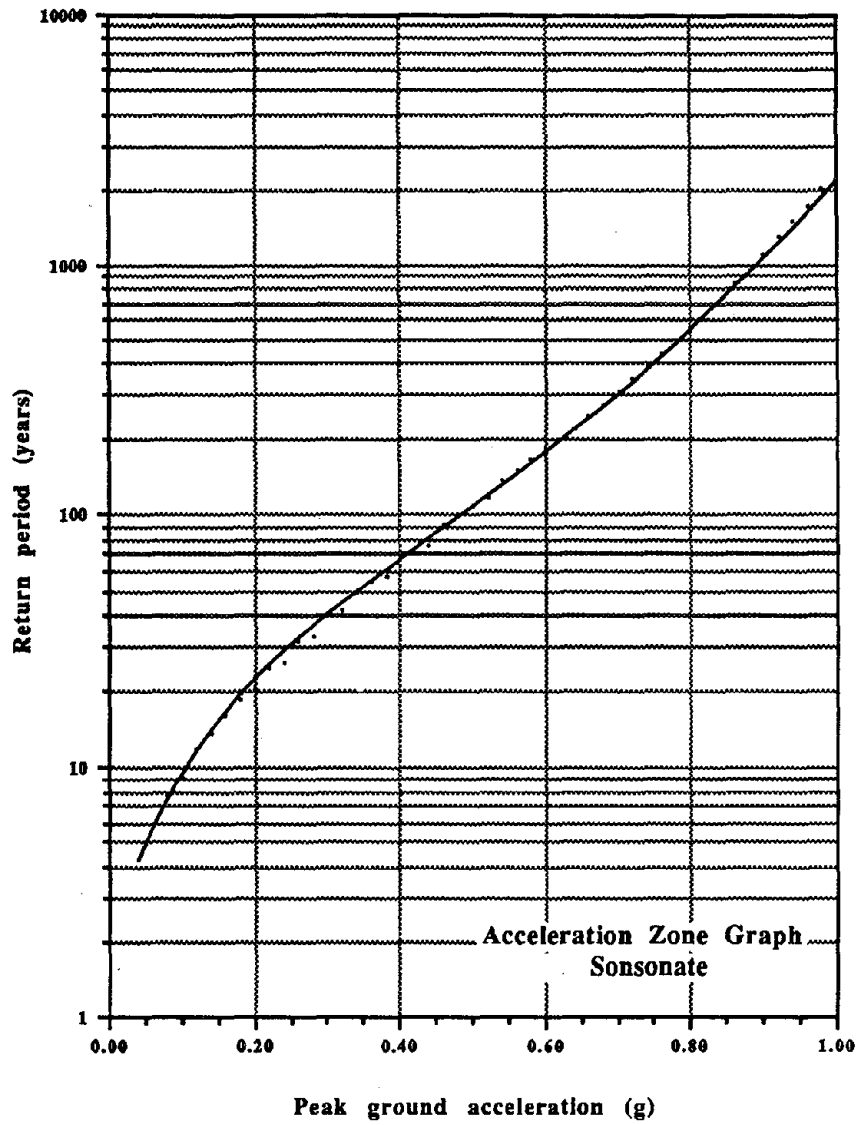


Figure 7.11.

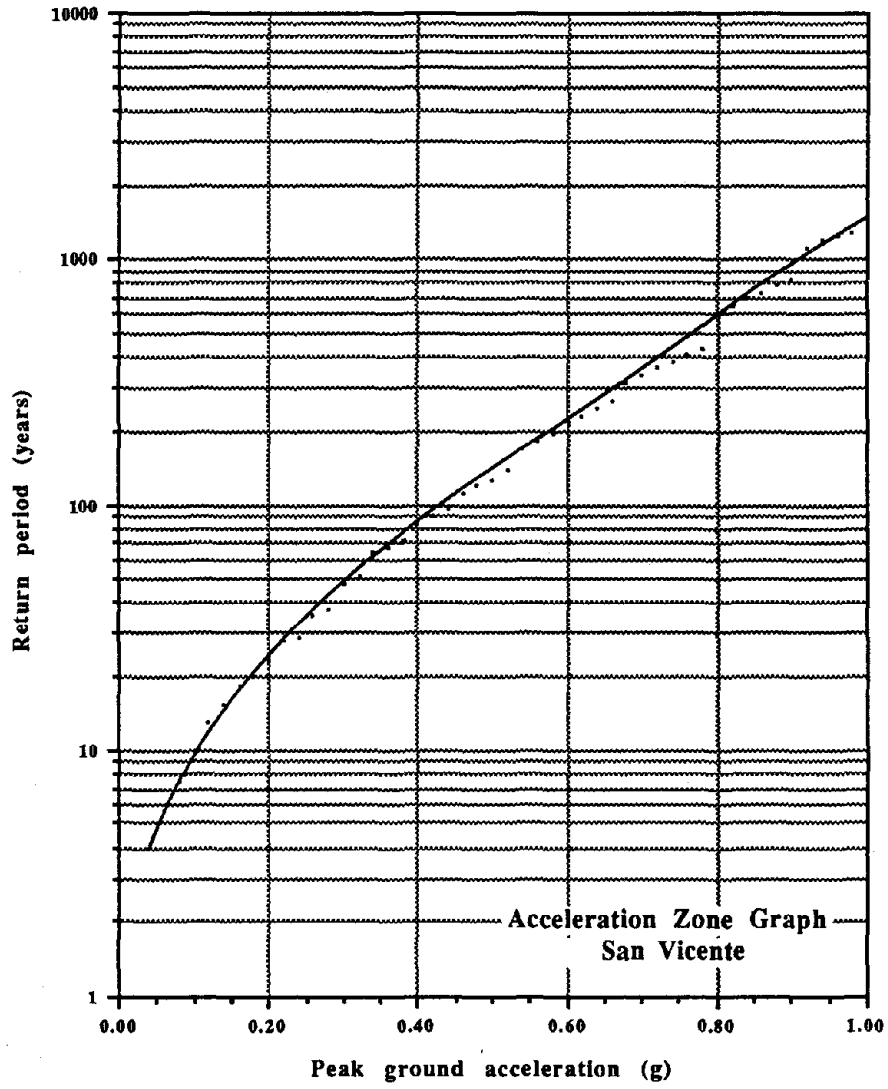


Figure 7.12.

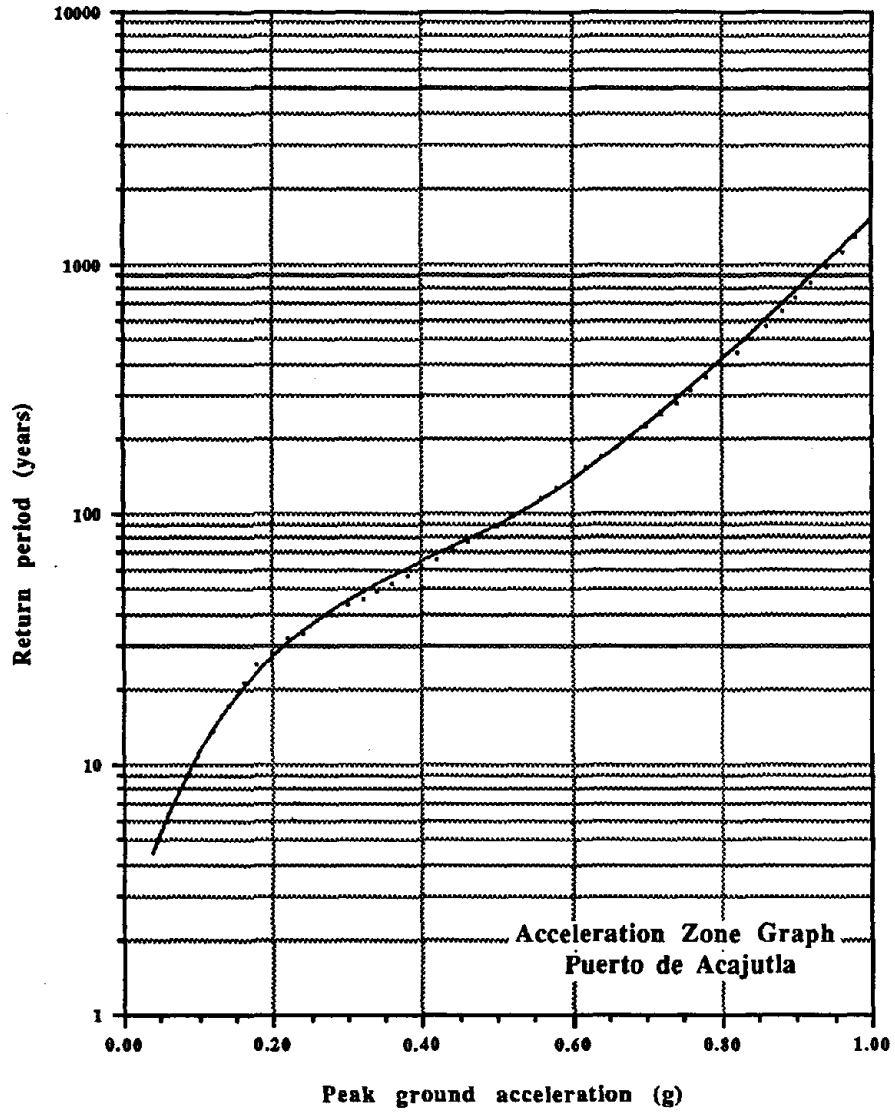


Figure 7.13.

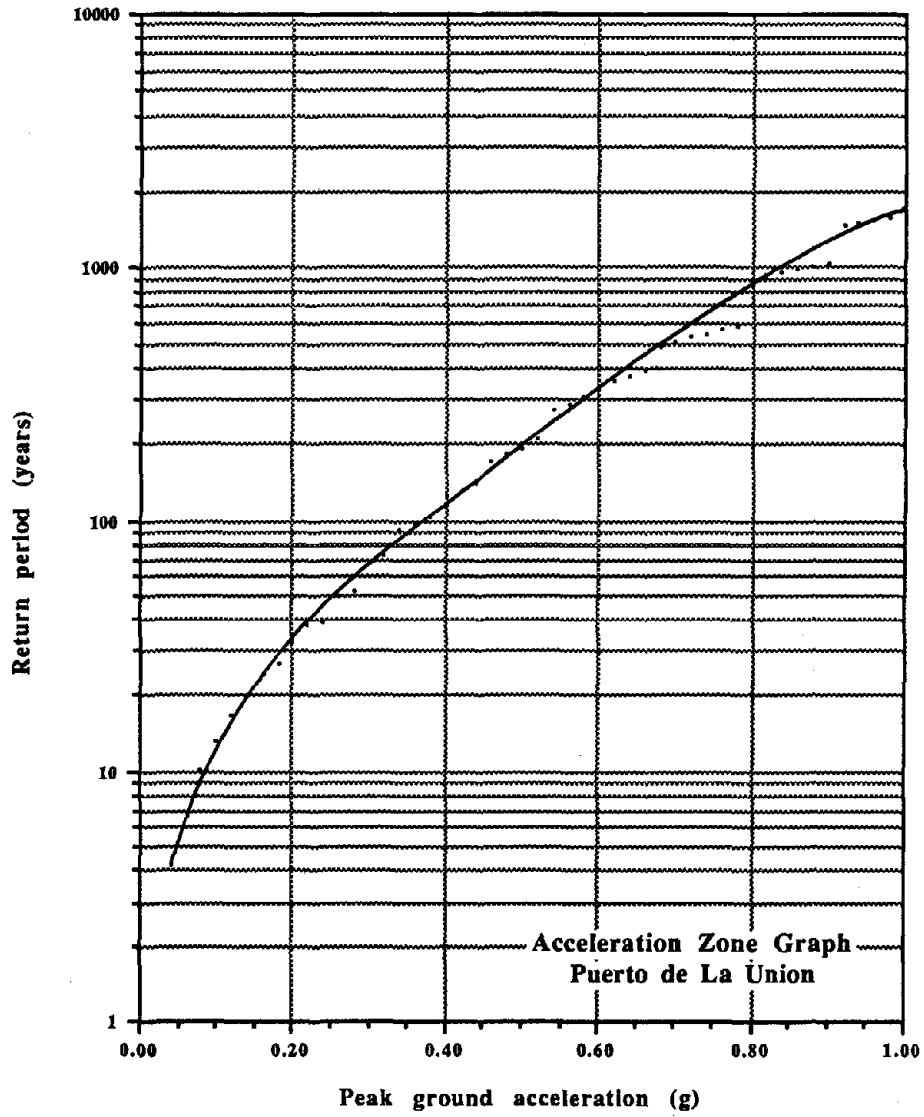


Figure 7.14.

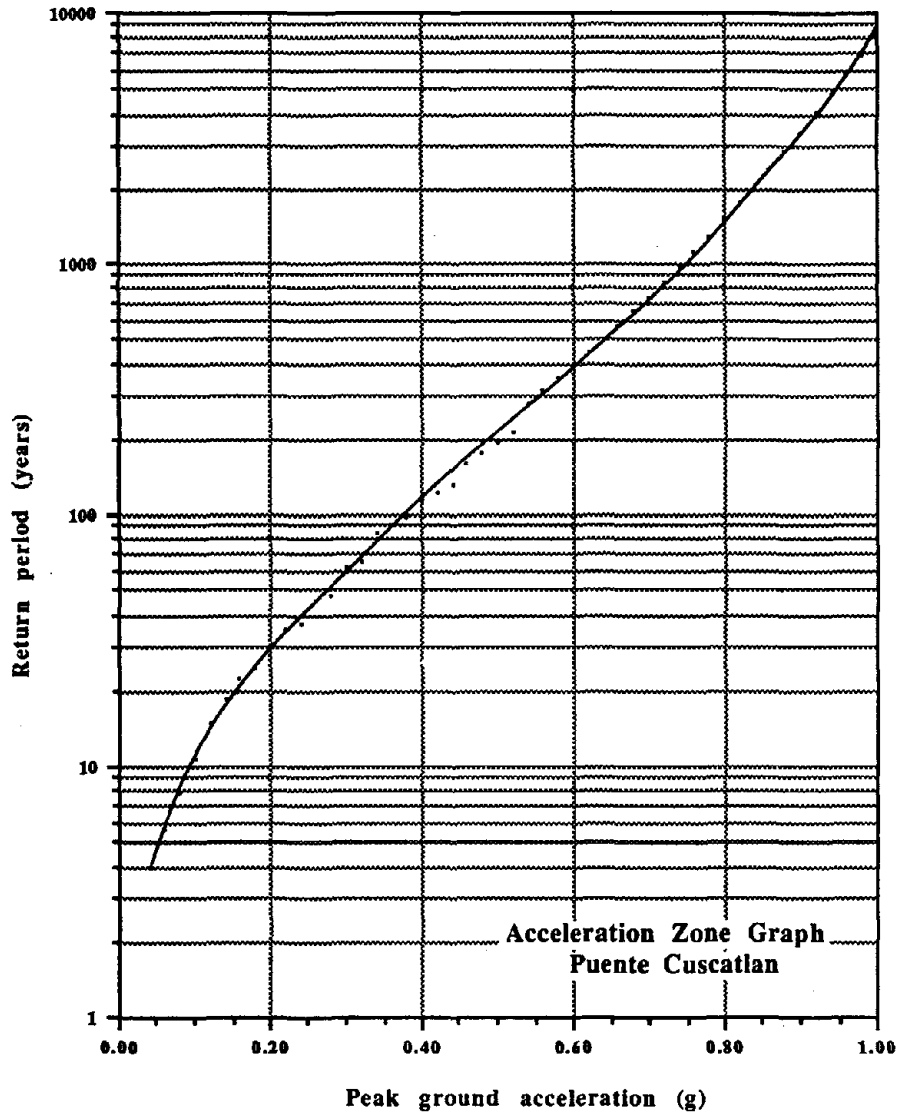


Figure 7.15.

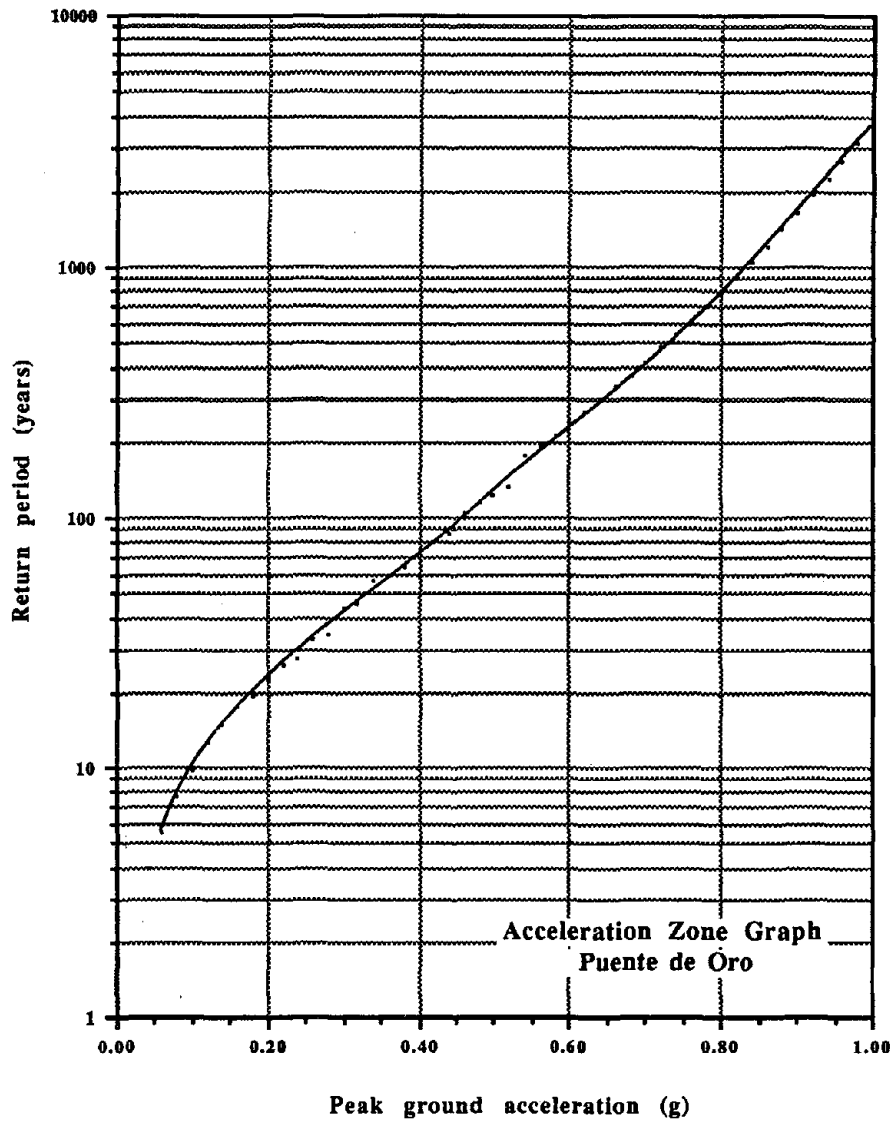


Figure 7.16.

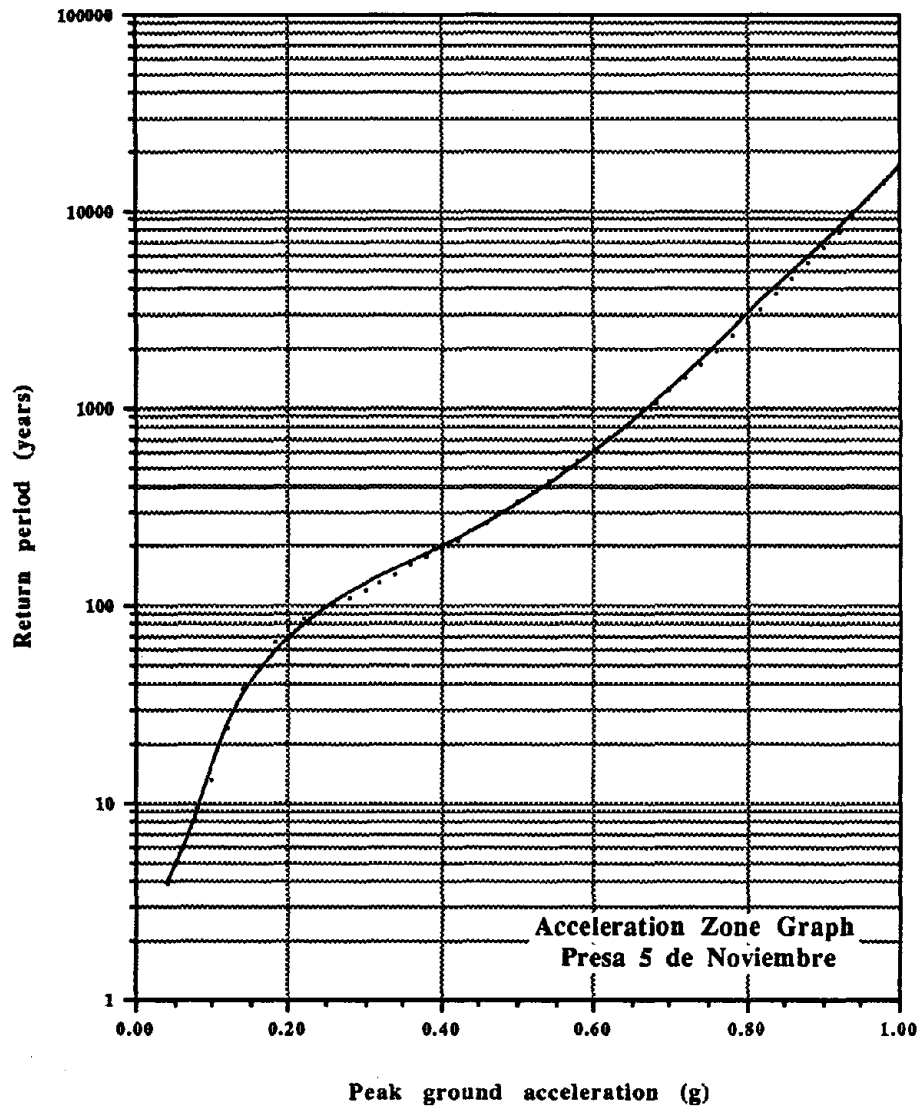


Figure 7.17.

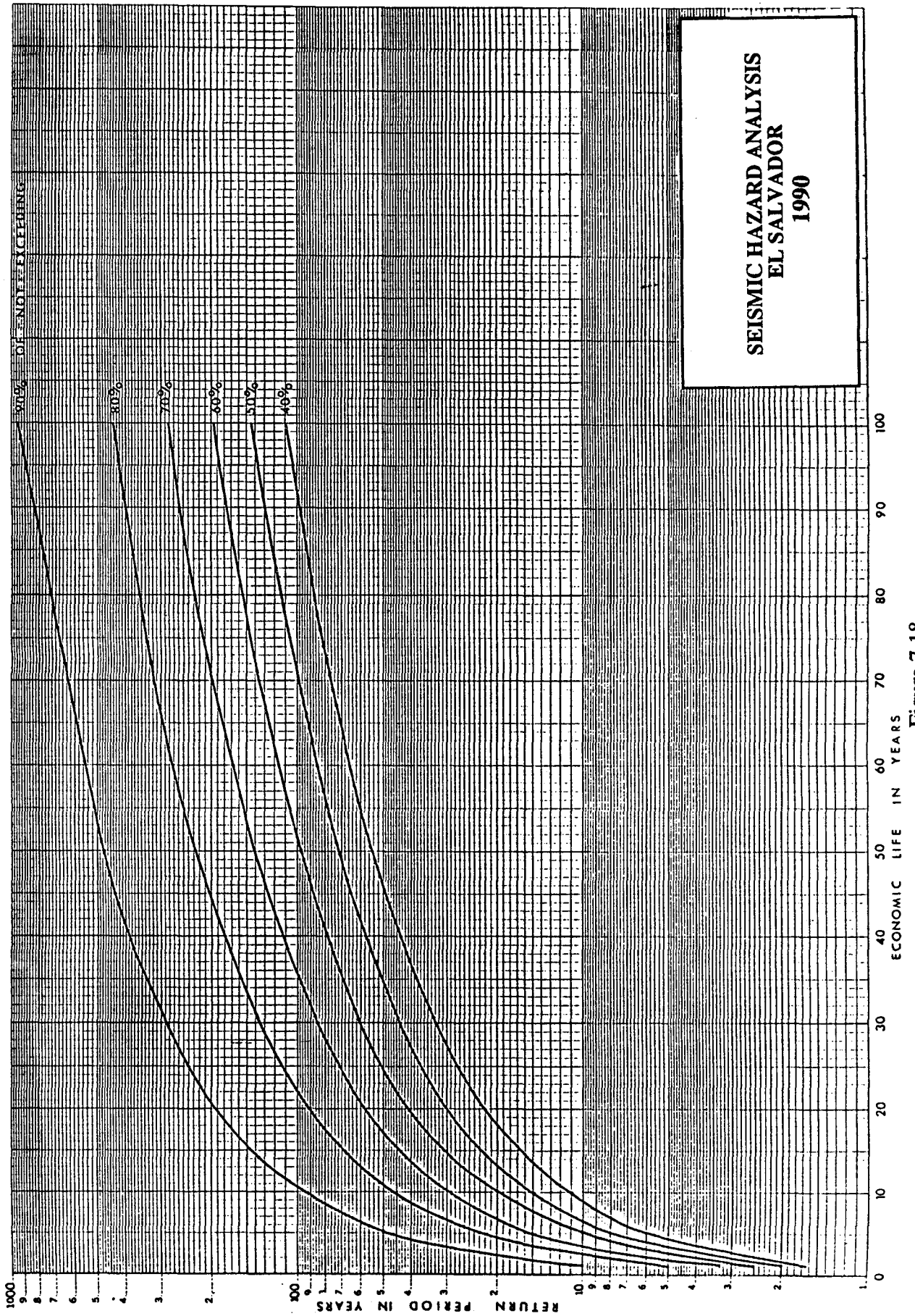


Figure 7.18.

building should be designed is 180 years and the return period for which the warehouse should be designed is 20 years. Now, from the San Salvador AZG (Figure 7.7), the corresponding PGA values are 0.70g and 0.20g for the office building and warehouse, respectively. If the same two facilities were to be built in San Miguel, the corresponding PGA values would be 0.39g and 0.14g.

It should also be indicated that even though the AZGs for San Salvador and Ahuachapan suggest for a return period of 1000 years a PGA greater than 1.0g, a 1.0g PGA value is recommended in this study for these cities. Further studies for these cities is strongly recommended taking in consideration local site conditions so that more accurate PGA values can be forecasted.

Finally, the following statements should be understood in using the concept of return period:

- 1) A return period is the mean waiting time for an event of interest. For example, the average (waiting) time between two events producing 0.20g in San Salvador is approximately 22 years.
- 2) The probability that an event corresponding to a return period RP will occur in any given year is given by $P = \frac{1}{RP}$. Thus, the probability of exceeding 0.20g in San Salvador in any given year is $1/22 = 0.0454$.
- 3) The probability that not a single event of the RP type will occur in RP years is given by $\frac{1}{e}$ where $e = 2.718$, the Naperian base. Thus, the probability that in 22 years, there will not be a single event producing a PGA of 0.20g in San Salvador is given by $1/e \approx 0.36$. Hence, there is a 64% chance that in 132 years there will be at least one event producing PGA of 0.20g or more in San Salvador.

For relative seismicity, it can be noticed in the AZGs charts (Figures 7.7 to 7.17) that San Salvador and Ahuachapan have the highest seismicity whereas the Presa 5 de Noviembre has the lowest seismicity. For a given hazard level, i.e. return period, a risk-consistent design for each location will demand the structure to resist a different level of PGA as specified in Figures 7.7 to 7.17. These types of figures are very useful in micro-zoning the country and formulation of building codes.

CHAPTER 8

SUMMARY AND CONCLUSIONS

This chapter summarizes the work conducted in this study. In addition, the main conclusions are indicated and some recommendations are made for the use of the results.

The seismic activity of the region of study was presented in terms of several tectonic provinces. These seismic regions: the Volcanic Chain Zone, the Benioff Zone, the Caribbean Plate Boundary and the Honduras Depression Zone were defined according to the seismic parameters of events occurred into the regions themselves, and the location of the faults between the zones.

An exhaustive search was conducted to obtain the existing data for the study region. Two kind of data were found: non-instrumental and instrumental. For both kind of data, a methodology of calculation of earthquake parameters was described and their relation to the seismic provinces was discussed. The acquired data was sorted according to the seismic provinces in which they occurred. This sorted data was analyzed to obtain frequency of earthquake occurrences with time in order to obtain the parameters needed for the probabilistic hazard models.

Two seismic hazard models were applied to the seismicity of the region, the stochastic slip-predictable and Bayesian models. Since the slip-predictable model was applied to only one seismic source, and since the computed peak ground accelerations resulted more conservative than using the Bayesian model for the same seismic source, a combined Markov-Bayesian model was adopted for the final seismic hazard computations. However, for comparison purposes hazard maps were also developed using only the Bayesian model. Iso-acceleration maps were developed for return periods of events of 100, 500 and 1000 years based on both models, the Markov-Bayesian and Bayesian models. In addition, acceleration zone graphs, which describe the peak ground acceleration values vs. return period, were developed for eleven locations in El Salvador.

Several aspects of the results obtained were found interesting to note:

- As it was expected, in seismic sources where enough information is available to apply the slip-predictable model, more conservative peak ground acceleration values were obtained.
- It was also observed that attenuation relationships developed for the region represent well the observed peak ground accelerations. Two attenuation functions were developed: near-field and far-field attenuation functions.
- It is also important to indicate that the presented iso-acceleration maps and AZGs graphs were computed for the Volcanic Chain soil conditions where a sharp fluctuation of peak ground accelerations have been observed for range of epicentral distances from 1 to 8 km. For more accurate hazard analysis in specific sites, local soil conditions studies should be performed.
- From the study of the seismic provinces of the region, the major sources of earthquake activity were found in the Benioff Zone. Additionally, a potential threat of a large earthquake ($M_s > 7.5$) in the near future from a Benioff seismic source 50 miles away from San Salvador was found. However, earthquakes occurring in local seismic sources were found more damaging than subduction earthquakes.
- The highest risk was observed along the axis of the Volcanic Chain where accelerations are higher than 0.80g for 500 years return period.
- The lowest risk was observed in the northern part of El Salvador where accelerations are less than 0.60g in 500 years return period.

Finally, it is recommended that the results obtained in this study should be further used in the development of seismic code formulation for structural analysis purposes. Ground acceleration values, a , may be established for a given structure and location and then converted to seismic load information. With this information, structures designed for these load levels, could have a desired reliability R_D of damage protection and a much higher reliability R_C against total building condemnation or incipient collapse during the lifetime of the structure.

REFERENCES

- Anagnos, T. and Kiremidjian, A.S., 1988, A Review of Earthquake Occurrence Models for Seismic Hazard Analysis: *Prob. Engr. Mech.*, 3, No. 1.
- Anderson, T.H., Burkat, B., Clemons, R.E., Bohnenberger, O.H. and Blount, D.N., 1973, Geology of the Western Altos Cuchumatanes, Northwestern Guatemala: *Geol. Soc. Am. Bull.*, 84, 805-826.
- Aki, K., 1966, Generation and Propagation of G Waves from the Nigata Earthquake of June 16, 1964: Estimation of Earthquake Movement, Released Energy and Stress-Strain Drop from G Wave Spectrum: *Bull. Earthq. Res. Inst.*, 44, 23-88.
- Bonilla, M.G., Mark, R.K. and Lienkaemper, J.J., 1984, Statistical Relations Among Earthquake Magnitude, Surface, Rupture Length, and Surface Fault Displacement: *Bull. Seism. Soc. Am.*, 74, 2379-2411.
- Boore, D.M. and Joyner, W.B., 1982, The Empirical Prediction of Ground Motion: *Bull. Seism. Soc. Am.*, 72, No. 6, S43-S60.
- Bucknam, R.C., Plafker, G. and Sharp, R.V., 1978, Fault Movement (Afterslip) Following the Guatemala Earthquake of February 4, 1976: *Geol.*, 6, 170-173.
- Burbach, G., Van, N., Frohlich, C., Pennington, W.D. and Matumoto, T., 1984, Seismicity and Tectonics of the Subducted Cocos Plate: *Jour. of Geo. Resch.*, 89, 7719-7735.
- Campbell, K., 1981, Near-Source of Peak Horizontal Acceleration: *Bull. of Seism. Soc. Ame.*, 71, No.6, 2039-2070.
- Carr, M.J., Rose Jr., W.I. and Stoiber, R.E., 1982, Regional Distribution and Character of Active Andesitic Volcanism: Central America, in *Andesites: Orogenic Andesites and Related Rocks*, edited by R.S. Thorpe, 149-166, John Wiley, New York.
- Carr, M.J. and Stoiber, R.E., 1977, Geologic Setting of Some Destructive Earthquakes in Central America: *Geol. Soc. Am. Bull.*, 88, 151-156.
- Chiang, W., Guidi, G.A., Mortgat, C.P., Schoof, C.C. and Shah, H.C., 1984, *Computer Programs for Seismic Hazard Analysis: The John A. Blume Earthquake Engineering Center, Stanford University, Report No. 62.*
- Consorzio Salvador e., 1988, San Salvador-Programa di Ricostruzione. *Direzione Generale per la Cooperazione allo Sviluppo*. Repubblica Italiana, Ministero degli Affari Esteri.
- Davies, G. and Brune, J., 1971, Regional and Global Fault Slip Rate from Seismicity: *Natr. Phys. Sci.*, 229, 101-107.
- Dean, B.W. and Drake, C.L., 1978, Focal Mechanism Solutions and Tectonics of the Middle America Arc: *Jour. Geol.*, 86, No. 1, 111-128.

- Dengo, G. and Bohnenberger, O., 1969, Structural Development of Northern Central America: *Am. Assoc. Pet. Geol. Mem.*, 11, 203-220.
- Esteva, L. and Villaverde, R., 1973, Seismic Risk Design Spectra and Structural Reliability: *Proceedings of Fifth World Conference on Earthquake Engineering*, Rome, Italy, 2586-2597.
- Hasegawa, H.S., Basham, P.W. and Berry, M.J., 1981, Attenuation Relations for Strong Seismic Ground Motion in Canada: *Bull. Seism. Soc. Am.*, 71, 1943-1962.
- Harlow, D.H., White, R.A., Rymer, M.J., Alvarez, S. and Martinez, C., The San Salvador Earthquake of October 10, 1986 and Its Historical Context, paper in preparation.
- Heaton, T.H., Tajima, F. and Mori, A.W., 1982, Estimating Ground Motions Using Recorded Accelerograms. Report by Dames and Moore to Exxon Production Res. Co., Houston.
- Joyner, W. and Boore, D.M., 1988, Measurement, Characterization, and Prediction of Strong Ground Motion. *Proceedings of Earthquake Engineering and Soil Dynamics II, GTDN/ASCE*, Park City, Utah, June 27-30.
- Kelleher, J.A., Sykes, L.R. and Oliver, J., 1973, Possible Criteria for Predicting Earthquake Locations and their Applications to Major Plate Boundaries of the Pacific and Caribbean: *Jour. Geophys. Res.*, 78, 2547-2585.
- Kiremidjian, A.S., Shah, H.C. and Lubetkin, L., 1977, Seismic Hazard mapping for Guatemala: Report No. 26, The John A. Blume Earthquake Engineering Center, Stanford University.
- Kiremidjian, A.S. and Anagnos, T., 1984, Stochastic Slip-Predictable Model for Earthquake Occurrences: *Bull. Seism. Soc. Am.*, 74, 739-755.
- Kiremidjian, A.S., Sutch, P. and Shah, H.C., 1979, Seismic Hazard Analysis of Honduras: Report No. 38, The John A. Blume Earthquake Engineering Center, Stanford University.
- Kiremidjian, A.S. and Suzuki, S., 1987, A Stochastic Model for Site Ground Motions from Temporally Dependent Earthquakes: *Bull. Seism. Soc. Am.*, 77.
- Knudson, C.F., and Hausen, F., 1973, Accelerograph and Seismoscope Records from Managua, Nicaragua Earthquake: *EERI Conference Proceedings*, San Francisco, California, 1, 181-203.
- Lomnitz, C. and Schultz, R., 1966, The San Salvador Earthquake of May 3, 1965: *Bull. Seis. Soc. Am.*, 56, No. 2, 561-575.
- Molnar, P. and Sykes, L.R., 1969, Tectonics of the Caribbean and Middle America Region from Focal Mechanisms and Seismicity: *Geol. Soc. Am. Bull.*, 80, 1639-1684.
- Mortgat, C.P. and Shah, H.C., 1979, A Bayesian Model for Seismic Hazard Mapping: *Bull. Seism. Soc. Am.*, 69, 1237-1251.

- Neter, J., Wasserman, W., and Kutner, M. H., 1985, Applied Linear Statistical Models. *Richard D. Irwin Inc.*, second edition.
- Sabetta, F. and Pugliese, A., 1987, Attenuation of Peak Horizontal Acceleration and Velocity from Italian Strong-Motion Records: *Bull. Seism. Soc. Am.*, 77, 1491-1513.
- Sanchez, E.I. and Mojica, J.A., 1984, Estudio de Espectros de Respuesta para el Area Metropolitana de San Salvador como Base para una Microzonificacion Sismica: Tesis para optar al grado de Ingeniero Civil, Universidad Centroamericana "Jose Simeon Canas", San Salvador.
- Schwartz, D.P., Cluff, L.S. and Donnelly, T.W., 1979, Quaternary Faulting Along the Caribbean-North American Plate Boundary in Central America: *Tectonophysics*, 52, 431-445.
- Schwartz, D.P., Coppersmith, K.J. and Swan III, F.H., 1984, Methods for Estimating Maximum Earthquake Magnitude: *Eighth World Conference of Earthquake Engineering*, I, 279-285.
- Shakal, A.F. and Bernreuter, D.L., 1981, Empirical Analysis of Near-Source Ground Motion: U.S. Nuclear Regulatory Commission NUREG/CR - 2095.
- Shakal, A., Huang, M. and Linares, R., 1987, The San Salvador Earthquake of October 10, 1986 - Processed Strong Motion Data: *Earthq. Spec.*, 3, No. 3.
- Singh, S.K., Mena, E., Castro, R. and Carmona, C., 1987, Empirical Predictions of Ground Motion in Mexico City from Coastal Earthquakes: *Bull. Seism. Soc. Am.*, 77, No. 5, 1862-1867.
- Shah, H.C., Mortgat, C.P., Kiremidjian, A.S. and Zsutty, T.C., 1975, A Study of Seismic Risk for Nicaragua, Part I: The John A. Blume Earthquake Engineering Center, Report No. 11, Department of Civil Engineering, Stanford University.
- Thatcher, W. and Hanks, T.C., 1973, Source Parameters of Southern California Earthquakes: *Jour. Geophys. Res.*, 86, 5053-5060.
- Utsu, T. and Seki, A., 1954, A Relation Between the Area of Aftershock Region and the Energy of Main Shock: *Jour. Seism. Soc. Jpn.*, 7, 233-240.
- White, R.A., 1988, Catalog of Historic Seismicity in the Vicinity of the Chixoy-Polochic and Motagua Faults, Guatemala: Open-File Report 84-88, U.S.G.S., Menlo Park, California.
- White, R.A. and Cifuentes, Q., Seismic History of the Middle America Trench Spanning the Guatemala Triple Junction and an Earthquake Forecast for Western El Salvador: Submitted to B.S.S.A.
- White, R.A. and Harlow, D.H., Hypocentral Parameters of Significant Shallow Volcanic Chain Earthquake of Central America Since 1900: Submitted to B.S.S.A.

White, R.A., 1985, The Guatemala Earthquake of 1816 on the Chixoy-Polochic Fault:
Bull. Seis. Soc. Am., 75, No. 2, 455-473.

APPENDIX A

EARTHQUAKE DATA FROM 1525 TO 1710

TABLE 2. EARTHQUAKES ALONG CHIAPAS, MEXICO TO EL SALVADOR (ALL SOURCES) FROM 1525 TO 1710

Year Mo/Dy	Int(MM):Location	Description	[duration]
1526 7/20	VIII: Antigua; VII?: VFuego(G), StaAna(S) SSalvador(S); VI-7: Tecpan(G)	(8/15?) earthquake knocked down soldiers; affected affected; apparently unaffected	[long]
1530 5/29	Int?: Ciudad Vieja, Quezaltenango, SMarcos(G)	great earthquakes	
1533, early	Int?: Guatemala(G), Tehuantepeque(M)	It shook often; events stronger in Guatemala than Tehuantepeque	
1556	VI-VII: SSalvador(S)	minor damage from several earthquakes	
1565 8/30	VIII: Antigua, Comalapa, Almolonga, Solola VII+: Escuintla, Chimaltango(G), lasCasas(M)	there was a great earthquake; many houses fell extraordinary violence	["3 psalms" -490? sec]
1566 5	VIII: Quezaltenango, Taxisco(G), Sonsonate(S)	houses collapsed; aftershocks for 9 days	
1575	VIII: Chiapas(M) to Nicaragua, Antigua(G)	great destruction in all of Chiapas province to that of to Nicaragua	
1575 6/02	VIII: SSalv, Sierra Texcuangos towns(S)	(5/23?) let major earthquake here; all houses fell earthquakes; considerable damage	
1576	VII: Antigua(G)	earthquake at midnight destroyed many buildings	[3 hrs]
1577 11/29	VIII: Antigua, SMarcos, Solola(G)	total destruction; church ruined	
1581	VIII: SSalvador(S)	began 2 yrs of earthquakes less than 9 days apart; many dead	
1585 1/16	VII+: Antigua, Solola(G)	earthquake destroyed some houses	
1586 12/05	VII: Antigua; VI: Solola(G)	church buildings and 160 poorer houses ruined	
1586 12/23	VII-VIII: Antigua(G)	cathedral tower and main chapel destroyed	
1591 3/14	VIII: las Casas(M)	13 dead; 1 great shake..for an instant (shallow?)	[instant]
1594 4/21	VII-VIII: SSalvador(S)	buildings cracked/ruined; 29 dead; aftershocks for 4-6 months	
1607 10/09	VII: Antigua(G)	hospital damaged; earthquakes (aftershocks?) for 9 days	
1631 2/18	VII: Antigua; VI+: Mixco(G)	great earthquakes; church destroyed	
1650	VIII: SSalvador(S)	all buildings badly damaged; aftershocks to mid-April;	
1651 2/18	VII-VIII?: Antigua, Amatlan(G)	old facade of cathedral damaged	
1652	VII-: las Casas(M)	destroyed buildings; worst in 70 years	["1 creed" -30+ sec]
1658(1656?)	VIII: SSalvador + Sonsonate provs(S)	earthquakes alarmed populace	
1659	VI: Antigua(G)	partial ruin; series of earthquakes, worst on 5/01	
1663 5/01	VII-?: Antigua(G)	partial ruin	
1666	VII-?: Antigua(G)	all buildings fell/unusable; greatest earthquake here so far	
1671 8/16	VIII: SSalvador(S)	great earthquake (damage?)	
1676+	VI-VII?: Andres Itzapa, Antigua(G)	church very badly damaged by earthquakes	
1679 3/04	VII+: Comalapa; VI+: Antigua(G)	series of earthquakes, worst on 7/22	
1681 7/22	Int?: Antigua(G)	series of earthquakes	
1683 5	Int?: Antigua(G)	series of earthquakes	
1684 8	Int?: Antigua(G)	series of earthquakes	
1687+	VII?: las Casas(M)	damage	
1687- 9,10	Int?: Antigua(G)	earthquakes	
1688 10/10	VII: Mexico, Guatemala, (VII+: Chiapas?)	earthquake felt	
1689 2/12	VIII: SPedro Ruertas, Antigua(G)	all major buildings destroyed	
1689 2/23	VIII: Antigua(G)	stronger than event of 2/12/89	
1691	VII?: Antigua(G)	damage	
1693	Int?: SNIquei(S)	earthquake and thundering sounds	
1702 8/14	VII+: Ahuachapan(S)	church ruined	
1707	Int?: SSalvador(S)	possible earthquake	

Abbreviations used in Tables 1 to 3: Int(MM) is an estimate of Modified Mercalli (MM) intensity, Int? indicates intensity unknown; Location, S -San, Sta -Santa, V -Volcano, L -Lake; prov(s) -Province(s), n, s, e, w -northern, southern, eastern, and western, respectively; town names having three words are shortened as San Pedro Nonualco -SPNonualco; countries are abbreviated as (M) -Mexico, (G) -Guatemala, and (S) -El Salvador; Description, q(s) -earthquakes, foq(s) -foreshock(s), aftq(s) -aftershocks, bids -buildings; under H_{int} is an estimate of the moment magnitude from the maximum diameter of the Modified Mercalli Intensity VII (L_{VII}) and VIII (L_{VIII}) contours; Duration of felt shaking is given in {} under [duration] in seconds unless minutes are specified; M_s is instrumentally-determined surface wave magnitude, unless mb -body wave magnitude or M_t -tsunami magnitude (Abe, 1979) is specified, or, if preceded by M indicates a "unified magnitude" from Gutenberg and Richter (1954); M_s is from Abe (1981) unless followed a three letter station code; Instrumental locations are from the NOAA hypocenter file unless followed by (K) -Kellerer and others (1973).

APPENDIX B

**EARTHQUAKE DATA FOR EL SALVADOR SORTED
BY SOURCES**

SOURCE SYMBOLS

GUTE	B. Gutenberg and Richter, C. and Gutenberg, B.
LEEDS	D. Leeds
SSA	Seismological Society of America-Earthquake Notes
WHITE	R. White
BSSA	Bulletin of the Seismological Society of America
ISS	International Seismological Summary
GELL	R. J. Geller
TAC	Tacubaya, Mexico Seismological Station
SYKES	L. R. Sykes and Ewing, M. and Molnar, P. And Sykes, L. R.
CGS	Coast and Geodetic Survey
ISC	International Seismological Center
NOS	National Ocean Survey
ERL	Enviromental Research Laboratories
PDE	Preliminary Determination of Earthquakes
NMNH	National Museum of Natural History
SCHUL	R. Schulz
RVR	L. Rutten and Van Raadshooven, B.
ROTHE	J. P. Rothe
KELLE	J. Kelleher et al.

445 446 447 448 449 450 451 452 453 454 455 456 457 458 459 460 461 462 463 464 465 466 467 468 469 470 471 472 473 474 475 476 477 478 479 480 481 482 483 484 485 486 487 488 489 490 491 492 493 494 495 496 497 498 499 500 501 502 503 504 505 506 507 508 509 510 511 512 513 514 515 516 517 518 519 520 521 522 523 524 525 526 527 528 529 530 531 532 533 534 535 536 537 538 539 540 541 542 543 544 545 546 547 548 549 550 551 552 553 554 555 556 557 558 559 560 561 562 563 564 565 566 567 568 569 570 571 572 573 574 575 576 577 578 579 580 581 582 583 584 585 586 587 588 589 590 591 592 593 594 595 596 597 598 599 600 601 602 603 604 605 606 607 608 609 610 611 612 613 614 615 616 617 618 619 620 621 622 623 624 625 626 627 628 629 630 631 632 633 634 635 636 637 638 639 640 641 642 643 644 645 646 647 648 649 650 651 652 653 654 655 656 657 658 659 660 661 662 663 664 665 666 667 668 669 670 671 672 673 674 675 676 677 678 679 680 681 682 683 684 685 686 687 688 689 690 691 692 693 694 695 696 697 698 699 700 701 702 703 704 705 706 707 708 709 710 711 712 713 714 715 716 717 718 719 720 721 722 723 724 725 726 727 728 729 730 731 732 733 734 735 736 737 738 739 740 741 742 743 744 745 746 747 748 749 750 751 752 753 754 755 756 757 758 759 760 761 762 763 764 765 766 767 768 769 770 771 772 773 774 775 776 777 778 779 780 781 782 783 784 785 786 787 788 789 790 791 792 793 794 795 796 797 798 799 800 801 802 803 804 805 806 807 808 809 810 811 812 813 814 815 816 817 818 819 820 821 822 823 824 825 826 827 828 829 830 831 832 833 834 835 836 837 838 839 840 841 842 843 844 845 846 847 848 849 850 851 852 853 854 855 856 857 858 859 860 861 862 863 864 865 866 867 868 869 870 871 872 873 874 875 876 877 878 879 880 881 882 883 884 885 886 887 888 889 890 891 892 893 894 895 896 897 898 899 900 901 902 903 904 905 906 907 908 909 910 911 912 913 914 915 916 917 918 919 920 921 922 923 924 925 926 927 928 929 930 931 932 933 934 935 936 937 938 939 940 941 942 943 944 945 946 947 948 949 950 951 952 953 954 955 956 957 958 959 960 961 962 963 964 965 966 967 968 969 970 971 972 973 974 975 976 977 978 979 980 981 982 983 984 985 986 987 988 989 990 991 992 993 994 995 996 997 998 999 1000

134 135 136 137 138 139 140 141 142 143 144 145 146 147 148 149 150 151 152 153 154 155 156 157 158 159 160 161 162 163 164 165 166 167 168 169 170 171 172 173 174 175 176 177 178 179 180 181 182 183 184 185 186 187 188 189 190 191 192 193 194 195 196 197 198 199 200 201 202 203 204 205 206 207 208 209 210 211 212 213 214 215 216 217 218 219 220 221 222 223 224 225 226 227 228 229 230 231 232 233 234 235 236 237 238 239 240 241 242 243 244 245 246 247 248 249 250 251 252 253 254 255 256 257 258 259 260 261 262 263 264 265 266 267 268 269 270 271 272 273 274 275 276 277 278 279 280 281 282 283 284 285 286 287 288 289 290 291 292 293 294 295 296 297 298 299 300 301 302 303 304 305 306 307 308 309 310 311 312 313 314 315 316 317 318 319 320 321 322 323 324 325 326 327 328 329 330 331 332 333 334 335 336 337 338 339 340 341 342 343 344 345 346 347 348 349 350 351 352 353 354 355 356 357 358 359 360 361 362 363 364 365 366 367 368 369 370 371 372 373 374 375 376 377 378 379 380 381 382 383 384 385 386 387 388 389 390 391 392 393 394 395 396 397 398 399 400 401 402 403 404 405 406 407 408 409 410 411 412 413 414 415 416 417 418 419 420 421 422 423 424 425 426 427 428 429 430 431 432 433 434 435 436 437 438 439 440 441 442 443 444 445 446 447 448 449 450 451 452 453 454 455 456 457 458 459 460 461 462 463 464 465 466 467 468 469 470 471 472 473 474 475 476 477 478 479 480 481 482 483 484 485 486 487 488 489 490 491 492 493 494 495 496 497 498 499 500 501 502 503 504 505 506 507 508 509 510 511 512 513 514 515 516 517 518 519 520 521 522 523 524 525 526 527 528 529 530 531 532 533 534 535 536 537 538 539 540 541 542 543 544 545 546 547 548 549 550 551 552 553 554 555 556 557 558 559 560 561 562 563 564 565 566 567 568 569 570 571 572 573 574 575 576 577 578 579 580 581 582 583 584 585 586 587 588 589 590 591 592 593 594 595 596 597 598 599 600 601 602 603 604 605 606 607 608 609 610 611 612 613 614 615 616 617 618 619 620 621 622 623 624 625 626 627 628 629 630 631 632 633 634 635 636 637 638 639 640 641 642 643 644 645 646 647 648 649 650 651 652 653 654 655 656 657 658 659 660 661 662 663 664 665 666 667 668 669 670 671 672 673 674 675 676 677 678 679 680 681 682 683 684 685 686 687 688 689 690 691 692 693 694 695 696 697 698 699 700 701 702 703 704 705 706 707 708 709 710 711 712 713 714 715 716 717 718 719 720 721 722 723 724 725 726 727 728 729 730 731 732 733 734 735 736 737 738 739 740 741 742 743 744 745 746 747 748 749 750 751 752 753 754 755 756 757 758 759 760 761 762 763 764 765 766 767 768 769 770 771 772 773 774 775 776 777 778 779 780 781 782 783 784 785 786 787 788 789 790 791 792 793 794 795 796 797 798 799 800 801 802 803 804 805 806 807 808 809 810 811 812 813 814 815 816 817 818 819 820 821 822 823 824 825 826 827 828 829 830 831 832 833 834 835 836 837 838 839 840 841 842 843 844 845 846 847 848 849 850 851 852 853 854 855 856 857 858 859 860 861 862 863 864 865 866 867 868 869 870 871 872 873 874 875 876 877 878 879 880 881 882 883 884 885 886 887 888 889 890 891 892 893 894 895 896 897 898 899 900 901 902 903 904 905 906 907 908 909 910 911 912 913 914 915 916 917 918 919 920 921 922 923 924 925 926 927 928 929 930 931 932 933 934 935 936 937 938 939 940 941 942 943 944 945 946 947 948 949 950 951 952 953 954 955 956 957 958 959 960 961 962 963 964 965 966 967 968 969 970 971 972 973 974 975 976 977 978 979 980 981 982 983 984 985 986 987 988 989 990 991 992 993 994 995 996 997 998 999 1000

ORDER	CRONER	DATA	SOURCE	DAY	MON	YEAR	MOOR	MINUTE	SECOND	LATITUDE	LONGITUDE	DELM	MB	MAGNITUDE
3	MM	11	14	14	12	71				13	300N	89	45	7.00
4	MM	11	12	12	12	71				13	220N	88	59	7.10
7	MM	11	12	12	12	71				13	750N	91	10	7.40
8	MM	11	10	10	17	71				13	800N	90	49	7.40
9	MM	11	10	10	17	71				13	300N	89	59	7.40
10	MM	11	10	10	17	71				13	900N	91	10	7.40
11	MM	11	10	10	17	71				13	900N	91	10	7.40
14	MM	11	10	10	17	71				13	300N	89	49	7.40
15	MM	11	10	10	17	71				13	500N	89	59	7.40
17	MM	11	10	10	17	71				13	100N	87	11	7.40
18	MM	11	10	10	17	71				13	100N	87	11	7.40
23	MM	11	10	10	17	71				13	100N	87	11	7.40
27	MM	11	10	10	17	71				13	500N	89	49	7.40
30	MM	11	10	10	17	71				13	500N	89	49	7.40
31	MM	11	10	10	17	71				13	400N	91	10	7.40
32	MM	11	10	10	17	71				13	400N	91	10	7.40
33	MM	11	10	10	17	71				13	400N	91	10	7.40
34	MM	11	10	10	17	71				13	400N	91	10	7.40
35	MM	11	10	10	17	71				13	400N	91	10	7.40
36	MM	11	10	10	17	71				13	400N	91	10	7.40
37	MM	11	10	10	17	71				13	400N	91	10	7.40
38	MM	11	10	10	17	71				13	400N	91	10	7.40
39	MM	11	10	10	17	71				13	400N	91	10	7.40
40	MM	11	10	10	17	71				13	400N	91	10	7.40
41	MM	11	10	10	17	71				13	400N	91	10	7.40
42	MM	11	10	10	17	71				13	400N	91	10	7.40
43	MM	11	10	10	17	71				13	400N	91	10	7.40
44	MM	11	10	10	17	71				13	400N	91	10	7.40
45	MM	11	10	10	17	71				13	400N	91	10	7.40
46	MM	11	10	10	17	71				13	400N	91	10	7.40
47	MM	11	10	10	17	71				13	400N	91	10	7.40
48	MM	11	10	10	17	71				13	400N	91	10	7.40
49	MM	11	10	10	17	71				13	400N	91	10	7.40
50	MM	11	10	10	17	71				13	400N	91	10	7.40
51	MM	11	10	10	17	71				13	400N	91	10	7.40
52	MM	11	10	10	17	71				13	400N	91	10	7.40
53	MM	11	10	10	17	71				13	400N	91	10	7.40
54	MM	11	10	10	17	71				13	400N	91	10	7.40
55	MM	11	10	10	17	71				13	400N	91	10	7.40
56	MM	11	10	10	17	71				13	400N	91	10	7.40
57	MM	11	10	10	17	71				13	400N	91	10	7.40
58	MM	11	10	10	17	71				13	400N	91	10	7.40
59	MM	11	10	10	17	71				13	400N	91	10	7.40
60	MM	11	10	10	17	71				13	400N	91	10	7.40
61	MM	11	10	10	17	71				13	400N	91	10	7.40
62	MM	11	10	10	17	71				13	400N	91	10	7.40
63	MM	11	10	10	17	71				13	400N	91	10	7.40
64	MM	11	10	10	17	71				13	400N	91	10	7.40
65	MM	11	10	10	17	71				13	400N	91	10	7.40
66	MM	11	10	10	17	71				13	400N	91	10	7.40
67	MM	11	10	10	17	71				13	400N	91	10	7.40
68	MM	11	10	10	17	71				13	400N	91	10	7.40
69	MM	11	10	10	17	71				13	400N	91	10	7.40
70	MM	11	10	10	17	71				13	400N	91	10	7.40
71	MM	11	10	10	17	71				13	400N	91	10	7.40
72	MM	11	10	10	17	71				13	400N	91	10	7.40
73	MM	11	10	10	17	71				13	400N	91	10	7.40
74	MM	11	10	10	17	71				13	400N	91	10	7.40
75	MM	11	10	10	17	71				13	400N	91	10	7.40
76	MM	11	10	10	17	71				13	400N	91	10	7.40
77	MM	11	10	10	17	71				13	400N	91	10	7.40
78	MM	11	10	10	17	71				13	400N	91	10	7.40
79	MM	11	10	10	17	71				13	400N	91	10	7.40
80	MM	11	10	10	17	71				13	400N	91	10	7.40
81	MM	11	10	10	17	71				13	400N	91	10	7.40
82	MM	11	10	10	17	71				13	400N	91	10	7.40
83	MM	11	10	10	17	71				13	400N	91	10	7.40
84	MM	11	10	10	17	71				13	400N	91	10	7.40
85	MM	11	10	10	17	71				13	400N	91	10	7.40
86	MM	11	10	10	17	71				13	400N	91	10	7.40
87	MM	11	10	10	17	71				13	400N	91	10	7.40
88	MM	11	10	10	17	71				13	400N	91	10	7.40
89	MM	11	10	10	17	71				13	400N	91	10	7.40
90	MM	11	10	10	17	71				13	400N	91	10	7.40
91	MM	11	10	10	17	71				13	400N	91	10	7.40
92	MM	11	10	10	17	71				13	400N	91	10	7.40
93	MM	11	10	10	17	71				13	400N	91	10	7.40
94	MM	11	10	10	17	71				13	400N	91	10	7.40
95	MM	11	10	10	17	71				13	400N	91	10	7.40
96	MM	11	10	10	17	71				13	400N	91	10	7.40
97	MM	11	10	10	17	71				13	400N	91	10	7.40
98	MM	11	10	10	17	71				13	400N	91	10	7.40
99	MM	11	10	10	17	71				13	400N	91	10	7.40
100	MM	11	10	10	17	71				13	400N	91	10	7.40

724 729 730 733 735 739 741 744 747 749 750 751 752 753 754 755 756 757 758 759 760 761 762 763 764 765 766 767 768 769 770 771 772 773 774 775 776 777 778 779 780 781 782 783 784 785 786 787 788 789 790 791 792 793 794 795 796 797 798 799 800 801 802 803 804 805 806 807 808 809 810 811 812 813 814 815 816 817 818 819 820 821 822 823 824 825 826 827 828 829 830 831 832 833 834 835 836 837 838 839 840 841 842 843 844 845 846 847 848 849 850 851 852 853 854 855 856 857 858 859 860 861 862 863 864 865 866 867 868 869 870 871 872 873 874 875 876 877 878 879 880 881 882 883 884 885 886 887 888 889 890 891 892 893 894 895 896 897 898 899 900 901 902 903 904 905 906 907 908 909 910 911 912 913 914 915 916 917 918 919 920 921 922 923 924 925 926 927 928 929 930 931 932 933 934 935 936 937 938 939 940 941 942 943 944 945 946 947 948 949 950 951 952 953 954 955 956 957 958 959 960 961 962 963 964 965 966 967 968 969 970 971 972 973 974 975 976 977 978 979 980 981 982 983 984 985 986 987 988 989 990 991 992 993 994 995 996 997 998 999 1000

430MB 440MB 450MB 460MB 470MB 480MB 490MB 500MB 510MB 520MB 530MB 540MB 550MB 560MB 570MB 580MB 590MB 600MB 610MB 620MB 630MB 640MB 650MB 660MB 670MB 680MB 690MB 700MB 710MB 720MB 730MB 740MB 750MB 760MB 770MB 780MB 790MB 800MB 810MB 820MB 830MB 840MB 850MB 860MB 870MB 880MB 890MB 900MB 910MB 920MB 930MB 940MB 950MB 960MB 970MB 980MB 990MB 1000MB

*****MOTAGUA FAULT ZONE*****

MOTAGUA FAULT ZONE

CRONOLOGICAL	ORDER	DATA	SOURCE	DAY	MONTH	YEAR	HOUR	MINUTE	SECOND	LATITUDE	LONGITUDE	DEPTH	MB MAGNITUDE	MAGNITUDE
5	1	WHITE2	WHITE2	12	09	1971	13			14.941N	90.750W	0	6.50	6.50
41	2	WHITE2	WHITE2	06	05	1981	18			14.941N	91.167W	0	6.50	6.50
184	3	ESSA	ESSA	19	05	1984	10	47	36	14.800N	91.000W	0	0.00	0.00
189	4	GELL	GELL	24	12	1984	14	35	48	14.800N	91.000W	0	0.00	0.00
237	5	ISSMUL	ISSMUL	15	02	1987	09	26	42	15.300N	89.400W	0	0.00	0.00
261	6	GELL	GELL	12	01	1988	11	20	00	15.300N	89.400W	0	0.00	0.00
269	7	WHITE2	WHITE2	10	08	1988	14	09	05	15.250N	89.133W	0	0.50	0.80
270	8	GELL	GELL	10	08	1988	14	09	05	15.345N	89.063W	0	0.50	0.50
287	9	ISS	ISS	27	10	1988	11	24	05	15.000N	91.000W	0	0.00	0.00
477	10	GELL	GELL	03	01	1992	08	40	12	15.000N	90.900W	0	0.00	0.00
482	11	GELL	GELL	03	01	1992	08	40	12	15.000N	90.900W	0	0.00	0.00
629	12	CSS-B	CSS-B	19	10	1995	05	11	25	14.800N	89.800W	33	390MB	95
937	13	CSS-B	CSS-B	19	10	1995	05	11	25	14.800N	89.800W	33	390MB	95
1199	14	ISS	ISS	28	01	1997	02	30	09	14.800N	91.000W	0	380MB	0.80
1679	15	ISS	ISS	12	08	1972	00	00	00	15.000N	90.500W	33	0.00	0.00
1934	16	ERL	ERL	24	12	1972	00	20	19	15.000N	90.500W	33	0.00	0.00
2305	17	ISS	ISS	04	02	1976	09	01	43	15.430N	89.523W	33	460MB	12
2330	18	ISS	ISS	04	02	1976	09	01	43	15.430N	89.523W	33	540MB	14
2330	19	ISS	ISS	04	02	1976	12	57	24	15.300N	89.1234W	33	450MB	11
2330	20	ISS	ISS	04	02	1976	12	57	24	15.300N	89.1234W	33	450MB	11
2331	21	ISS	ISS	05	02	1976	10	17	04	14.800N	91.000W	33	470MB	11
2331	22	ISS	ISS	05	02	1976	10	17	04	14.800N	91.000W	33	470MB	11
2332	23	PDE	PDE	09	02	1976	11	48	46	15.571N	89.073W	33	520MB	5
2332	24	PDE	PDE	09	02	1976	11	48	46	15.571N	89.073W	33	520MB	5
2332	25	PDE	PDE	10	02	1976	06	05	14	14.833N	89.778W	33	490MB	3
2332	26	PDE	PDE	10	02	1976	06	05	14	14.833N	89.778W	33	490MB	3
2334	27	PDE	PDE	07	03	1976	03	15	41	14.869N	90.943W	33	510MB	4
2334	28	PDE	PDE	07	03	1976	03	15	41	14.869N	90.943W	33	510MB	4
2334	29	PDE	PDE	13	03	1976	15	30	44	14.780N	91.000W	33	540MB	3
2334	30	PDE	PDE	13	03	1976	15	30	44	14.780N	91.000W	33	540MB	3
2335	31	ISS	ISS	03	06	1977	20	18	00	15.016N	89.507W	33	490MB	4
2335	32	ISS	ISS	03	06	1977	20	18	00	15.016N	89.507W	33	490MB	4
2337	33	ISS	ISS	10	01	1979	19	30	09	15.000N	90.800W	33	510MB	4
2337	34	ISS	ISS	10	01	1979	19	30	09	15.000N	90.800W	33	510MB	4
2337	35	ISS	ISS	15	05	1979	02	14	18	15.000N	91.000W	33	460MB	4
2337	36	ISS	ISS	15	05	1979	02	14	18	15.000N	91.000W	33	460MB	4
2337	37	ISS	ISS	15	05	1979	02	14	18	15.000N	91.000W	33	460MB	4
2337	38	ISS	ISS	15	05	1979	02	14	18	15.000N	91.000W	33	460MB	4
2337	39	ISS	ISS	15	05	1979	02	14	18	15.000N	91.000W	33	460MB	4
2337	40	ISS	ISS	15	05	1979	02	14	18	15.000N	91.000W	33	460MB	4
2337	41	ISS	ISS	15	05	1979	02	14	18	15.000N	91.000W	33	460MB	4
2337	42	ISS	ISS	15	05	1979	02	14	18	15.000N	91.000W	33	460MB	4
2337	43	ISS	ISS	15	05	1979	02	14	18	15.000N	91.000W	33	460MB	4
2337	44	ISS	ISS	15	05	1979	02	14	18	15.000N	91.000W	33	460MB	4
2337	45	ISS	ISS	15	05	1979	02	14	18	15.000N	91.000W	33	460MB	4
2337	46	ISS	ISS	15	05	1979	02	14	18	15.000N	91.000W	33	460MB	4
2337	47	ISS	ISS	15	05	1979	02	14	18	15.000N	91.000W	33	460MB	4
2337	48	ISS	ISS	15	05	1979	02	14	18	15.000N	91.000W	33	460MB	4
2337	49	ISS	ISS	15	05	1979	02	14	18	15.000N	91.000W	33	460MB	4
2337	50	ISS	ISS	15	05	1979	02	14	18	15.000N	91.000W	33	460MB	4
2337	51	ISS	ISS	15	05	1979	02	14	18	15.000N	91.000W	33	460MB	4
2337	52	ISS	ISS	15	05	1979	02	14	18	15.000N	91.000W	33	460MB	4
2337	53	ISS	ISS	15	05	1979	02	14	18	15.000N	91.000W	33	460MB	4
2337	54	ISS	ISS	15	05	1979	02	14	18	15.000N	91.000W	33	460MB	4
2337	55	ISS	ISS	15	05	1979	02	14	18	15.000N	91.000W	33	460MB	4
2337	56	ISS	ISS	15	05	1979	02	14	18	15.000N	91.000W	33	460MB	4
2337	57	ISS	ISS	15	05	1979	02	14	18	15.000N	91.000W	33	460MB	4
2337	58	ISS	ISS	15	05	1979	02	14	18	15.000N	91.000W	33	460MB	4
2337	59	ISS	ISS	15	05	1979	02	14	18	15.000N	91.000W	33	460MB	4
2337	60	ISS	ISS	15	05	1979	02	14	18	15.000N	91.000W	33	460MB	4
2337	61	ISS	ISS	15	05	1979	02	14	18	15.000N	91.000W	33	460MB	4
2337	62	ISS	ISS	15	05	1979	02	14	18	15.000N	91.000W	33	460MB	4
2337	63	ISS	ISS	15	05	1979	02	14	18	15.000N	91.000W	33	460MB	4
2337	64	ISS	ISS	15	05	1979	02	14	18	15.000N	91.000W	33	460MB	4
2337	65	ISS	ISS	15	05	1979	02	14	18	15.000N	91.000W	33	460MB	4
2337	66	ISS	ISS	15	05	1979	02	14	18	15.000N	91.000W	33	460MB	4
2337	67	ISS	ISS	15	05	1979	02	14	18	15.000N	91.000W	33	460MB	4
2337	68	ISS	ISS	15	05	1979	02	14	18	15.000N	91.000W	33	460MB	4
2337	69	ISS	ISS	15	05	1979	02	14	18	15.000N	91.000W	33	460MB	4
2337	70	ISS	ISS	15	05	1979	02	14	18	15.000N	91.000W	33	460MB	4
2337	71	ISS	ISS	15	05	1979	02	14	18	15.000N	91.000W	33	460MB	4
2337	72	ISS	ISS	15	05	1979	02	14	18	15.000N	91.000W	33	460MB	4
2337	73	ISS	ISS	15	05	1979	02	14	18	15.000N	91.000W	33	460MB	4
2337	74	ISS	ISS	15	05	1979	02	14	18	15.000N	91.000W	33	460MB	4
2337	75	ISS	ISS	15	05	1979	02	14	18	15.000N	91.000W	33	460MB	4
2337	76	ISS	ISS	15	05	1979	02	14	18	15.000N	91.000W	33	460MB	4
2337	77	ISS	ISS	15	05	1979	02	14	18	15.000N	91.000W	33	460MB	4
2337	78	ISS	ISS	15	05	1979	02	14	18	15.000N	91.000W	33	460MB	4
2337	79	ISS	ISS	15	05	1979	02	14	18	15.000N	91.000W	33	460MB	4
2337	80	ISS	ISS	15	05	1979	02	14	18	15.000N	91.000W	33	460MB	4
2337	81	ISS	ISS	15	05	1979	02	14	18	15.000N	91.000W	33	460MB	4
2337	82	ISS	ISS	15	05	1979	02	14	18	15.000N	91.000W	33	460MB	4
2337	83	ISS	ISS	15	05	1979	02	14	18	15.000N	91.000W	33	460MB	4
2337	84	ISS	ISS	15	05	1979	02	14	18	15.000N	91.000W	33	460MB	4
2337	85	ISS	ISS	15	05	1979	02	14	18	15.000N	91.000W	33	460MB	4
2337	86	ISS	ISS	15	05	1979	02	14	18	15.000N	91.000W	33	460MB	4
2337	87	ISS	ISS	15	05	1979	02	14	18	15.000N	91.000W	33	460MB	4
2337	88	ISS	ISS	15	05	1979	02	14	18	15.000N	91.000W	33	460MB	4
2337	89	ISS	ISS	15	05	1979	02	14	18	15.000N	91.000W	33	460MB	4
2337	90	ISS	ISS	15	05	1979	02	14	18	15.000N	91.000W	33	460MB	4
2337	91	ISS	ISS	15	05	1979	02	14	18	15.000N	91.000W	33	460MB	4
2337	92	ISS	ISS	15	05	1979	02	14	18	15.000N	91.000W	33	460MB	4
2337	93	ISS	ISS	15	05	1979	02	14	18	15.000N	91.000W	33	460MB	4
2337	94	ISS	ISS	15	05	1979	02	14	18	15.000N	91.000W	33	460MB	4
2337	95	ISS	ISS	15	05	1979	02	14	18	15.000N	91.000W	33	460MB	4
2337	96	ISS	ISS	15	05	1979	02	14	18	15.000N	91.000W	33	460MB	4
2337	97	ISS	ISS	15	05	1979	02	14	18	15.000N	91.000W	33	460MB	4
2337	98	ISS	ISS	15	05	1979	02	14	18	15.000N	91.000W	33	460MB	4
2337	99	ISS	ISS	15	05	1979	02	14	18	15.00				

 MONDURAS DEPRESSION ZONE

ORDER	CRONOLOGICAL	D SOURCE	DAY	MONTH	YEAR	HOUR	MINUTE	SECOND	LATITUDE	LONGITUDE	DEPTH	M B MAGNITUDE	MAGNITUDE
89	119	WMTI	29	12	15	02	23	00	14.600N	88.583W	0	0	6.30
114	133	ISS	21	05	26	17	53	30	14.520N	88.700W	0	0	0.0
122	134	ISS	21	09	26	02	53	30	14.500N	88.700W	0	0	0.0
225	134	ISS	28	09	29	14	58	30	14.500N	88.000W	0	0	0.0
459	134	ISS	06	06	59	14	51	02	14.500N	87.500W	0	0	0.0
539	134	GELLES	20	08	61	09	49	41	15.670N	87.090W	30	400MB	4.10
641	134	SYKES	03	01	64	17	08	08	14.400N	87.900W	33	470MB	4.13
753	134	ISS	09	04	69	02	38	00	14.470N	87.950W	10	0	4.49
1317	134	ISS	12	02	69	07	01	00	14.274N	87.544W	13	480MB	4.00
1370	134	ISS	02	02	71	07	39	00	14.231N	87.465W	17	500MB	4.78
1402	134	ISS	08	02	71	07	39	00	14.200N	87.465W	0	0	4.29
1403	134	ISS	08	02	71	07	39	00	14.200N	87.465W	0	0	4.12
1404	134	ISS	08	02	71	07	39	00	14.200N	87.465W	0	0	4.12
1405	134	ISS	08	02	71	07	39	00	14.200N	87.465W	0	0	4.12
1406	134	ISS	08	02	71	07	39	00	14.200N	87.465W	0	0	4.12
1407	134	ISS	08	02	71	07	39	00	14.200N	87.465W	0	0	4.12
1408	134	ISS	08	02	71	07	39	00	14.200N	87.465W	0	0	4.12
1409	134	ISS	08	02	71	07	39	00	14.200N	87.465W	0	0	4.12
1410	134	ISS	08	02	71	07	39	00	14.200N	87.465W	0	0	4.12
1411	134	ISS	08	02	71	07	39	00	14.200N	87.465W	0	0	4.12
1412	134	ISS	08	02	71	07	39	00	14.200N	87.465W	0	0	4.12
1413	134	ISS	08	02	71	07	39	00	14.200N	87.465W	0	0	4.12
1414	134	ISS	08	02	71	07	39	00	14.200N	87.465W	0	0	4.12
1415	134	ISS	08	02	71	07	39	00	14.200N	87.465W	0	0	4.12
1416	134	ISS	08	02	71	07	39	00	14.200N	87.465W	0	0	4.12
1417	134	ISS	08	02	71	07	39	00	14.200N	87.465W	0	0	4.12
1418	134	ISS	08	02	71	07	39	00	14.200N	87.465W	0	0	4.12
1419	134	ISS	08	02	71	07	39	00	14.200N	87.465W	0	0	4.12
1420	134	ISS	08	02	71	07	39	00	14.200N	87.465W	0	0	4.12
1421	134	ISS	08	02	71	07	39	00	14.200N	87.465W	0	0	4.12
1422	134	ISS	08	02	71	07	39	00	14.200N	87.465W	0	0	4.12
1423	134	ISS	08	02	71	07	39	00	14.200N	87.465W	0	0	4.12
1424	134	ISS	08	02	71	07	39	00	14.200N	87.465W	0	0	4.12
1425	134	ISS	08	02	71	07	39	00	14.200N	87.465W	0	0	4.12
1426	134	ISS	08	02	71	07	39	00	14.200N	87.465W	0	0	4.12
1427	134	ISS	08	02	71	07	39	00	14.200N	87.465W	0	0	4.12
1428	134	ISS	08	02	71	07	39	00	14.200N	87.465W	0	0	4.12
1429	134	ISS	08	02	71	07	39	00	14.200N	87.465W	0	0	4.12
1430	134	ISS	08	02	71	07	39	00	14.200N	87.465W	0	0	4.12
1431	134	ISS	08	02	71	07	39	00	14.200N	87.465W	0	0	4.12
1432	134	ISS	08	02	71	07	39	00	14.200N	87.465W	0	0	4.12
1433	134	ISS	08	02	71	07	39	00	14.200N	87.465W	0	0	4.12
1434	134	ISS	08	02	71	07	39	00	14.200N	87.465W	0	0	4.12
1435	134	ISS	08	02	71	07	39	00	14.200N	87.465W	0	0	4.12
1436	134	ISS	08	02	71	07	39	00	14.200N	87.465W	0	0	4.12
1437	134	ISS	08	02	71	07	39	00	14.200N	87.465W	0	0	4.12
1438	134	ISS	08	02	71	07	39	00	14.200N	87.465W	0	0	4.12
1439	134	ISS	08	02	71	07	39	00	14.200N	87.465W	0	0	4.12
1440	134	ISS	08	02	71	07	39	00	14.200N	87.465W	0	0	4.12
1441	134	ISS	08	02	71	07	39	00	14.200N	87.465W	0	0	4.12
1442	134	ISS	08	02	71	07	39	00	14.200N	87.465W	0	0	4.12
1443	134	ISS	08	02	71	07	39	00	14.200N	87.465W	0	0	4.12
1444	134	ISS	08	02	71	07	39	00	14.200N	87.465W	0	0	4.12
1445	134	ISS	08	02	71	07	39	00	14.200N	87.465W	0	0	4.12
1446	134	ISS	08	02	71	07	39	00	14.200N	87.465W	0	0	4.12
1447	134	ISS	08	02	71	07	39	00	14.200N	87.465W	0	0	4.12
1448	134	ISS	08	02	71	07	39	00	14.200N	87.465W	0	0	4.12
1449	134	ISS	08	02	71	07	39	00	14.200N	87.465W	0	0	4.12
1450	134	ISS	08	02	71	07	39	00	14.200N	87.465W	0	0	4.12
1451	134	ISS	08	02	71	07	39	00	14.200N	87.465W	0	0	4.12
1452	134	ISS	08	02	71	07	39	00	14.200N	87.465W	0	0	4.12
1453	134	ISS	08	02	71	07	39	00	14.200N	87.465W	0	0	4.12
1454	134	ISS	08	02	71	07	39	00	14.200N	87.465W	0	0	4.12
1455	134	ISS	08	02	71	07	39	00	14.200N	87.465W	0	0	4.12
1456	134	ISS	08	02	71	07	39	00	14.200N	87.465W	0	0	4.12
1457	134	ISS	08	02	71	07	39	00	14.200N	87.465W	0	0	4.12
1458	134	ISS	08	02	71	07	39	00	14.200N	87.465W	0	0	4.12
1459	134	ISS	08	02	71	07	39	00	14.200N	87.465W	0	0	4.12
1460	134	ISS	08	02	71	07	39	00	14.200N	87.465W	0	0	4.12

 JOCOTAN-CHAMELECON FAULT ZONE

ORDER	CRONOLOGICAL	D SOURCE	DAY	MONTH	YEAR	HOUR	MINUTE	SECOND	LATITUDE	LONGITUDE	DEPTH	M B MAGNITUDE	MAGNITUDE
21	187	WMTI	15	10	74	01	38	36	14.765N	89.583W	0	0	6.50
187	187	GELLE	03	12	84	02	34	43	14.600N	89.594W	0	0	7.20
188	187	SYKES	17	12	84	00	51	50	15.000N	89.000W	0	0	6.25
932	187	ISS	30	10	87	09	48	50	15.700N	88.950W	33	380MB	6.80
1389	187	ISS	26	10	87	03	59	24	15.400N	88.800W	33	410MB	6.25
1390	187	ISS	14	07	88	01	27	06	15.370N	88.843W	33	410MB	6.25
1391	187	ISS	05	07	88	05	23	06	15.370N	88.843W	33	410MB	6.25
1392	187	ISS	05	07	88	05	23	06	15.370N	88.843W	33	410MB	6.25
1393	187	ISS	05	07	88	05	23	06	15.370N	88.843W	33	410MB	6.25
1394	187	ISS	05	07	88	05	23	06	15.370N	88.843W	33	410MB	6.25
1395	187	ISS	05	07	88	05	23	06	15.370N	88.843W	33	410MB	6.25
1396	187	ISS	05	07	88	05	23	06	15.370N	88.843W	33	410MB	6.25
1397	187	ISS	05	07	88	05	23	06	15.370N	88.843W	33	410MB	6.25
1398	187	ISS	05	07	88	05	23	06	15.370N	88.843W	33	410MB	6.25
1399	187	ISS	05	07	88	05	23	06	15.370N	88.843W	33	410MB	6.25
1400	187	ISS	05	07	88	05	23	06	15.370N	88.843W	33	410MB	6.25
1401	187	ISS	05	07	88	05	23	06	15.370N	88.843W	33	410MB	6.25
1402	187	ISS	05	07	88	05	23	06	15.370N	88.843W	33	410MB	6.25
1403	187	ISS	05	07	88	05	23	06	15.370N	88.843W	33	410MB	6.25
1404	187	ISS	05	07	88	05	23	06	15.370N	88.843W	33	410MB	6.25
1405	187	ISS	05	07	88	05	23	06	15.370N	88.843W	33	410MB	6.25
1406	187	ISS	05	07	88	05	23	06	15.370N	88.843W	33	410MB	6.25
1407	187	ISS	05	07	88	05	23	06	15.370N	88.843W	33	410MB	6.25
1408	187	ISS	05	07	88	05	23	06	15.370N	88.843W	33	410MB	6.25
1409	187	ISS	05	07	88	05	23	06	15.370N	88.843W	33	410MB	6.25
1410	187	ISS	05	07	88	05	23	06	15.370N	88.843W	33	410MB	6.25
1411	187	ISS	05	07	88	05	23	06	15.370N	88.843W	33	410MB	6.25
1412	187	ISS	05	07	88	05	23	06	15.370N	88.843W	33	410MB	6.25
1413	187	ISS	05	07	88	05	23	06	15.370N	88.843W	33	410MB	6.25
1414	187	ISS	05	07	88	05	23	06	15.370N	88.843W	33	410MB	6.25
1415	187	ISS	05	07	88	05	23	06	15.370N	88.843W	33	410MB	6.25
1416	187	ISS	05	07	88	05	23	06	15.370N	88.843W	33	410MB	6.25
1417	187	ISS	05	07	88	05	23	06	15.370N	88.843W	33	410MB	6.25
1418	187	ISS	05	07	88	05	23	06	15.370N</				

APPENDIX C
SEISMIC PROVINCES

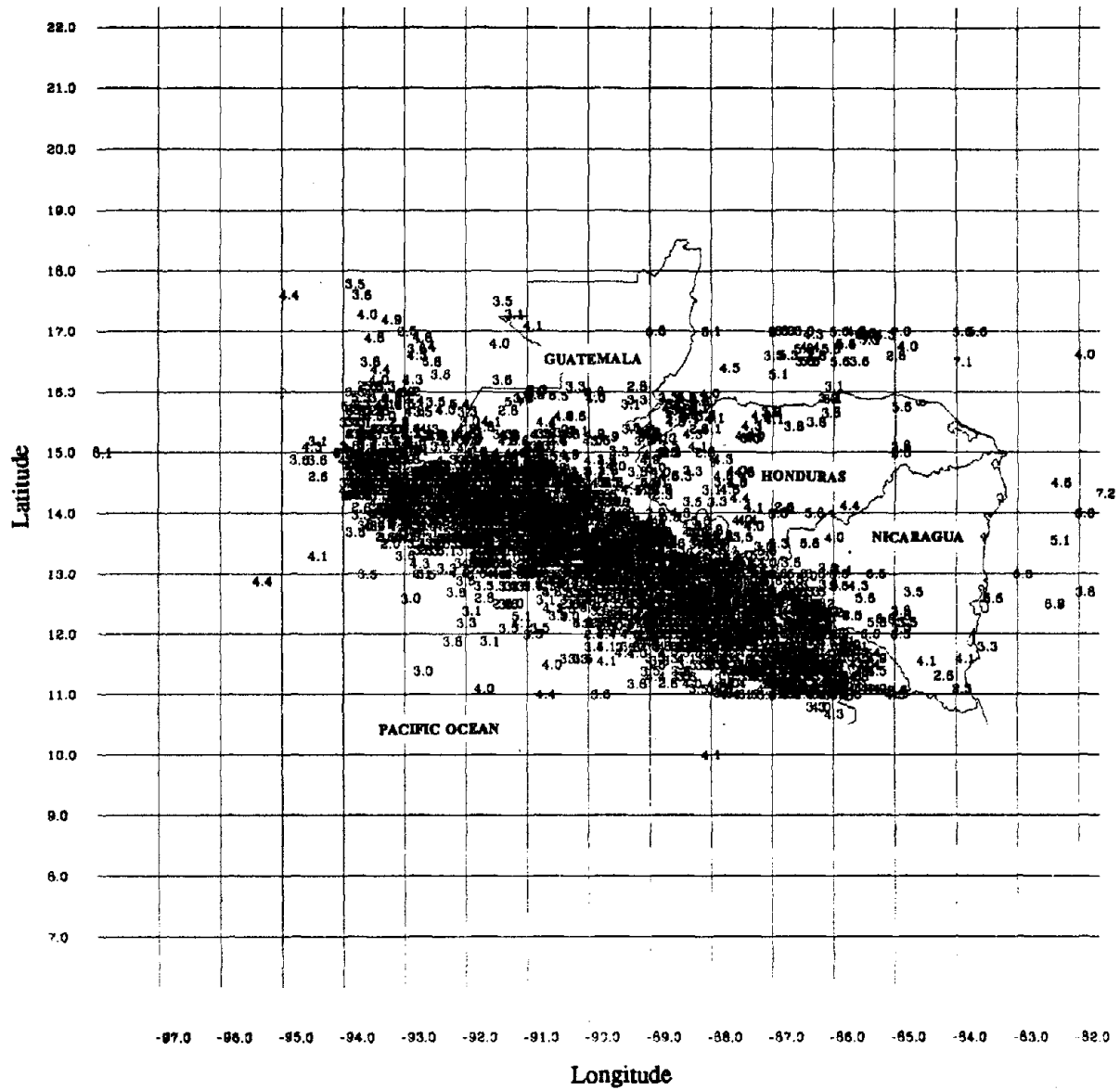


Figure C.1. Earthquake epicenters from all seismic sources for all depths and $M \geq 3.0$ since 1538.

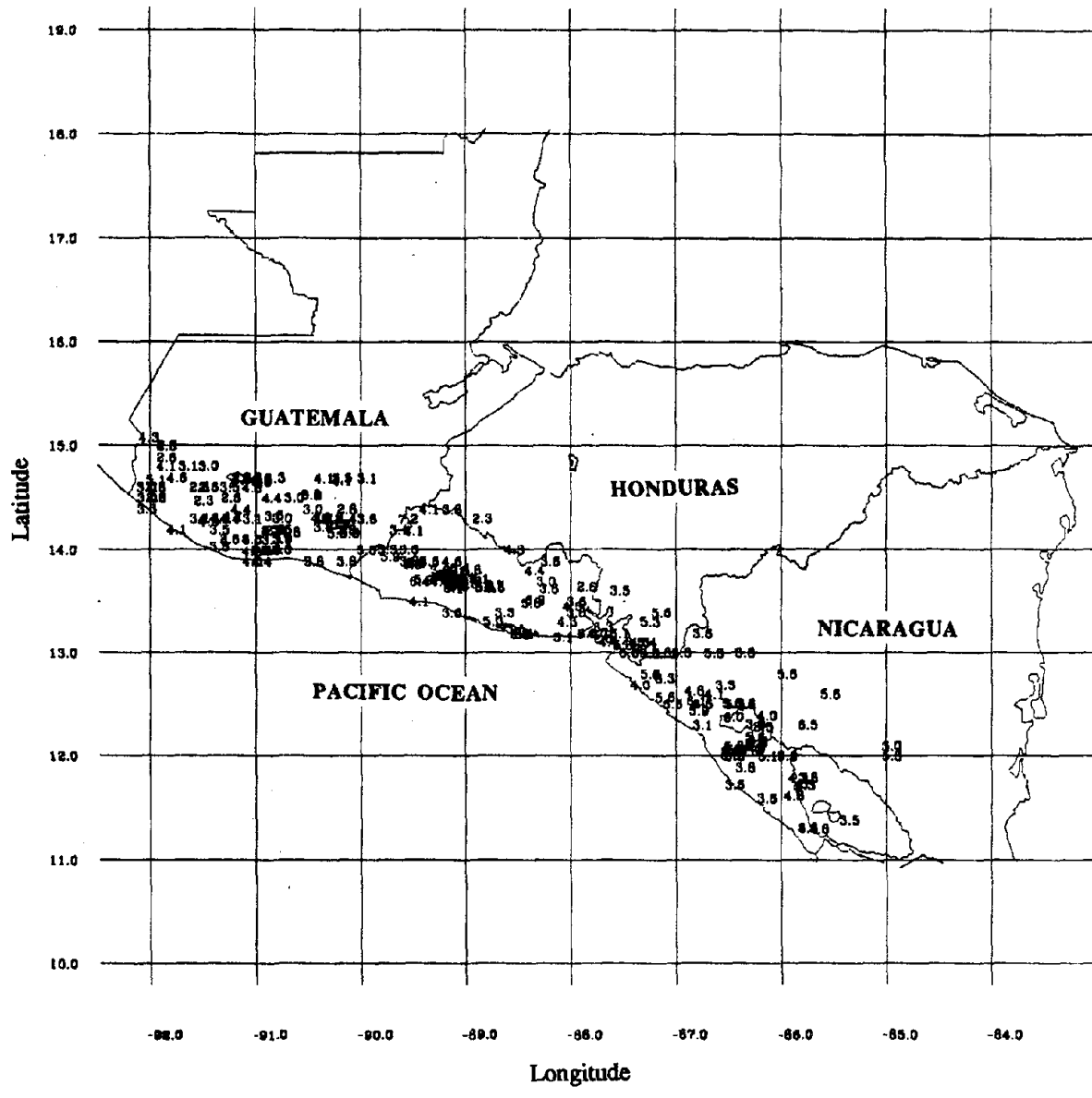


Figure C.2. Earthquake epicenters for the Volcanic Chain for $M \geq 3.0$ since 1730.

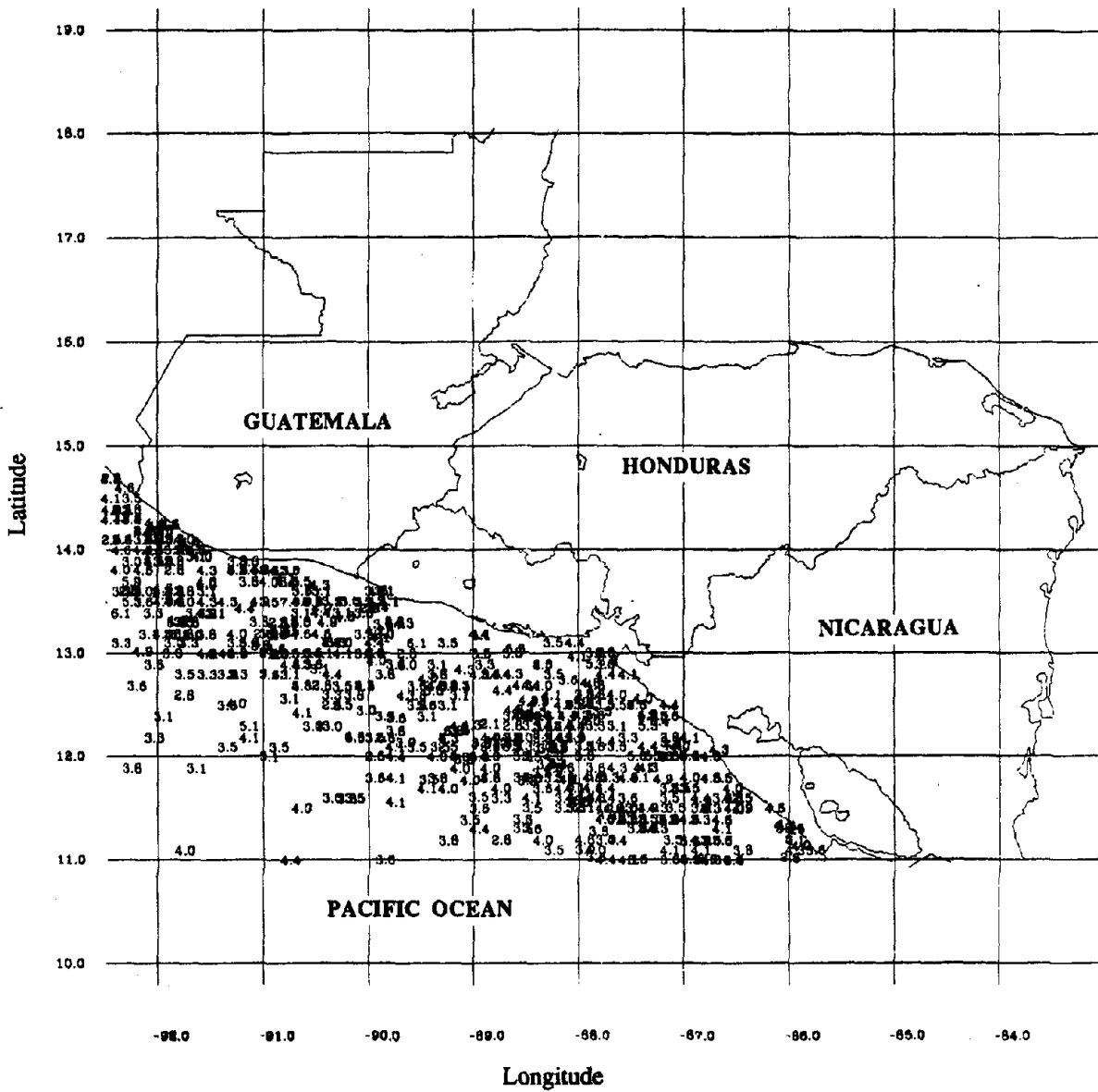


Figure C.3. Earthquake epicenters for the Shallow Benioff Zone for $M \geq 3.0$ since 1711.

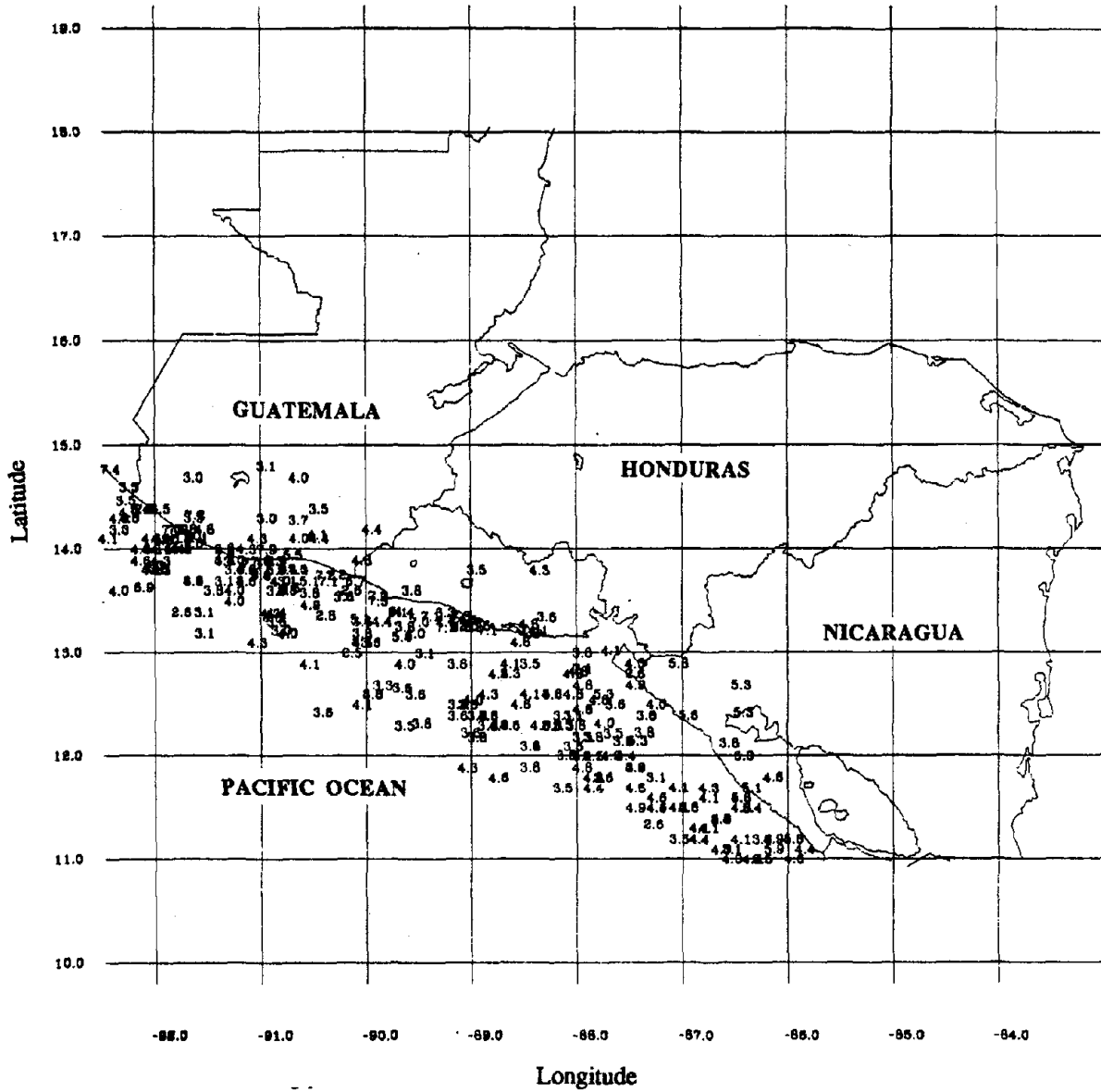


Figure C.4. Earthquake epicenters for the Intermediate Benioff Zone for $M \geq 3.0$ since 1711.

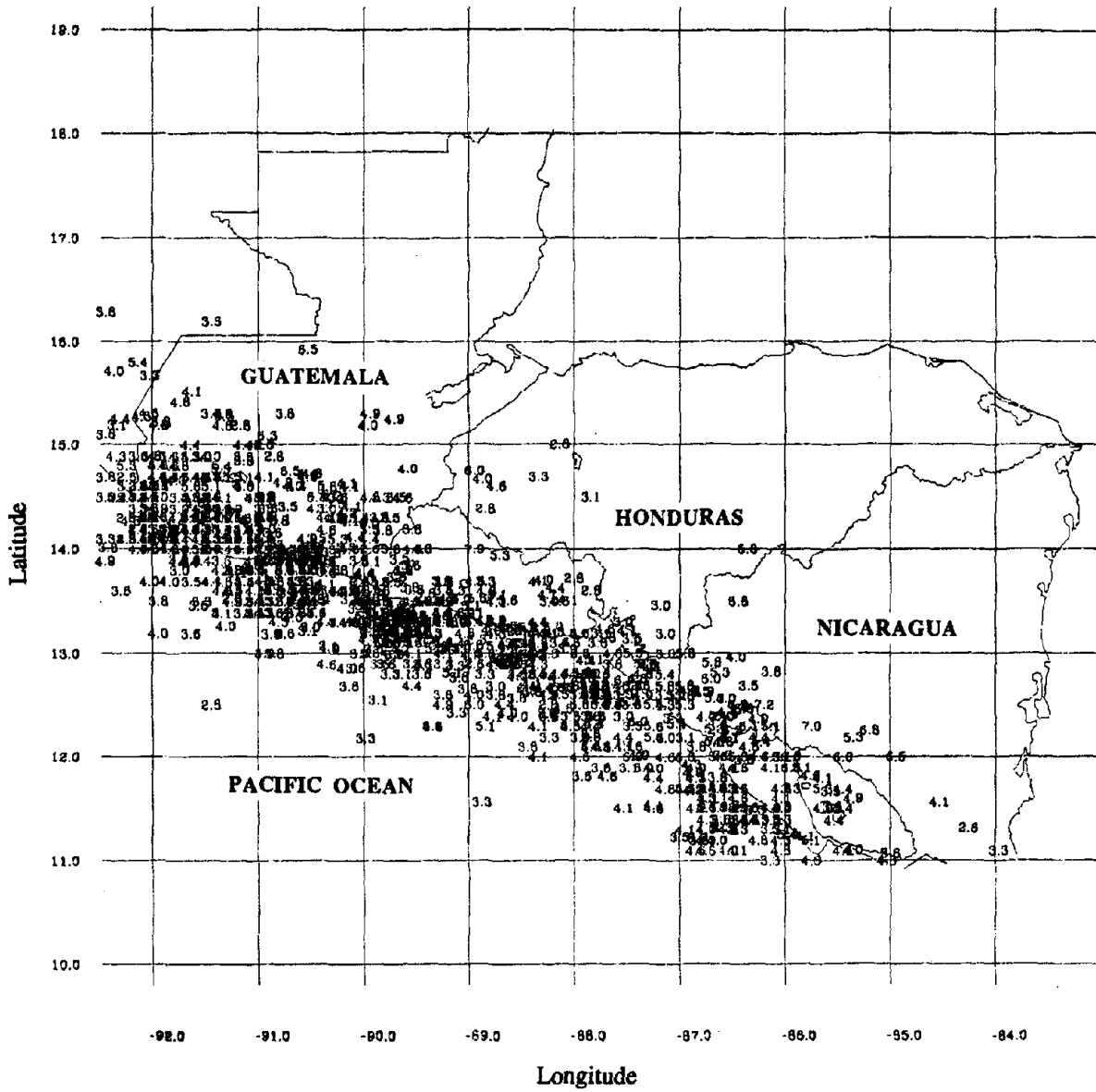


Figure C.5. Earthquake epicenters for the Deep Benioff Zone for $M \geq 3.0$ since 1711.

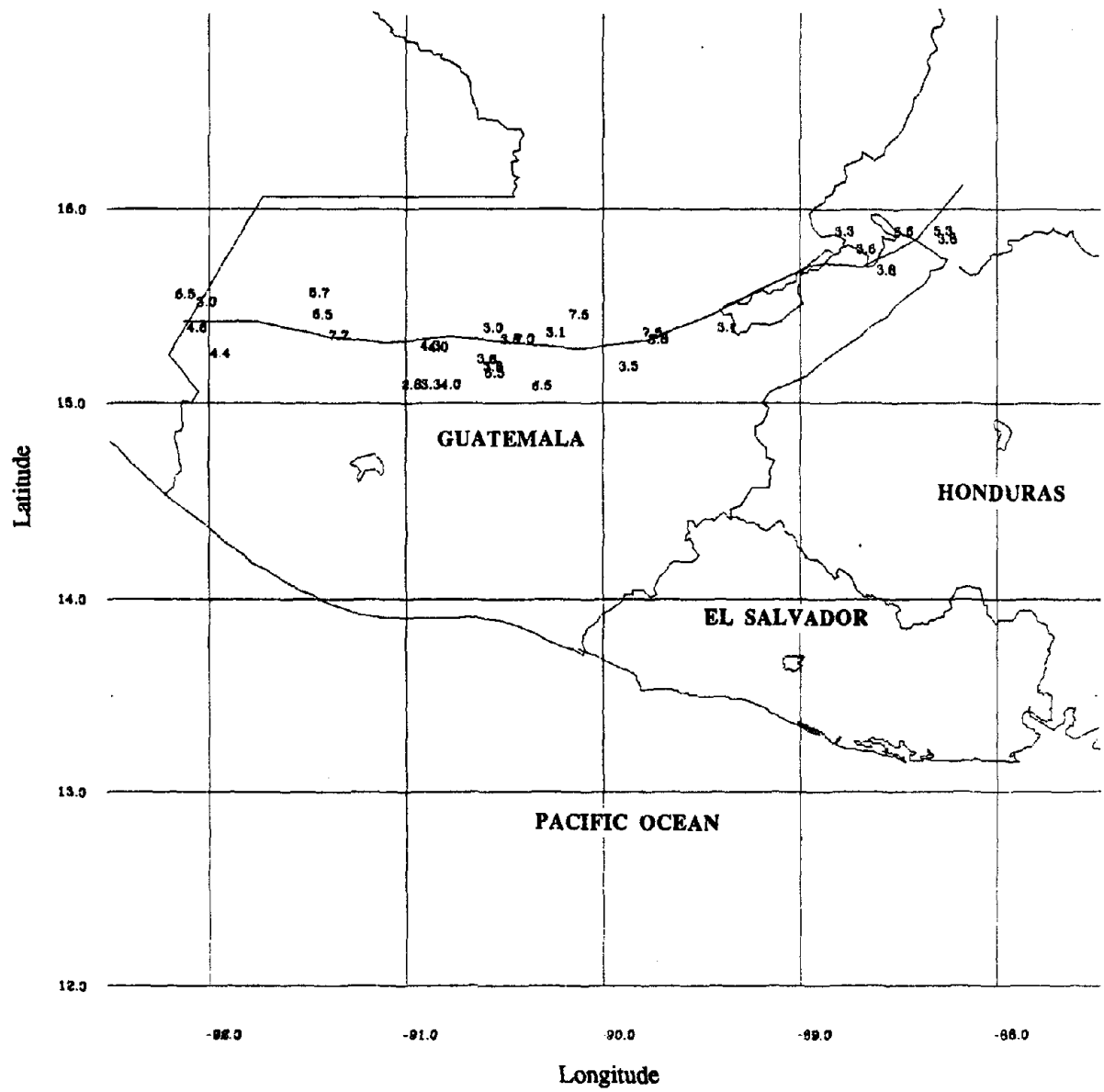


Figure C.6. Earthquake epicenters for the Chixoy-Polochic Fault Zone for $M \geq 3.0$ since 1538.

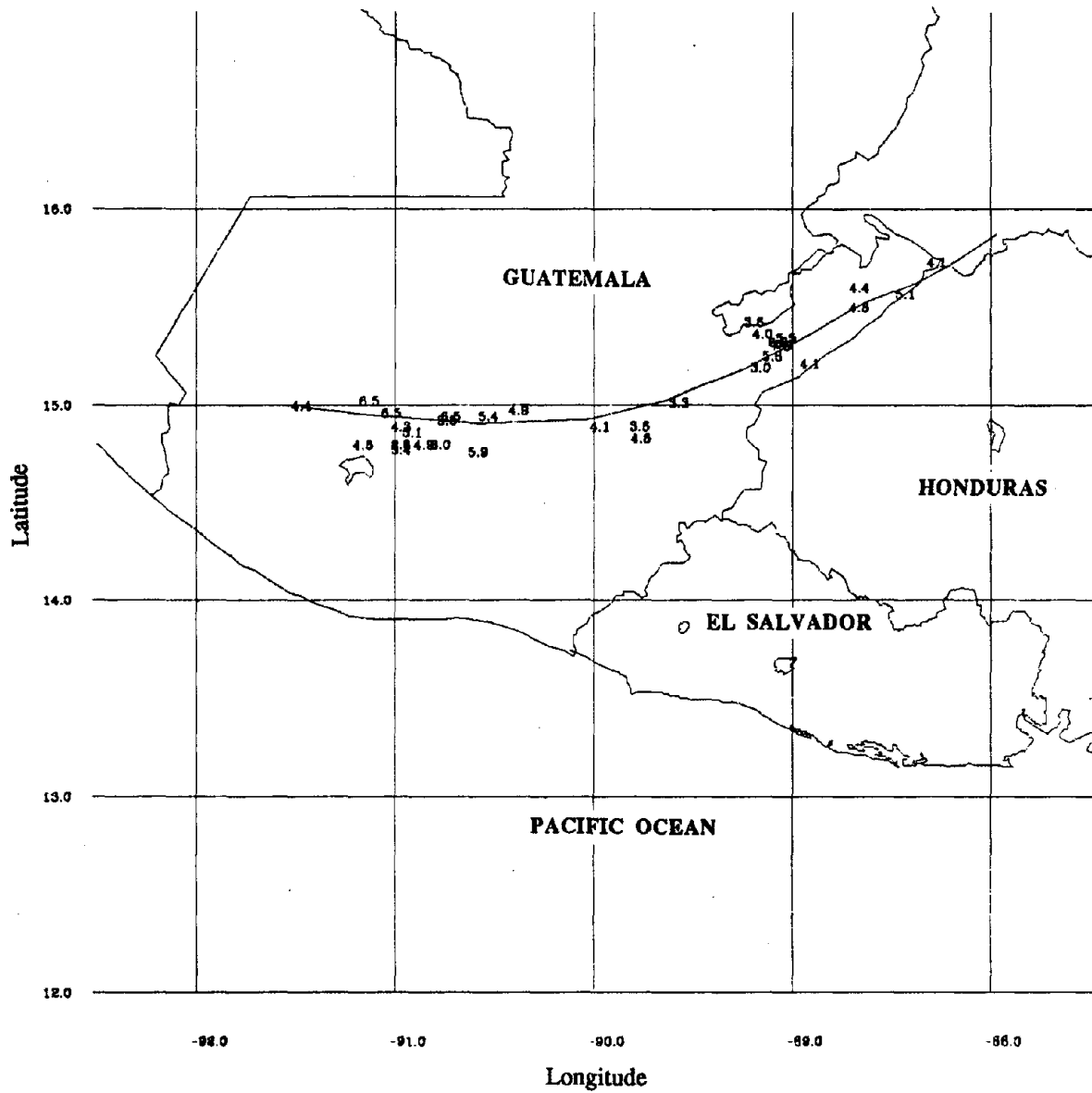


Figure C.7. Earthquake epicenters for the Motagua Fault Zone for $M \geq 3.0$ since 1700.

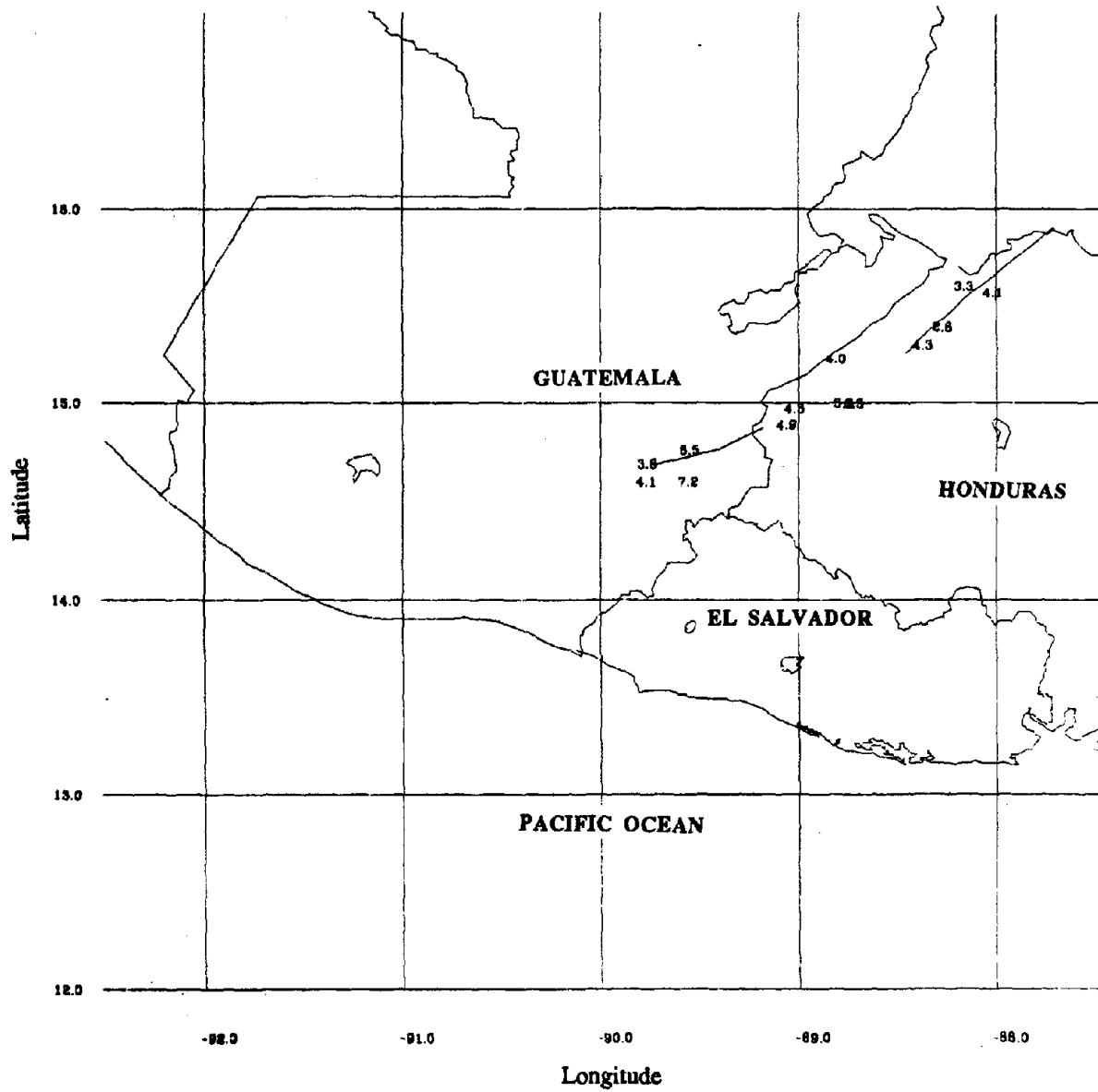


Figure C.8. Earthquake epicenters for the Jocotan-Chamelecon Fault Zone for $M \geq 3.0$ since 1700.

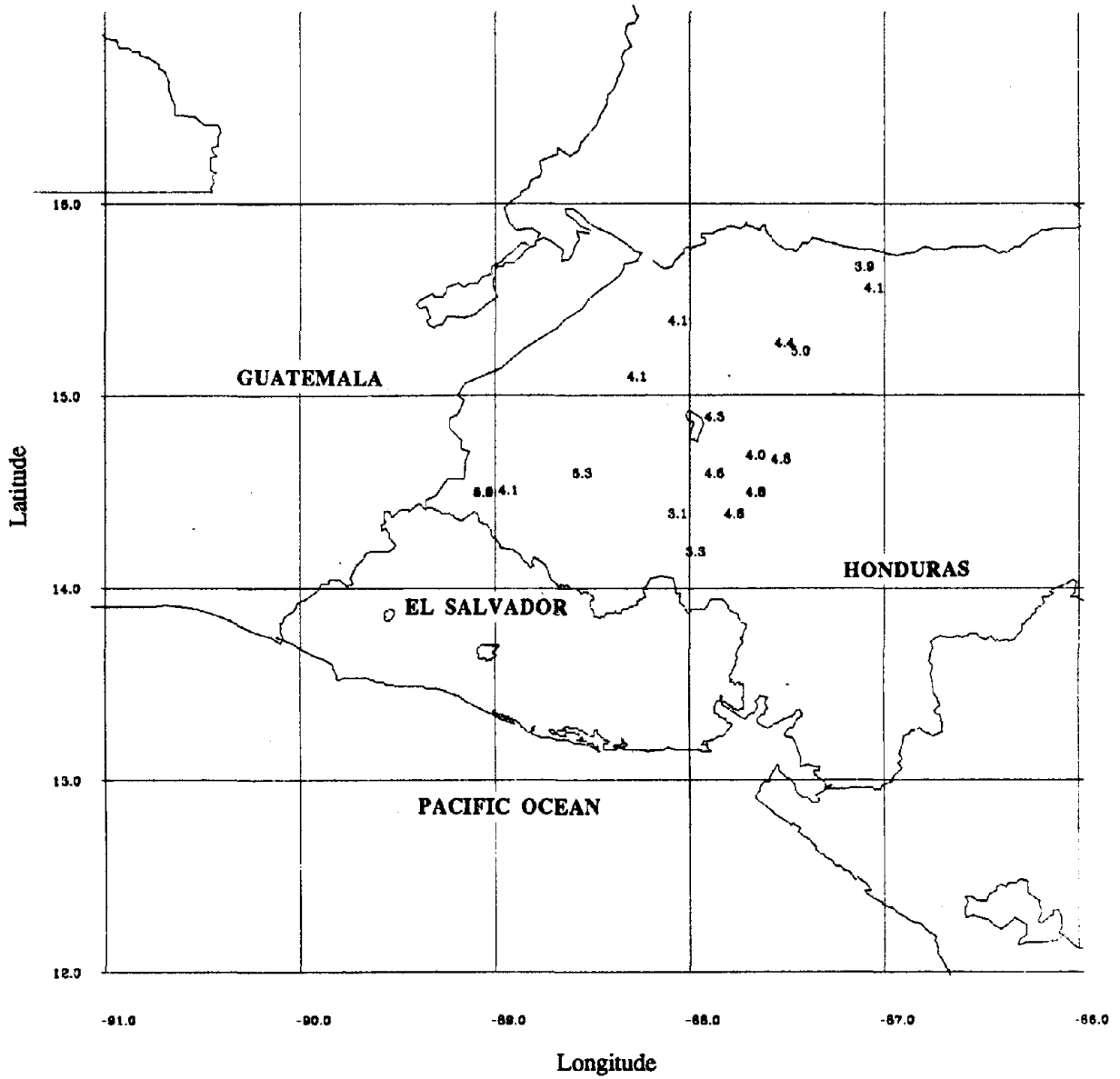


Figure C.9. Earthquake epicenters for the Honduras Depression Zone for $M \geq 3.0$ since 1915.

APPENDIX D
EARTHQUAKE RECURRENCE RELATIONSHIPS

APPENDIX D

EARTHQUAKE RECURRENCE RELATIONSHIPS

D.1 Introduction.

This appendix presents a review of different calculation methods of an earthquake recurrence relationship. In the past, Gutenberg and Richter (1956), Wiechert (1980), and Dong et al. (1984) suggested, respectively, the use of the least squares method, the maximum likelihood method, and the maximum entropy method for the development of earthquake recurrence relationships. These methods are described and applied to the seismicity of several seismic sources in El Salvador. The evaluation and adequacy of these relationships is discussed below.

D.2 The Least Squares Method.

The simplest and most common method of representing information on earthquake occurrences is by a least squares best fitted line. This method states that the occurrence of earthquakes during a period of time is approximated by the following relationship:

$$\ln N(M) = \alpha + \beta M \quad (D.1)$$

where $N(M)$ is the number of events above a magnitude M . α and β are regression constants obtained through least squares fit to the data. This equation assumes temporal and spatial independence of all events. α and β are given by

$$\alpha = \frac{\sum_i \ln N(m_i) + \sum_i m_i \beta}{n} \quad (D.2)$$

and

$$\beta = \frac{\sum_i m_i \sum_i \ln N(m_i) - n \sum_i \ln N(m_i)}{n \sum_i m_i^2 - (\sum_i m_i)^2} \quad (D.3)$$

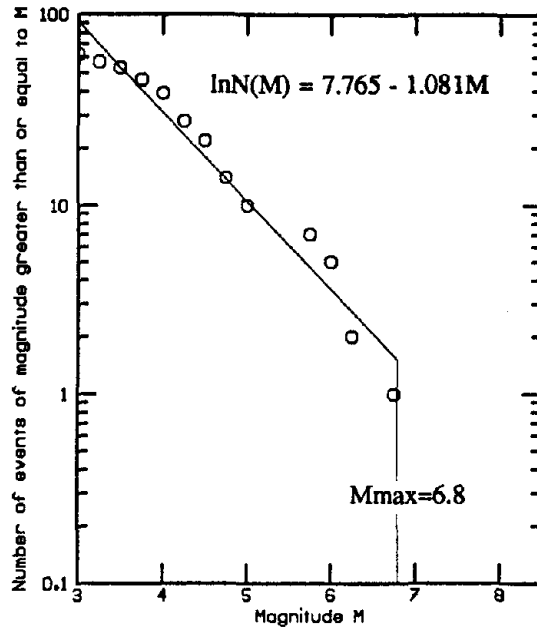


Figure D.1. Recurrence relationship for the Guatemalan Segment of the Volcanic Chain Zone for a time period of 256 yrs.

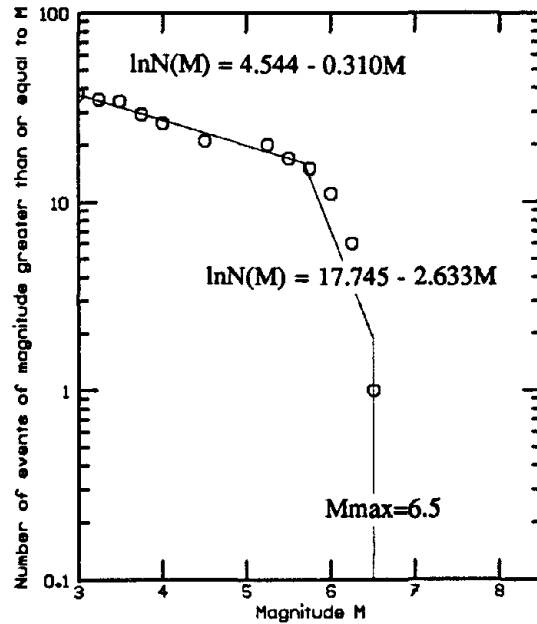


Figure D.2. Recurrence relationship for the Central El Salvador Segment of the Volcanic Chain Zone for a time period of 256 yrs.

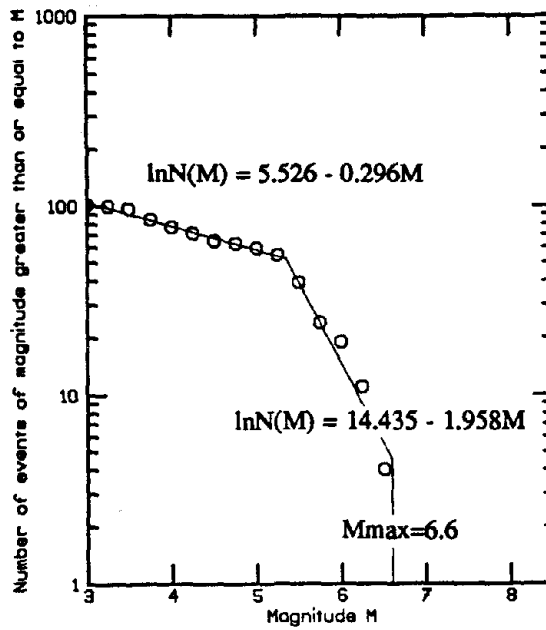


Figure D.3. Recurrence relationship for the Eastern El Salvador Segment of the Volcanic Chain Zone for a time period of 256 yrs.

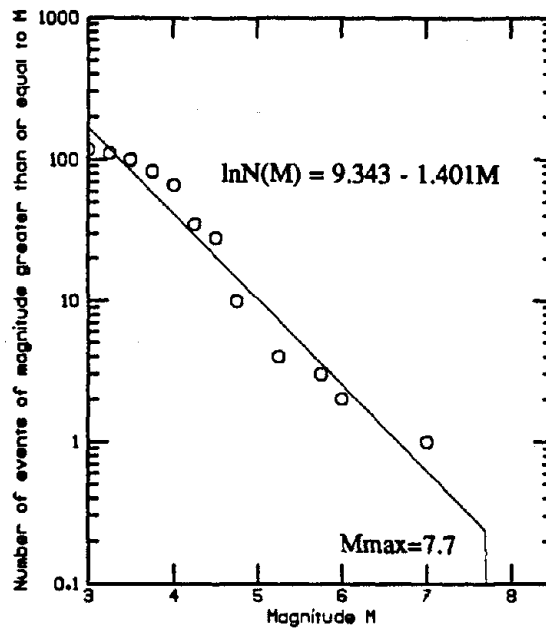


Figure D.4. Recurrence relationship for the Segment 1 of the Shallow Benioff Zone for a time period of 275 yrs.

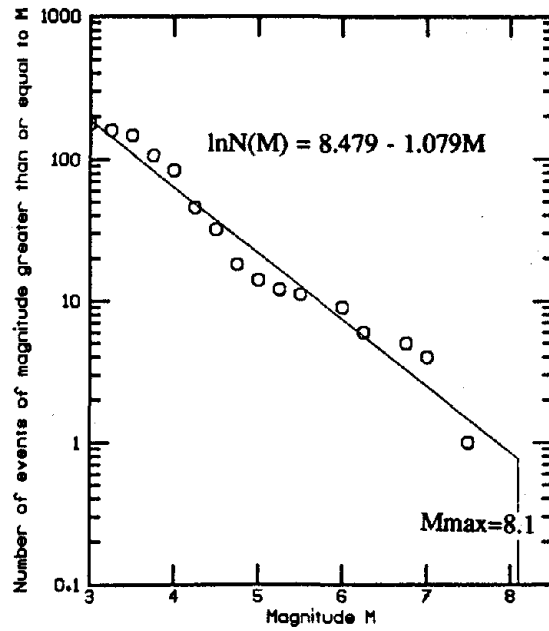


Figure D.5. Recurrence relationship for the Segment 2 of the Shallow Benioff Zone for a time period of 275 yrs.

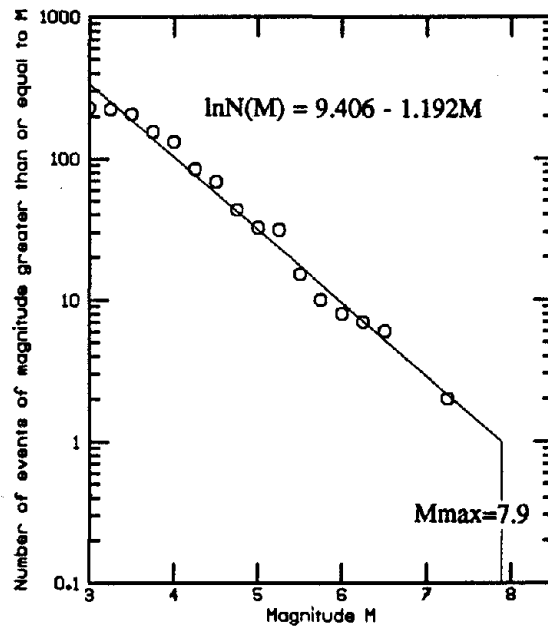


Figure D.6. Recurrence relationship for the Segment 3 of the Shallow Benioff Zone for a time period of 275 yrs.

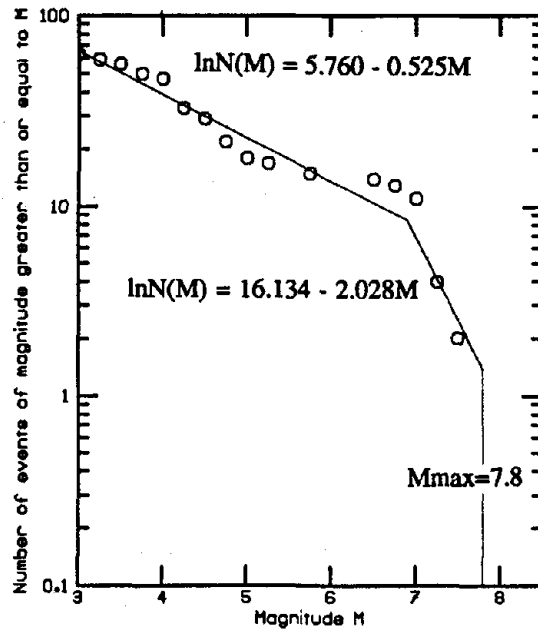


Figure D.7. Recurrence relationship for the Segment 1 of the Intermediate Benioff Zone for a time period of 275 yrs.

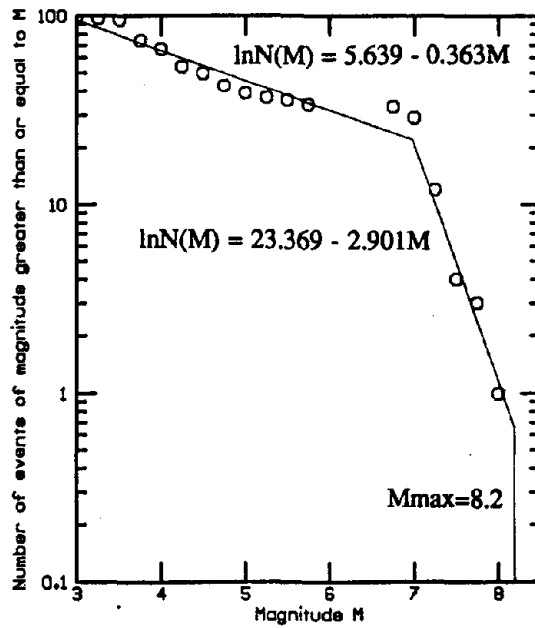


Figure D.8. Recurrence relationship for the Segment 2 of the Intermediate Benioff Zone for a time period of 275 yrs.

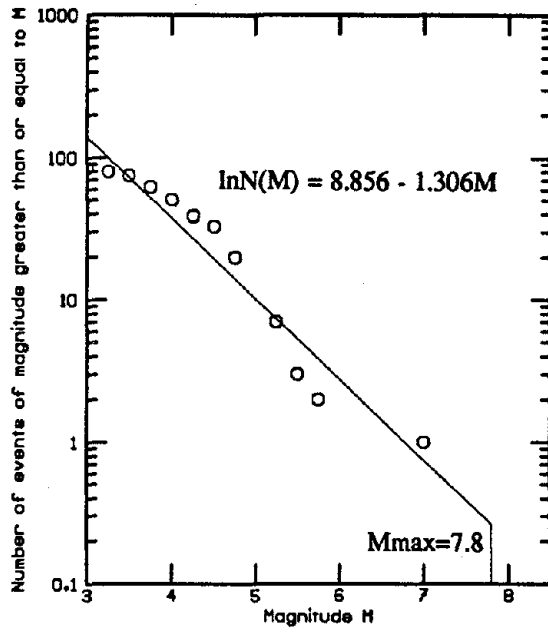


Figure D.9. Recurrence relationship for the Segment 3 of the Intermediate Benioff Zone for a time period of 275 yrs.

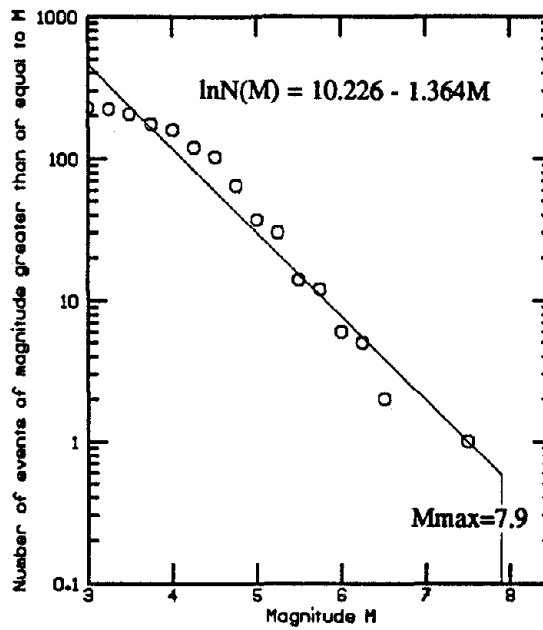


Figure D.10. Recurrence relationship for the Segment 1 of the Deep Benioff Zone for a time period of 275 yrs.

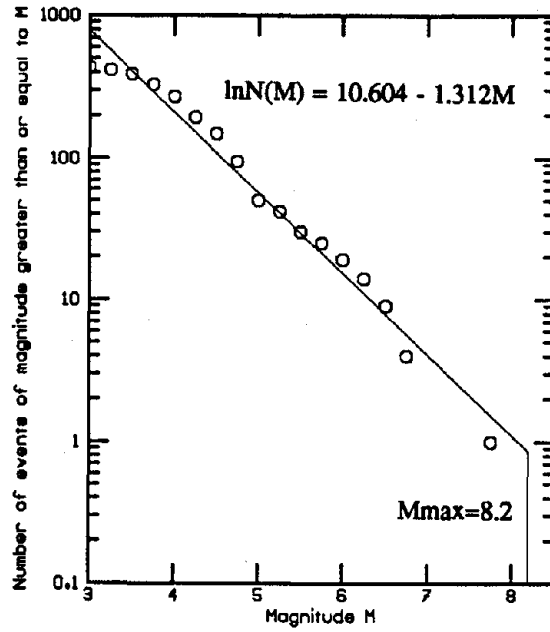


Figure D.11. Recurrence relationship for the Segment 2 of the Deep Benioff Zone for a time period of 275 yrs.

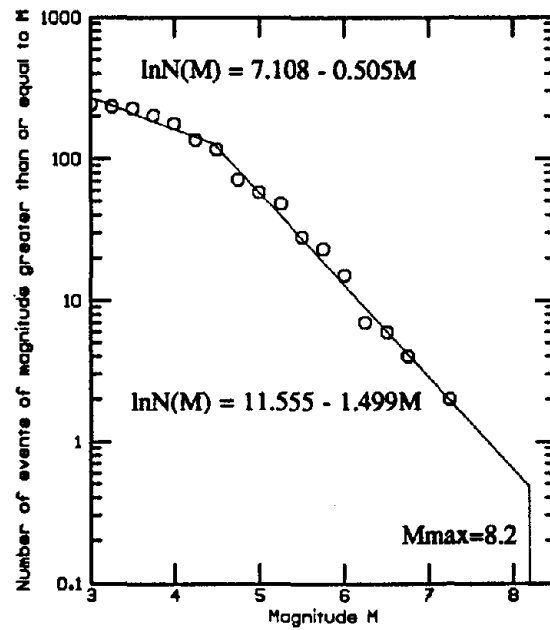


Figure D.12. Recurrence relationship for the Segment 3 of the Deep Benioff Zone for a time period of 275 yrs.

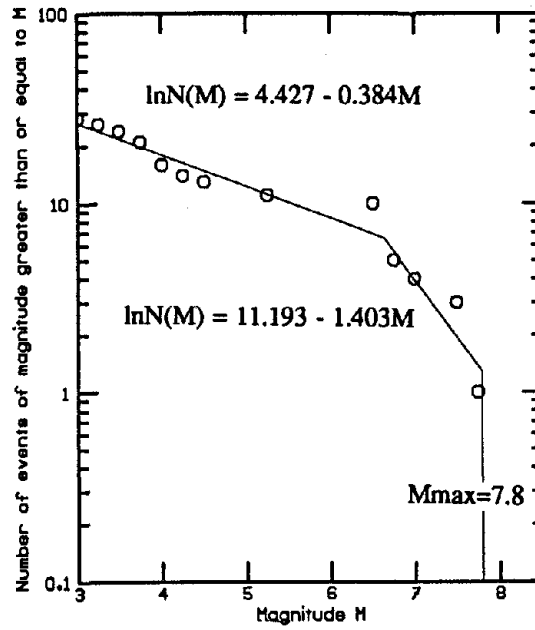


Figure D.13. Recurrence relationship for the Chixoy-Polochic Fault for a time period of 448 yrs.

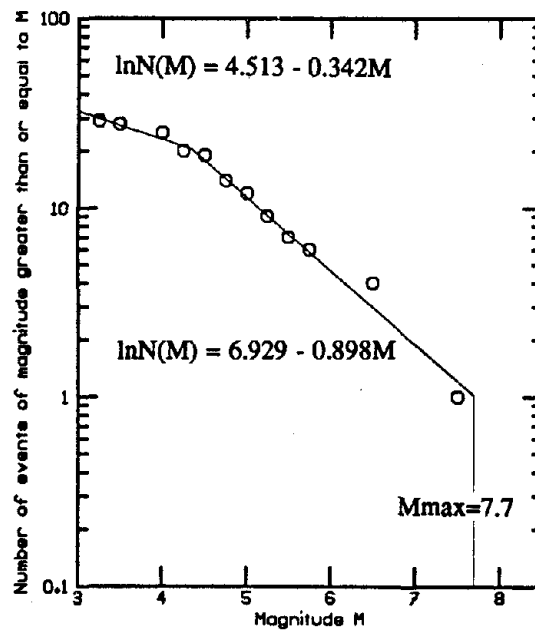


Figure D.14. Recurrence relationship for the Motagua Fault for a time period of 273 yrs.

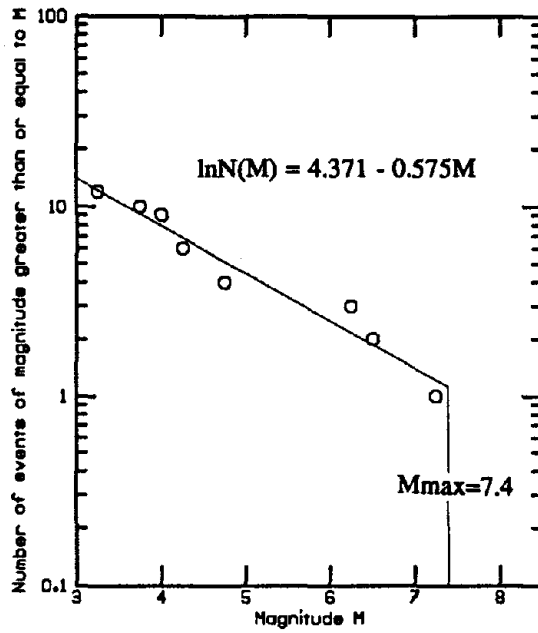


Figure D.15. Recurrence relationship for the Jocotan-Chamelecon for a time period of 243 yrs.

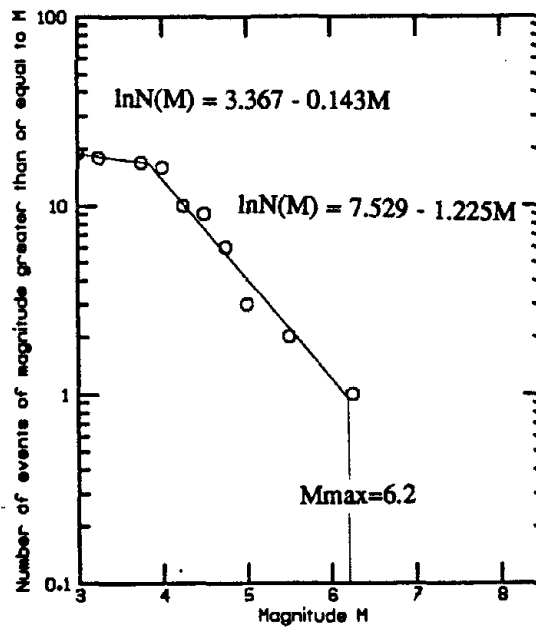


Figure D.16. Recurrence relationship for the Honduras Depression Zone for a time period of 71 yrs.

The Figures D.1-D.16 show plottings of best fitted lines and actual data grouped in intervals of 1/4 of magnitude. As is expected, the lines represent quite well the data sets. Bilinear recurrence relationships were developed when differences in slope were observed between small and large magnitude of frequency of occurrence.

D.3 The Maximum Likelihood Method.

In this method, maximum likelihood estimation of the earthquake parameters α and β in the relationship $N(M) = \alpha \exp(-\beta M)$ are extended to the case of earthquakes grouped in magnitude intervals observed in different time periods. In the development of this scheme, Wiechert (1980) considered the following aspects: a) different periods of observation, t_i ; b) classification of data in magnitude intervals, $M_i \pm \delta$; and c) an assumed maximum magnitude, M_x . Integrating over magnitude intervals and normalizing a given truncated recurrence density, a likelihood function is obtained. An extreme of this function is represented by

$$\frac{\sum_i t_i M_i \exp(-\beta M_i)}{\sum_j t_j \exp(-\beta M_j)} = \frac{\sum_i n_i M_i}{N} = \bar{M} \quad (D.4)$$

where β can be obtained by solving equation D.4 using an iterative scheme. N is the total number of earthquakes. \bar{M} is the sample mean of the magnitude.

In addition, α is given by

$$\alpha = \frac{N \sum_i \exp(-\beta M_i)}{\sum_j t_j \exp(-\beta M_j)} \quad (D.5)$$

To study the adequacy of the method for the region of study, two sources are considered: segment 3 of the Intermediate Benioff Zone and the Chixoy-Polochic fault. The maximum possible magnitude is estimated to be 7.8 for both sources. Their recurrence parameters were obtained applying the method to the data and the results are summarized in Table D.1.

	Segment 3 IBZ	Chixoy-Polochic fault
α	68.34	18.79
β	0.9724	1.0328

Table D.1 Earthquake recurrence parameters

Figures D.17 and D.18 show comparisons of the fitted lines and the data normalized with time. It can be observed that the lines do not represent the data well in both cases. This, is primarily due to the large differences of observation time for the different magnitude intervals. For the Intermediate Benioff Zone segment, the number of occurrences at large magnitudes are overestimated by a factor of 5 per year. For the Chixoy-Polochic fault, in the magnitude interval of 5.25 to 5.50 the number of occurrences are underestimated by a factor of 6 per year. For the remaining seismic sources, similar results were obtained; therefore, this method was not considered for further applications in this study.

D.4 The Maximum Entropy Principle Method.

In this section, the Maximum Entropy Principle (MEP) is used to obtain unbiased recurrence relationships. In addition, a modified MEP method developed by Dong et al. (1984) is used for nonhomogeneous data bases. A description of the method is first presented and then is applied to several seismic sources in El Salvador.

D.4.1 The Non Modified MEP Method.

In this method, the entropy of the magnitude M is maximized, subject to given constraints. Thus, the probability density function of M for a range of magnitudes from M_0 to M_u is given by

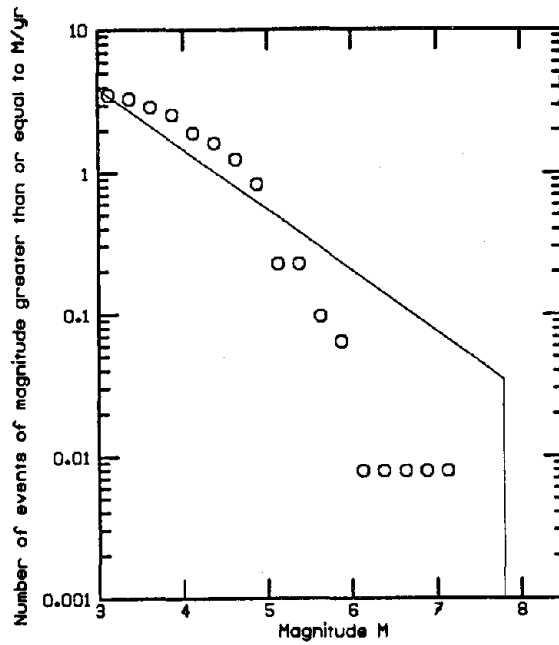


Figure D.17. Recurrence relationship for the segment 3 of the IBZ using the Maximum Likelihood method. The dots represent actual data grouped in intervals of 1/4 of magnitude.

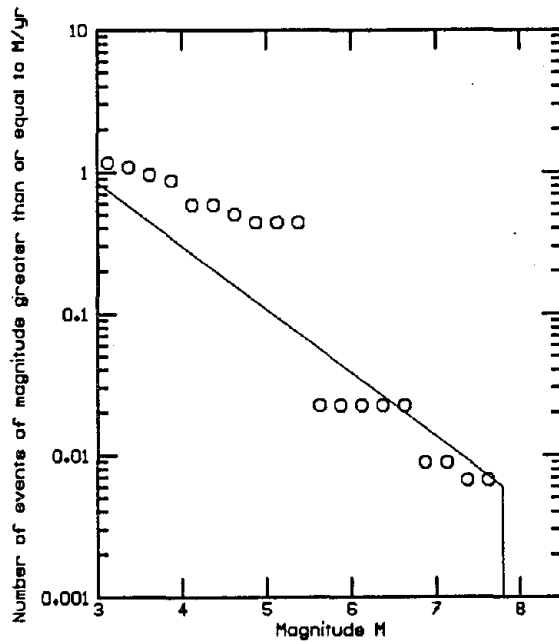


Figure D.18. Recurrence relationship for the Chixoy-Polochic fault using the Maximum Likelihood method. The dots represent actual data grouped in intervals of 1/4 of magnitude.

$$f_M(m) = \frac{\gamma_1 \exp(-\gamma_1 m)}{\exp(-\gamma_1 M_o) - \exp(-\gamma_1 M_u)} \quad (D.6)$$

where γ_1 can be determined by

$$\frac{1}{\gamma_1} + \frac{M_o \exp(-\gamma_1 M_o) - M_u \exp(-\gamma_1 M_u)}{\exp(-\gamma_1 M_o) - \exp(-\gamma_1 M_u)} = \bar{M} \quad (D.7)$$

Solving equation D.7 for γ_1 and substituting this value in equation D.6, the minimally unbiased probability density function of M is obtained.

D.4.2 The Modified Maximum Entropy Method.

In this method, the return period (RP_H) for large events between magnitudes M'_u and M_u is estimated. Define M_H as the magnitude between M'_u and M_u , then

$$\mu_H = \frac{1}{RP_H} \quad (D.8)$$

where μ_H is the mean rate of magnitude M_H events. The probability that the magnitude of the event will be between these magnitudes is given by

$$P_H = P(M'_u < M_H < M_u) = \frac{\mu_H}{\mu} = \frac{T}{NRP_H} \quad (D.9)$$

where μ is the mean rate of the data set, T is the period of instrumental data base, and N is the total number of events in time T . Additionally, the ordinate of the density function at $m=M_H$ should be adjusted as follows:

$$f_M(M_H) = \frac{P_H}{M_u - M'_u} = f_H \quad (D.10)$$

Similarly, as in the non modified MEP method the approximate solution of $f_M(m)$ is

$$f_M(m) = f_H \frac{m - M_o}{M_H - M_o} + \frac{1 - P_H - Af_H}{\left\{ \frac{1}{\gamma_1} (\exp(-\gamma_1 M_o) - \exp(-\gamma_1 M'_u)) - A \exp(-\gamma_1 M_H) \right\}} \cdot \left\{ \exp(-\gamma_1 m) - \frac{m - M_o}{M_H - M_o} \exp(-\gamma_1 M_H) \right\} \quad (D.11)$$

where the parameter γ_1 is determined by

$$\frac{1 - P_H - Af_H}{\left\{ \frac{1}{\gamma_1} (\exp(-\gamma_1 M_o) - \exp(-\gamma_1 M'_u)) - A \exp(-\gamma_1 M_H) \right\}} = \frac{\bar{M} - f_H B}{\left\{ \frac{1}{\gamma_1^2} (\exp(-\gamma_1 M_o) - \exp(-\gamma_1 M'_u)) + \frac{1}{\gamma_1} (M_o \exp(-\gamma_1 M_o) - M'_u \exp(-\gamma_1 M'_u)) - B \exp(-\gamma_1 M_H) \right\}} \quad (D.12)$$

and

$$A = \frac{(M'_u - M_o)^2}{2(M_H - M_o)} \quad (D.13)$$

$$B = \frac{(M'_u - M_o)^2 (2M'_u + M_o)}{6(M_H - M_o)} \quad (D.14)$$

The Figures D.19 and D.20 show plottings of the recurrence relationships obtained by the non modified MEP and least squares methods for segments 1 and 2 of the Deep Benioff Zone. It can be seen that the MEP method overestimates the number of occurrences in almost all ranges of magnitudes considered. Sensitivity analysis for the MEP methods are recommended but since similar results were obtained for other sources of the study area, those studies will be disregarded in this project. The MEP methods will not be considered in further calculations in this study.

In summary, three methods were used to investigate the best representation of earthquake occurrences for the study region. The least squares method was found the most adequate among them. To overcome the problem of incompleteness of the data set at lower

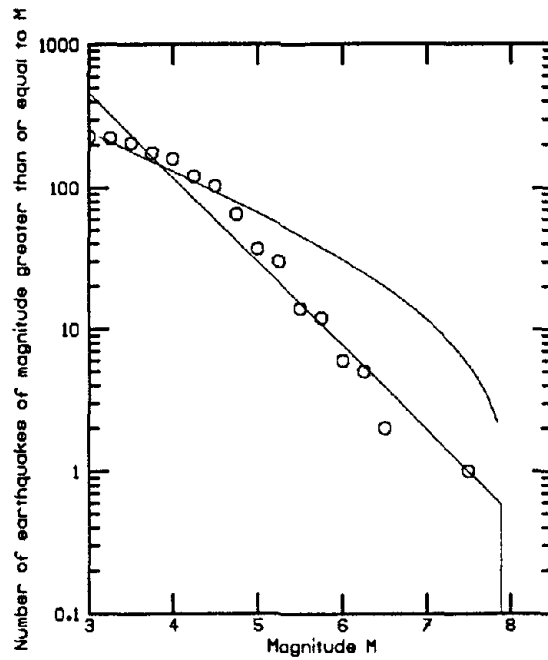


Figure D.19. Comparison of recurrence relationships obtained by using the non modified MEP (curved line) and the least squares (straight line) methods for the segment 1 of the DBZ.

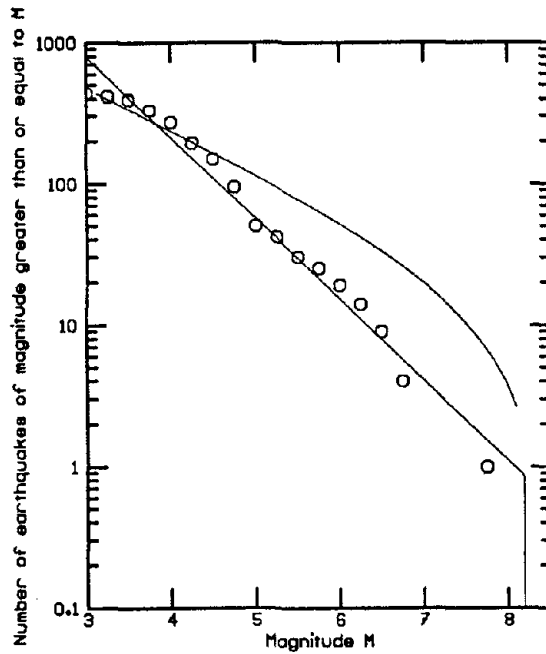


Figure D.20. Comparison of recurrence relationships obtained by using the non modified MEP (curved line) and the least squares (straight line) methods for the segment 2 of the DBZ.

magnitudes, a bilinear regression model was adopted. For hazard analysis calculations only this method will be used.

APPENDIX E
BAYESIAN PARAMETERS

Source : Volcanic Chain - Guatemalan segment.				
Time data base (T): 256 yr Number of recorded events (N): 46 v' from log-linear fit : $\lambda'' = \lambda' + T = 256 + 256 = 512$ $v'' = v' + N = 35.7 + 46 = 81.7$ $\eta''_{M_i} = \eta'_{M_i} + N = 35.7 + 46 = 81.7$				
Magnitude (M _i)	Nb of recorded occurrences in M _i bands (R _{M_i})	Cumulative Nb of occurrences (log-linear fit Fig. D.1) (N _c)	Nb of occurrences in M _i bands (log-linear fit) (ε'' _{M_i})	ε' _{M_i} + R _{M_i} (ε'' _{M_i})
4.00	11	35.7	8.4	19.4
4.25	7	27.3	6.5	13.5
4.50	11	20.8	4.9	15.9
4.75	3	15.9	3.8	6.8
5.00	6	12.1	2.8	8.8
5.25	1	9.3	2.2	3.2
5.50	0	7.1	1.7	1.7
5.75	0	5.4	1.3	1.3
6.00	4	4.1	1.0	5.0
6.25	2	3.1	0.7	2.7
6.50	0	2.4	0.6	0.6
6.75	0	1.8	0.4	0.4
7.00	1	1.4	1.4	2.4
7.25				
7.50				
7.75				
8.00				
8.25				

Table E.1. Seismic source parameters

Source : Volcanic Chain - Central El Salvador segment				
Time data base (T): 256 yr Number of recorded events (N): 29 v' from log-linear fit : 28.3 $\lambda'' = \lambda' + T = 256 + 256 = 512$ $v'' = v' + N = 28.3 + 29 = 57.3$ $\eta''M_i = \eta'M_i + N = 28.3 + 29 = 57.3$				
Magnitude (M_i)	Nb of recorded occurrences in M_i bands (R_{M_i})	Cumulative Nb of occurrences (log-linear fit Fig. D.2) (N_c)	Nb of occurrences in M_i bands (log-linear fit) ($\epsilon''M_i$)	$\epsilon'M_i + R_{M_i}$ ($\epsilon''M_i$)
4.00	4	28.3	2.1	6.1
4.25	4	26.2	2.0	6.0
4.50	0	24.2	1.8	1.8
4.75	1	22.4	1.6	2.6
5.00	0	20.8	1.6	1.6
5.25	0	19.2	1.4	1.4
5.50	4	17.8	1.4	5.4
5.75	2	16.4	6.7	8.7
6.00	6	9.7	4.7	10.7
6.25	4	5.0	2.4	6.4
6.50	4	2.6	2.6	6.6
6.75				
7.00				
7.25				
7.50				
7.75				
8.00				
8.25				

Table E.2. Seismic source parameters

Source : Volcanic Chain - East -El Salvador segment					
Time data base (T): 256 yr Number of recorded events (N): 84 v' from log-linear fit : 79.8 $\lambda'' = \lambda' + T = 256 + 256 = 512$ $v'' = v' + N = 79.8 + 84 = 163.8$ $\eta''_{Mi} = \eta'_{Mi} + N = 79.8 + 84 = 163.8$					
Magnitude (Mi)	Nb of recorded occurrences in Mi bands (R _{Mi})	Cumulative Nb of occurrences (log-linear fit Fig. D.3) (N _c)	Nb of occurrences in Mi bands (log-linear fit) (ε'' _{Mi})	ε' _{Mi} + R _{Mi} (ε'' _{Mi})	
4.00	10	79.8	5.7	15.7	
4.25	3	74.1	5.3	8.3	
4.50	8	68.8	4.9	12.9	
4.75	0	63.9	4.6	4.6	
5.00	6	59.3	4.2	10.2	
5.25	2	55.1	5.2	7.2	
5.50	17	49.9	19.3	36.3	
5.75	15	30.6	11.8	26.8	
6.00	10	18.8	7.3	17.3	
6.25	4	11.5	4.5	8.5	
6.50	8	7.0	2.7	10.7	
6.75					
7.00	1	4.3	4.3	5.3	
7.25					
7.50					
7.75					
8.00					
8.25					

Table E.3. Seismic source parameters

Source : Shallow Benioff Zone - Segment 1				
	Time data base (T): 275 yr Number of recorded events (N): 83 v' from log-linear fit : 48.4 $\lambda'' = \lambda' + T = 275 + 275 = 550$ $v'' = v' + N = 48.4 + 83 = 131.4$ $\eta'' M_i = \eta' M_i + N = 48.4 + 83 = 131.4$			
Magnitude (M _i)	Nb of recorded occurrences in M _i bands (R _{M_i})	Cumulative Nb of occurrences (log-linear fit Fig. D.4) (N _c)	Nb of occurrences in M _i bands (log-linear fit) (E''M _i)	E'M _i + R _{M_i} (E''M _i)
4.00	39	48.4	14.4	53.4
4.25	9	34.0	10.1	19.1
4.50	16	23.9	7.1	23.1
4.75	9	16.8	5.0	14.0
5.00	6	11.8	3.5	9.5
5.25	0	8.3	2.5	2.5
5.50	1	5.8	1.7	2.7
5.75	0	4.1	1.2	1.2
6.00	1	2.9	0.9	1.9
6.25	1	2.0	0.6	1.6
6.50	0	1.4	0.4	0.4
6.75	0	1.0	0.3	0.3
7.00	1	0.7	0.2	1.2
7.25	0	0.5	0.2	0.2
7.50	0	0.3	0.1	0.1
7.75	0	0.2	0.2	0.2
8.00				
8.25				

Table E.4. Seismic source parameters

Source : Shallow Benioff Zone - Segment 2				
Time data base (T): 275 yr Number of recorded events (N): 106 v' from log-linear fit : 73.5 $\lambda'' = \lambda' + T = 275 + 275 = 550$ $v'' = v' + N = 73.5 + 106 = 179.5$ $\eta''_{Mi} = \eta'_{Mi} + N = 73.5 + 106 = 179.5$				
Magnitude (Mi)	Nb of recorded occurrences in Mi bands (R _{Mi})	Cumulative Nb of occurrences (log-linear fit Fig. D.5) (N _c)	Nb of occurrences in Mi bands (log-linear fit) (ε'' _{Mi})	ε' _{Mi} + R _{Mi} (ε'' _{Mi})
4.00	39	73.5	17.3	56.3
4.25	21	56.2	13.3	34.3
4.50	26	42.9	19.2	45.2
4.75	2	32.7	7.7	9.7
5.00	4	25.0	5.9	9.9
5.25	2	19.1	4.5	6.5
5.50	1	14.6	3.5	4.5
5.75	2	11.1	2.6	4.6
6.00	2	8.5	2.0	4.0
6.25	1	6.5	1.5	2.5
6.50	1	5.0	1.2	2.2
6.75	0	3.8	0.9	0.9
7.00	2	2.9	0.7	2.7
7.25	2	2.2	0.5	2.5
7.50	1	1.7	0.4	1.4
7.75	0	1.3	0.3	0.3
8.00	0	1.0	1.0	1.0
8.25				

Table E.5. Seismic source parameters

Source : Shallow Benioff Zone - Segment 3				
Time data base (T): 275 yr Number of recorded events (N): 155 v' from log-linear fit : 119.9 $\lambda'' = \lambda' + T = 275 + 275 = 550$ $v'' = v' + N = 119.9 + 155 = 274.9$ $\eta''_{M_i} = \eta'_{M_i} + N = 119.9 + 155 = 274.9$				
Magnitude (M_i)	Nb of recorded occurrences in M_i bands (R_{M_i})	Cumulative Nb of occurrences (log-linear fit Fig. D.6) (N_c)	Nb of occurrences in M_i bands (log-linear fit) (ϵ'_{M_i})	$\epsilon'_{M_i} + R_{M_i}$ (ϵ''_{M_i})
4.00	53	119.9	30.9	83.9
4.25	18	89.0	22.9	40.9
4.50	33	66.1	17.0	50.0
4.75	8	49.1	12.7	20.7
5.00	11	36.4	9.4	20.4
5.25	1	27.0	6.9	7.9
5.50	18	20.1	5.2	23.2
5.75	3	14.9	3.8	6.8
6.00	3	11.1	2.9	5.9
6.25	0	8.2	2.1	2.1
6.50	4	6.1	1.6	5.6
6.75	1	4.5	1.1	2.1
7.00	0	3.4	0.9	0.9
7.25	0	2.5	0.7	0.7
7.50	2	1.8	0.4	2.4
7.75	0	1.4	0.4	0.4
8.00	0	1.0	1.0	1.0
8.25				

Table E.6. Seismic source parameters

Source : Intermediate Benioff Zone - Segment 1				
Time data base (T): 275 yr Number of recorded events (N): 50 v' from log-linear fit : 41.5 $\lambda'' = \lambda' + T = 275 + 275 = 550$ $v'' = v' + N = 41.5 + 50 = 91.5$ $\eta''M_i = \eta'M_i + N = 41.5 + 50 = 91.5$				
Magnitude (M_i)	Nb of recorded occurrences in M_i bands (R_{M_i})	Cumulative Nb of occurrences (log-linear fit Fig. D.7) (N_c)	Nb of occurrences in M_i bands (log-linear fit) ($\epsilon''M_i$)	$\epsilon''M_i + R_{M_i}$ ($\epsilon''M_i$)
4.00	10	41.5	5.1	15.1
4.25	7	36.4	4.5	11.5
4.50	7	31.9	3.9	10.9
4.75	4	28.0	3.5	7.5
5.00	4	24.5	3.0	7.0
5.25	1	21.5	2.6	3.6
5.50	2	18.8	2.3	4.3
5.75	0	16.6	2.1	2.1
6.00	1	14.5	1.8	2.8
6.25	0	12.7	1.5	1.5
6.50	1	11.2	1.4	2.4
6.75	0	9.8	0.9	0.9
7.00	5	8.9	3.5	8.5
7.25	5	5.4	2.2	7.2
7.50	2	3.2	1.2	3.2
7.75	1	2.0	2.0	3.0
8.00				
8.25				

Table E.7. Seismic source parameters

Source : Intermediate Benioff Zone - Segment 2				
	Time data base (T): 275 yr Number of recorded events (N): 73 v' from log-linear fit : 68.9 $\lambda'' = \lambda' + T = 275 + 275 = 550$ $v'' = v' + N = 68.9 + 73 = 141.9$ $\eta''M_i = \eta'M_i + N = 68.9 + 73 = 141.9$			
Magnitude (M_i)	Nb of recorded occurrences in M_i bands (R_{M_i})	Cumulative Nb of occurrences (log-linear fit Fig. D.8) (N_c)	Nb of occurrences in M_i bands (log-linear fit) ($\epsilon''M_i$)	$\epsilon'M_i + R_{M_i}$ ($\epsilon''M_i$)
4.00	14	68.9	6.0	20.0
4.25	5	62.9	5.5	10.5
4.50	9	57.4	4.9	13.9
4.75	2	52.5	4.6	6.6
5.00	4	47.9	4.1	8.1
5.25	2	43.8	3.8	5.8
5.50	2	40.0	3.5	5.5
5.75	1	36.5	3.2	4.2
6.00	1	33.3	2.9	3.9
6.25	0	30.4	2.6	2.6
6.50	0	27.8	2.4	2.4
6.75	1	25.4	2.2	3.2
7.00	9	23.2	8.3	17.3
7.25	15	14.9	7.7	22.7
7.50	5	7.2	3.7	8.7
7.75	2	3.5	1.8	3.8
8.00	0	1.7	0.9	0.9
8.25	1	0.8	0.8	1.8

Table E.8. Seismic source parameters

Source : Intermediate Benioff Zone - Segment 3				
Time data base (T): 275 yr Number of recorded events (N): 62 $v' = \lambda' + T = 275 + 275 = 550$ $v'' = v' + N = 44.5 + 62 = 106.5$ $\eta''M_i = \eta'M_i + N = 44.5 + 62 = 106.5$				
Magnitude (M_i)	Nb of recorded occurrences in M_i bands (R_{M_i})	Cumulative Nb of occurrences (log-linear fit Fig. D.9) (N_c)	Nb of occurrences in M_i bands (log-linear fit) ($\epsilon'M_i$)	$\epsilon'M_i + RM_i$ ($\epsilon''M_i$)
4.00	16	44.5	12.4	28.4
4.25	7	32.1	8.9	15.9
4.50	10	23.2	6.5	16.5
4.75	9	16.7	4.6	13.6
5.00	13	12.1	3.4	16.4
5.25	0	8.7	2.4	2.4
5.50	4	6.3	1.8	5.8
5.75	1	4.5	1.2	2.2
6.00	1	3.3	0.9	1.9
6.25	0	2.4	0.7	0.7
6.50	0	1.7	0.5	0.5
6.75	0	1.2	0.3	0.3
7.00	0	0.9	0.3	0.3
7.25	1	0.6	0.1	1.1
7.50	0	0.5	0.2	0.2
7.75	0	0.3	0.3	0.3
8.00				
8.25				

Table E.9. Seismic source parameters

Source : Deep Benioff Zone - Segment I				
Time data base (T): 275 yr Number of recorded events (N): 176 v' from log-linear fit : 139.8 $\lambda'' = \lambda' + T = 275 + 275 = 550$ $v'' = v' + N = 139.8 + 176 = 315.8$ $\eta''M_i = \eta'M_i + N = 139.8 + 176 = 315.8$				
Magnitude (M _i)	Nb of recorded occurrences in M _i bands (R _{M_i})	Cumulative Nb of occurrences (log-linear fit Fig. D.10) (N _c)	Nb of occurrences in M _i bands (log-linear fit) (E''M _i)	E'M _i + R _{M_i} (E''M _i)
4.00	36	139.8	40.4	76.4
4.25	20	99.4	28.7	48.7
4.50	37	70.7	20.4	57.4
4.75	18	50.3	14.6	32.6
5.00	28	35.7	10.3	38.3
5.25	7	25.4	7.3	14.3
5.50	16	18.1	5.2	21.2
5.75	2	12.9	3.8	5.8
6.00	7	9.1	2.6	9.6
6.25	0	6.1	1.9	1.9
6.50	4	4.6	1.3	5.3
6.75	0	3.3	1.0	1.0
7.00	0	2.3	0.6	0.6
7.25	0	1.7	0.5	0.5
7.50	1	1.2	0.4	1.4
7.75	0	0.8	0.2	0.2
8.00	0	0.6	0.6	0.6
8.25	0	0.6	0.6	0.6

Table E.10. Seismic source parameters

Source : Deep Benioff Zone - Segment 2					
Time data base (T): 275 yr Number of recorded events (N): 327 v' from log-linear fit : 249.6 $\lambda'' = \lambda' + T = 275 + 275 = 550$ $v'' = v' + N = 249.6 + 327 = 576.6$ $\eta'' M_i = \eta' M_i + N = 249.6 + 327 = 576.6$					
Magnitude (M _i)	Nb of recorded occurrences in M _i bands (R _{M_i})	Cumulative Nb of occurrences (log-linear fit Fig. D.11) (N _c)	Nb of occurrences in M _i bands (log-linear fit) (ε''M _i)	ε'M _i + R _{M_i} (ε''M _i)	
4.00	89	249.6	69.8	158.8	
4.25	49	179.8	50.3	99.3	
4.50	69	129.5	36.2	105.2	
4.75	25	93.3	26.1	51.1	
5.00	47	67.2	18.8	65.8	
5.25	7	48.4	13.5	20.5	
5.50	14	34.9	9.8	23.8	
5.75	4	25.1	7.0	11.0	
6.00	9	18.1	5.1	14.1	
6.25	1	13.0	3.6	4.6	
6.50	8	9.4	2.6	10.6	
6.75	1	6.8	1.9	2.9	
7.00	3	4.9	1.4	4.4	
7.25	0	3.5	1.0	1.0	
7.50	0	2.5	0.7	0.7	
7.75	0	1.8	0.5	0.5	
8.00	1	1.3	0.4	1.4	
8.25	0	0.9	0.9	0.9	

Table E.11. Seismic source parameters

Source : Deep Benioff Zone - Segment 3				
Time data base (T): 275 yr Number of recorded events (N): 202 v' from log-linear fit: 172.6 $\lambda'' = \lambda' + T = 275 + 275 = 550$ $v^d = v' + N = 172.6 + 202 = 350.5$ $\eta''M_i = \eta'M_i + N = 172.6 + 202 = 350.5$				
Magnitude (Mi)	Nb of recorded occurrences in Mi bands (RMi)	Cumulative Nb of occurrences (log-linear fit Fig. D.12) (Nc)	Nb of occurrences in Mi bands (log-linear fit) (ε'Mi)	ε'Mi + RMi (ε'Mi)
4.00	43	172.6	20.4	63.4
4.25	24	152.2	18.1	42.1
4.50	38	134.1	31.4	70.4
4.75	26	101.7	31.8	57.8
5.00	13	69.9	21.8	34.8
5.25	10	48.1	15.1	25.1
5.50	22	33.0	10.3	32.3
5.75	3	22.7	7.1	10.1
6.00	14	15.6	4.9	18.9
6.25	2	10.7	3.3	5.3
6.50	3	7.4	2.3	5.3
6.75	0	5.1	1.6	1.6
7.00	2	3.5	1.1	3.1
7.25	1	2.4	0.8	1.8
7.50	1	1.6	0.5	1.5
7.75	0	1.1	0.3	0.3
8.00	0	0.8	0.3	0.3
8.25	0	0.5	0.5	0.5

Table E.12. Seismic source parameters

Source : Chixoy - Polochic fault				
Time data base (T): 448 yr Number of recorded events (N): 21 v' from log-linear fit : 19.5 $\lambda'' = \lambda' + T = 448 + 448 = 896$ $v'' = v' + N = 19.5 + 21 = 39.9$ $\eta''M_i = \eta'M_i + N = 19.5 + 21 = 39.9$				
Magnitude (M_i)	Nb of recorded occurrences in M_i bands (R_{M_i})	Cumulative Nb of occurrences (log-linear fit Fig. D.13) (N_c)	Nb of occurrences in M_i bands (log-linear fit) ($\epsilon''M_i$)	$\epsilon'M_i + R_{M_i}$ ($\epsilon''M_i$)
4.00	7	18.9	1.7	8.7
4.25	0	17.2	1.6	1.6
4.50	2	15.6	1.4	3.4
4.75	1	14.2	1.3	2.3
5.00	0	12.9	1.2	1.2
5.25	0	11.7	1.1	1.1
5.50	1	10.6	0.9	1.9
5.75	0	9.7	0.9	0.9
6.00	0	8.8	0.8	0.8
6.25	0	8.0	0.8	0.8
6.50	4	7.2	0.5	4.5
6.75	2	6.7	2.0	4.0
7.00	1	4.7	1.4	2.4
7.25	0	3.3	1.0	1.0
7.50	2	2.3	0.7	2.7
7.75	1	1.6	1.6	2.6
8.00				
8.25				

Table E.13. Seismic source parameters

Source : Motagua fault				
Time data base (T): 286 yr Number of recorded events (N): 25 v' from log-linear fit : 24.2 $\lambda'' = \lambda' + T = 286 + 286 = 572$ $v'' = v' + N = 24.2 + 25 = 49.2$ $\eta'' M_i = \eta' M_i + N = 24.2 + 25 = 49.2$				
Magnitude (M _i)	Nb of recorded occurrences in M _i bands (R _{M_i})	Cumulative Nb of occurrences (log-linear fit Fig. D.14) (N _c)	Nb of occurrences in M _i bands (log-linear fit) (ε''M _i)	ε'M _i + R _{M_i} (ε''M _i)
4.00	1	24.2	2.0	3.0
4.25	4	22.2	2.2	6.2
4.50	3	20.0	4.0	7.0
4.75	3	16.0	3.2	6.2
5.00	2	12.8	2.6	4.6
5.25	3	10.2	2.0	5.0
5.50	3	8.2	1.7	4.7
5.75	0	6.5	1.3	1.3
6.00	2	5.2	1.0	3.0
6.25	0	4.2	0.9	0.9
6.50	3	3.3	0.6	3.6
6.75	0	2.7	0.6	0.6
7.00	0	2.1	0.4	0.4
7.25	0	1.7	0.3	0.3
7.50	1	1.4	0.3	1.3
7.75	0	1.1	1.1	1.1
8.00				
8.25				

Table E.14. Seismic source parameters

Source : Jocotan - Chamelecon fault				
Time data base (T): 286 yr Number of recorded events (N): 10 v' from log-linear fit : 8.5 $\lambda'' = \lambda' + T = 286 + 286 = 572$ $v'' = v' + N = 8.5 + 10 = 18.5$ $\eta''_{M_i} = \eta'_{M_i} + N = 8.5 + 10 = 18.5$				
Magnitude (M _i)	Nb of recorded occurrences in M _i bands (R _{M_i})	Cumulative Nb of occurrences (log-linear fit Fig. D.15) (N _c)	Nb of occurrences in M _i bands (log-linear fit) (ε'' _{M_i})	ε'' _{M_i} + R _{M_i} (ε'' _{M_i})
4.00	2	8.5	1.1	3.1
4.25	2	7.4	1.0	3.0
4.50	2	6.4	0.9	2.9
4.75	0	5.5	0.7	0.7
5.00	1	4.8	0.6	1.6
5.25	0	4.2	0.6	0.6
5.50	0	3.6	0.5	0.5
5.75	0	3.1	0.4	0.4
6.00	0	2.7	0.4	0.4
6.25	0	2.3	0.3	0.3
6.50	2	2.0	0.2	2.2
6.75	0	1.8	0.3	0.3
7.00	0	1.5	0.2	0.2
7.25	1	1.3	0.3	1.3
7.50	0	1.1	1.1	1.1
8.00				
8.25				

Table E.15. Seismic source parameters

Source : Honduras Depression Zone				
	Time data base (T): 71 yr Number of recorded events (N): 16 v' from log-linear fit : 16.1 $\lambda'' = \lambda' + T = 71 + 71 = 142$ $v'' = v' + N = 16.1 + 16 = 32.1$ $\eta''M_i = \eta'M_i + N = 16.1 + 16 = 32.1$			
Magnitude (M _i)	Nb of recorded occurrences in M _i bands (R _{M_i})	Cumulative Nb of occurrences (log-linear fit Fig. D.16) (N _c)	Nb of occurrences in M _i bands (log-linear fit) (E''M _i)	E'M _i + R _{M_i} (E''M _i)
4.00	3	16.1	4.2	7.2
4.25	4	11.9	3.1	7.1
4.50	2	8.8	2.4	4.4
4.75	2	6.4	1.7	3.7
5.00	4	4.7	1.2	5.2
5.25	0	3.5	0.9	0.9
5.50	0	2.6	0.7	0.7
5.75	1	1.9	0.5	1.5
6.00	0	1.4	0.4	0.4
6.25	1	1.0	1.0	2.0
6.50				
6.75				
7.00				
7.25				
7.50				
7.75				
8.00				
8.25				

Table E.16. Seismic source parameters

